The impact of temperature-dependent alternative splicing on protein expression of the helicase eIF4A2

Inaugural-Dissertation

to obtain the academic degree

Doctor rerum naturalium (Dr. rer. nat.)

submitted to the Department of Biology, Chemistry, Pharmacy

of Freie Universität Berlin

by

Ann-Kathrin Emmerichs

Berlin, 2023

Declaration

This work was carried out between August 2019 and April 2023 under the supervision of Prof. Dr. Florian Heyd at the Institute of Chemistry and Biochemistry, Freie Universität Berlin, Germany.

First reviewer:

Prof. Dr. Florian Heyd

RNA Biochemistry

Institute of Chemistry and Biochemistry

Freie Universität Berlin

Takustraße 6

14195 Berlin, Germany

Second reviewer:

Prof. Sutapa Chakrabari, Ph.D.

mRNA Metabolism

Institute of Chemistry and Biochemistry

Freie Universität Berlin

Takustraße 6

14195 Berlin

Date of defense: 30.06.2023

– H –

Selbstständigkeitserklärung

Gem. § 7 Abs. 4 der Promotionsordnung basierend auf den Mitteilungen im Amtsblatt der Freien Universität Berlin Nr. 21/2018 vom 23.05.2018.

Hierdurch versichere ich, dass ich die vorliegende Dissertation selbstständig und ohne unerlaubte Hilfe angefertigt habe.

Hierdurch versichere ich, dass meine Dissertation nicht auf meiner Masterarbeit aufbaut bzw. nicht daraus erwachsen ist.

Hierdurch versichere ich, dass meine Dissertation im Einvernehmen mit meinem Betreuer Prof. Dr. Florian Heyd in Teilen veröffentlicht wurde. Die Publikationen sind Bestandteil der Monographie.

Ann-Kathrin Emmerichs

Berlin, 2023

Table of Contents

Abstract

Alternative splicing is a co-transcriptional process in which multiple mature mRNAs isoforms can arise from a single pre-mRNA transcript. The translation of these different mRNAs significantly increases the size of the proteome. At the genomic level, alternative splicing leads to the regulation of gene expression as part of RNA processing. Alternative splicing allows the cell to respond quickly to changes in its environment, as it is a rapid process. Changes in a cell's environment are caused, for example, by toxins, infections or temperature variations. Since temperature fluctuations are a ubiquitous factor, further investigation of their effects on splicing, as well as gene and protein expression, was of interest. Homoiothermic organisms such as humans can maintain a constant body temperature, which makes them robust to more severe temperature fluctuations. In contrast, plants and poikilothermic animals are more affected by their ambient temperature.

To better understand the impact of temperature on global cellular processes, this work is interested in the effects of temperature-dependent alternative splicing on the protein expression of human helicases. In our study we identified a number of helicases whose expression was affected by changes in temperature.

As the DEAD-box RNA helicase eIF4A2 turned out to be the most interesting of the identified proteins, we put our main focus on its investigation. We showed that two temperature-dependent alternative exons regulate its protein expression. While exon 10A was the interest of several previous studies, exon 4 has been neglected in the past. Thus, we examined exon 4 and exon 10A individually and also the co-regulation of the two alternative exons. Therefore, we combined our initial *in vitro* approach with a specially established CRISPR/Cas9 based cell culture system. Both setups revealed that the inclusion of the alternative exon 4 is causative for a higher mRNA abundance, while the isoform containing exon 10A leads to mRNA degradation via the NMD pathway due to the inclusion of a premature stop codon. Analysis of RNA-seq data and minigenes showed that the two alternative exons are co-regulated despite their spatial distance. A comprehensive analysis of the proteome showed that the absence of exon 4 leads to a complete loss of protein (knockout), whereas exon 4 significantly increases the formation of the full-length protein (constitutive overexpression).

As an RNA helicase, the eukaryotic translation initiation factor eIF4A2 is involved in many cellular processes. We have shown that the ratio between eIF4A2 exon 4 and exon 10A is not only temperature dependent but also cell-type specific and that this ratio is regulated by their co-regulated alternative splicing. This tissue-specific expression is highly conserved in many species, raising questions about the exact function eIF4A2.

Helicases are essential proteins in cellular metabolism and are expressed in many species. Combined with the effect of temperature, eIF4A2 represents a fascinating RNA helicase that gives global insights into the regulation of helicases in a temperature-dependent manner. Global proteome analysis revealed many proteins of the respiratory chain complex I as direct targets of eIF4A2. Therefore, we propose a role of eIF4A2 in the electron transfer within the respiratory chain in mitochondria via regulating the expression of essential complex I components. Furthermore, our data are consistent with previous studies that showed eIF4A2 functions in neuronal development.

In summary, this work provides new insights into regulation of protein expression by alternative splicing in response to temperature using the eukaryotic RNA helicase eIF4A2 as an example.

Abstract

Zusammenfassung

Alternatives Spleißen ist ein ko-transkriptioneller Prozess, bei dem aus einem einzelnen prä-mRNA-Transkript mehrere reife mRNA-Isoformen entstehen können. Die Translation dieser verschiedenen mRNAs erhöht die Vielfalt des Proteoms erheblich. Auf genomischer Ebene führt das alternative Spleißen zur Regulierung der Genexpression als Teil der RNA-Prozessierung. Alternatives Spleißen ermöglicht es der Zelle, umgehend auf Veränderungen in ihrer Umgebung zu reagieren, da es sich um einen schnellen Prozess handelt. Veränderungen in der Umgebung einer Zelle werden zum Beispiel durch Toxine, Infektionen oder Temperaturfluktuationen verursacht. Da Temperaturschwankungen ein allgegenwärtiger Faktor sind, ist die Untersuchung ihrer Auswirkungen auf das Spleißen sowie die Gen- und Proteinexpression von großem Interesse. Homoiotherme Organismen, wie der Mensch, können ihre Körpertemperatur konstant aufrechterhalten, was sie robust gegenüber stärkeren Temperaturschwankungen macht. Im Gegensatz dazu werden Pflanzen und poikilotherme Tiere stärker von ihrer Umgebungstemperatur beeinflusst.

Um die globalen Auswirkungen der Temperatur auf zelluläre Prozesse besser zu verstehen, untersuchen wir in dieser Arbeit den Einfluss des temperaturabhängigen alternativen Spleißens auf die Proteinexpression menschlicher Helikasen. In unserer Studie haben wir eine Reihe von Helikasen identifiziert, deren Expression durch Temperaturveränderungen beeinflusst wird.

Da sich die DEAD-Box-RNA-Helikase eIF4A2 als das interessanteste der identifizierten Proteine herausstellte, haben wir unser Hauptaugenmerk auf dessen Untersuchung gelegt. Wir konnten zeigen, dass zwei temperaturabhängige alternative Exons die Expression des Proteins regulieren. Während Exon 10A bereits in früheren Studien untersucht wurde, wurde Exon 4 in der Vergangenheit eher vernachlässigt. Daher untersuchten wir Exon 4 und Exon 10A individuell, sowie die Ko-Regulation der beiden alternativen Exons. Dazu kombinierten wir unseren ursprünglichen In-vitro-Ansatz mit einem speziell entwickelten CRISPR/Cas9-basierten Zellkultursystem. In beiden Fällen zeigte sich, dass der Einschluss des alternativen Exons 4 zu einer höheren mRNA-Expression führt, während die Isoform mit Exon 10A aufgrund eines vorzeitigen Stopcodons den mRNA-Abbau über den NMD-Weg bewirkt. Die Analyse von RNA-Sequenzierungsdaten und Minigenen zeigte, dass die beiden alternativen Exons trotz ihres räumlichen Abstands ko-reguliert sind. Eine umfassende Analyse des Proteoms ergab, dass die Abwesenheit von Exon 4 zu einem vollständigen Verlust des Proteins führt (Knockout), während die Anwesenheit von Exon 4 die Bildung des Proteins in voller Länge deutlich erhöht (konstitutive Überexpression).

Als RNA-Helikase ist der eukaryotische Translationsinitiationsfaktor eIF4A2 an vielen zellulären Prozessen beteiligt. Wir konnten zeigen, dass das Verhältnis zwischen eIF4A2 Exon 4 und Exon 10A nicht nur temperaturabhängig, sondern auch zelltypspezifisch ist und dass dieses Verhältnis durch ihr gemeinsames alternatives Spleißen reguliert wird. Diese gewebespezifische Expression ist in vielen Spezies hoch konserviert, was Fragen nach der genauen Funktion von eIF4A2 aufwirft.

Helikasen sind essenzielle Proteine im zellulären Stoffwechsel und werden in vielen Spezies exprimiert. In Verbindung mit der Wirkung der Temperatur stellt eIF4A2 eine faszinierende RNA-Helikase dar, welche globale Einblicke in die temperaturabhängige Regulierung von Helikasen gewährt. Eine globale Proteom-Analyse ergab, dass viele Proteine des Komplex I der Atmungskette direkte Ziele von eIF4A2 sind. Daher schlagen wir vor, dass eIF4A2 eine Rolle beim Elektronentransfer innerhalb der Atmungskette in Mitochondrien spielt, indem es die Expression wesentlicher Komplex-I-Komponenten reguliert. Darüber hinaus stimmen unsere Daten mit früheren Studien überein, die zeigten, dass eIF4A2 bei der neuronalen Entwicklung eine bedeutende Rolle spielt.

Zusammenfassend lässt sich sagen, dass diese Arbeit neue Erkenntnisse über die Regulierung der Proteinexpression durch alternatives Spleißen in Abhängigkeit von der Temperatur am Beispiel der eukaryotischen RNA-Helikase eIF4A2 liefert.

1. Introduction

The central dogma of molecular biology by established Francis Crick in 1958, has built a keystone in understanding the passing of sequence information from desoxyribonucleic acid (DNA) to ribonucleic acid (RNA) to the protein level. On the genomic level, DNA stores the genetic information and gets transcribed into RNA which builds the transcriptome and can be translated into proteins building the proteome (Crick, 1970). This dogma was challenged by the discovery of retroviruses transferring information retrograde from RNA to DNA during reverse transcription, but has not yet been entirely disputed, as to this day genetic information doesn't converse from protein to nucleic acid (Temin and Mizutani, 1970). The central dogma is found in simple prokaryotes as well as in higher organisms like complex eukaryotes. While in simple prokaryotes a continuous DNA sequence is transcribed in its entirety and directly translates into a protein, in higher eukaryotes, the transcribed gene undergoes several processing and maturation events before its export to the cytoplasm. The transcription of DNA into RNA in the nucleus is mediated by the RNA polymerase II (Jacob and Monod, 1961). In the cytoplasm, the ribosomal machinery translates the transcripts into proteins (Clawson, Feldherr and Smuckler, 1985).

Processing of the precursor messenger RNA (pre-mRNA) begins as early as the transcription stage. In fact, in higher eukaryotes, where AS is more prominent, splicing occurs predominantly co-transcriptionally. To be further translated, the pre-mRNA needs to be processed into a mature mRNA. This happens by attaching an N7-methylguanosine (m^7G) to the 5' ribose by a 5' to 5' triphosphate linkage. Right before termination, the 3' end is cleaved and a poly(A) tail of up to 200 adenosine residues is synthesized at the end of the transcript. Capping and polyadenylation are modifications stabilize the transcript and supporting nuclear export, followed by translation initiation (Shatkin and Manley, 2000).

Furthermore, the pre-mRNA consists of exons (protein-coding sequences) which are often disrupted by introns (non-coding sequences). Within the first two pre-mRNA processing/maturation steps of eukaryotic gene expression, splice sites are identified, and introns are removed by a final maturation step called splicing. To produce the mature mRNA isoform and its encoded proteins, this step is essential (Gehring and Roignant, 2021). Splicing is catalyzed by a molecular RNA-protein machinery, the spliceosome, which ensures the accuracy of this pre-mRNA processing step.

1.1 Pre-mRNA structure

In eukaryotes, the defined boundaries of the introns are flanked by short, conserved motifs. These sequences, termed splice sites are recognized by the spliceosome to define the exon-intron boundaries. This splice site recognition process needs to be nucleotide specific since defects in splicing have dramatic consequences for the cell. Introns can be up to 200,000 nucleotides in size and have low protein-coding potential. The retention of an intron within an mRNA can cause the insertion of in-frame stop codons, resulting in prematurely terminated proteins (Krämer, 1996).

In higher eukaryotes, the consensus sequence of the 5' splice site (5'SS) determines the boundary between an intron and its upstream exon (Figure 1). This sequence AG|GURAGU (R = purine) is much more variable in human cells compared to yeast (Zhang, 1998). The downstream border of an exon/intron is termed a 3' splice site (3'SS). This splice site is depicted by the YAG| (Y = pyrimidine) sequence. For both splice sites, the underlined nucleotides are almost invariant, and the splice site (depicted by the vertical line). Additionally, a stretch of pyrimidine residues (C or U) is located between the 3'SS and the branch site (BS) in most vertebrate introns. The branch site displays the sequence **Y**NCUR**A**Y (nucleotides involved in BP formation). Usually, the branch site is located 18-40 nucleotides upstream of the 3'SS. Functionally this important splicing motif is essential, as it gets recognized and bound by spliceosomal factors in humans (Green, 1986; Krämer, 1996).

Introduction

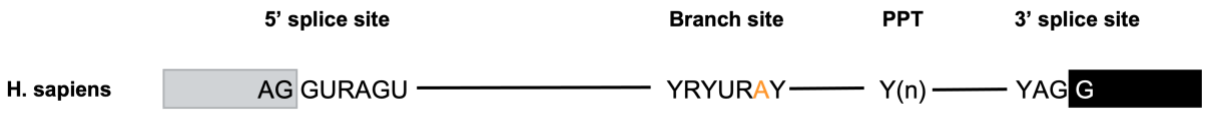

Figure 1. Conserved pre-mRNA splicing sequence in *homo sapiens*
Schematic representation of human pre-mRNA including an intron bordered by two exons. Specified in black and white letters are the conserved intron defining consensus sequences, the branch-point is shown in yellow. Exons are depicted by grey and black boxes, the intron by a black line. Adapted from (Will and Luhrmann, 2011).

1.1.1 The pre-mRNA splicing mechanism

Removal of introns from the pre-mRNA is achieved by two sequential SN2-type transesterification reactions. The 2'hydroxyl group of the branch-point (BP) adenosine attacks the phosphodiester bond of the 5'SS, to release the 5' exon. In this first step, a 3' exon-intron lariat intermediate is arranged, connecting the BP adenosine and the guanosine at the 5' end of the intron by a 2'-5' phosphodiester bond. In the second reaction, the phosphodiester bond at the 3'SS gets attacked by the 3' hydroxyl group of the upstream exon (Figure 2). This leads to exon ligation and the release of the intron in the lariat conformation (Moore and Sharp, 1993).

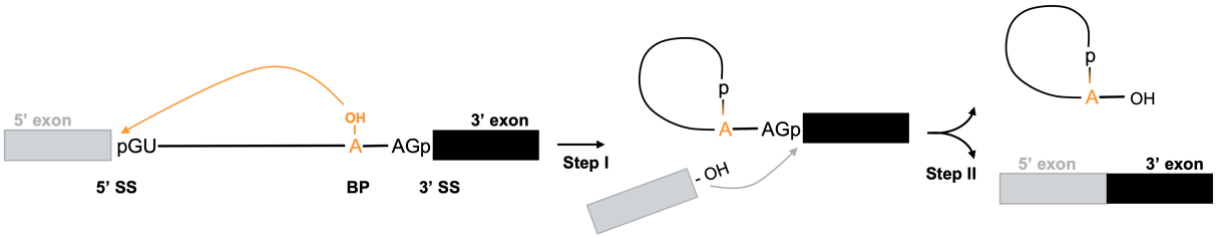

Figure 2. Transesterification reactions of a splicing reaction
The two sequential transesterification reactions are schematically illustrated. In the first reaction the branch-point's 2'OH group on the phosphodiester bond, located at the 5' splice site gets attacked leading to a free 5' exon and intron-3' exon intermediate. In the second reaction, which involves the 3' splice site, the free 3'OH group of the 5'exon targets the phosphodiester bond. The two exons get ligated, and the intron lariat released. The "p" depicts the involved phosphate groups. Adapted from (Will and Luhrmann, 2011).

Self-splicing group II introns and the mechanism of pre-mRNA splicing share important functional features like consensus sequence at the splice sites and branchpoint. Additionally, both use two transesterification reactions to form identical intermediates and end products. Unlike group II introns, pre-mRNA intron removal depends on the splicing machinery. While group II introns can form catalytically active structures and their splicing is therefore ATP-independent, spliceosome-dependent removal of pre-mRNA introns consumes energy during spliceosome assembly (Seetharaman *et al.*, 2006; Lambowitz and Zimmerly, 2011).

1.1.2 The spliceosome

In eukaryotes, this nuclear pre-mRNA splicing process is catalyzed by a mulitmegadalton ribonucleoprotein (RNP) complex, termed spliceosome. The five small nuclear ribonucleoproteins (snRNPs) U1, U2, U5 and U4/U6 and numerous non-snRNP proteins build this dynamic complex, also referred to as the major spliceosome (Will and Luhrmann, 2011) (Figure 3).

The major spliceosome is U2-dependent and coexists with the U12-dependent minor spliceosome which consists of the U11, U12, U4atac, U6atac and U5 snRNPs. While the major spliceosome catalyzes intron splicing with a GT-AG splice site, the minor spliceosome catalyzes AT-AC SS introns with distinct BP and polypyrimidine tract sequences. U12 dependent splicing concerns only less than 1 % of all introns (Turunen *et al.*, 2013).

The binding of the introns 5'SS by the U1 snRNA initiates spliceosome assembly by the U1-specific proteins, leading to the intermediate termed E complex. In addition SF1, U2AF65 and U2AF35 recognize the BPS, PY and 3'SS (Heinrichs *et al.*, 1990; Merendino *et al.*, 1999; Zhang and Rosbash, 1999). At this point already, all relevant splicing elements have been recognized by the distinct splicing factors. The helicases UAP56 and Prp5 are required to allow the E complex and the U2 snRNP to integrate into the A complex. The removal of SF1 from the pre-mRNA and the interaction of the U2 snRNP with the branch-site region are consequences of this ATP-dependent rearrangement. The interaction between U2 SF3a/b proteins with U2AF65 and the branch-site adenosine ensures the precise identification of the splicing motif (Zhang and Green, 2001; Will *et al.*, 2002).

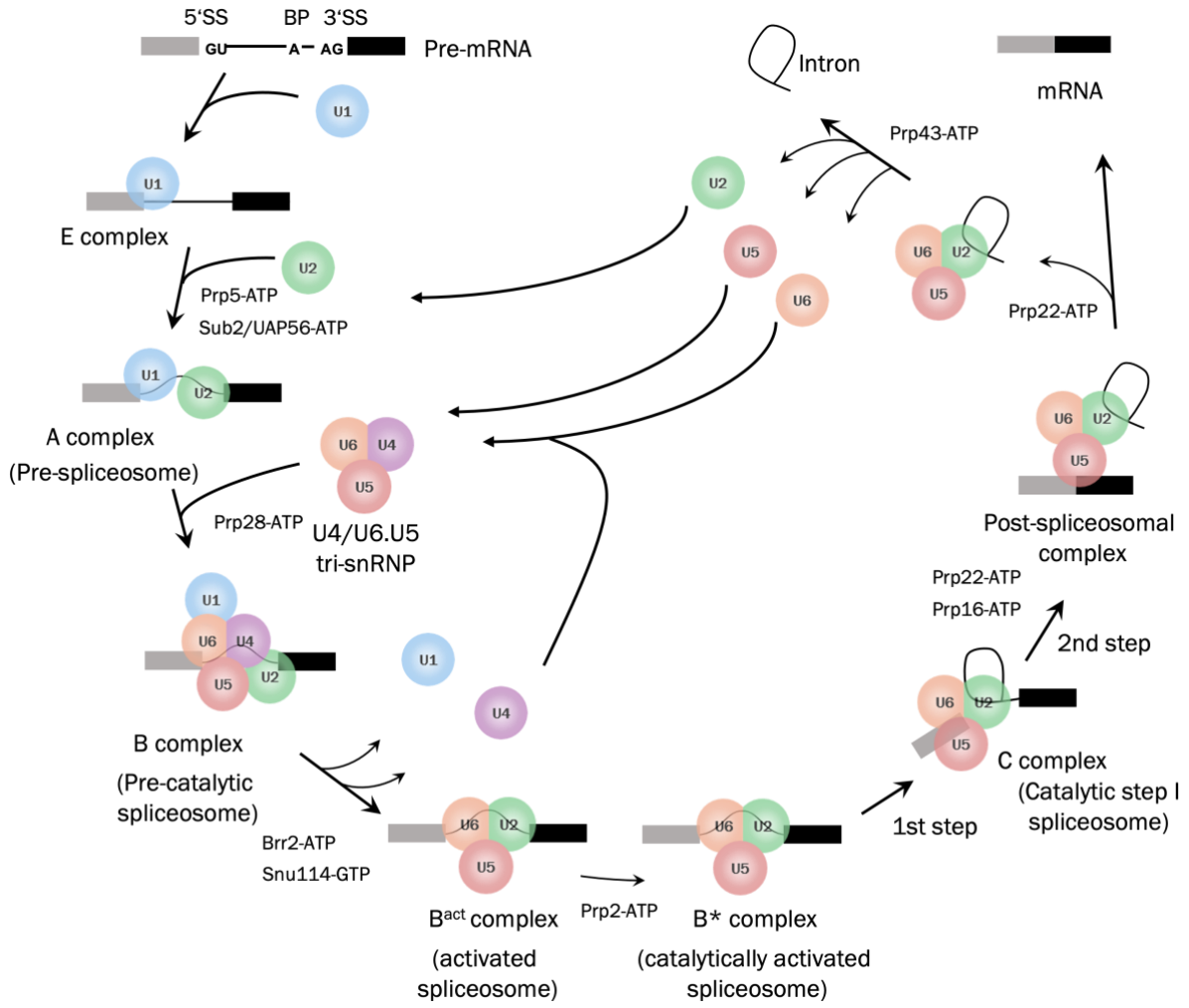

Figure 3. Splicing cycle by the major spliceosome
Simplified schematic model of the sequential spliceosome assembly and disassembly in one splicing cycle. U1 binding to the 5' splice site forming the E complex initiates the assembly. A complex formation occurs due to a stable binding of U2 to the branch point. The pre-B complex is formed after loose association of the tri-snRNP followed by its stable integration and the loss of U1 which leads to the B complex. The B complex gets catalytically activated (B^{act} complex) by the release of U4 caused by other structural rearrangements and the action of Prp2 (B* complex). In the last step, the complex C is formed by the first transesterification reaction and the second reaction leads to the mature mRNA and the intron lariat. For the next round of splicing, the spliceosomal components dissociate and are recycled. Scheme modified from (Will and Luhrmann, 2011).

The final role of U2 binding for the following steps of splicing is to bulge out the branch-site adenosine. The U4/U6 di-snRNP assembles with U5, resulting in a tri-snRNP, which then builds the unstable pre-B complex by associating with the A complex. The tri-snRNP gets tethered by the formation of the U2/U6 helix II. To stabilize the loose binding of the tri-snRNP to the spliceosome, the pre-catalytic B complex is formed by the destabilization of the U1 binding to the 5'SS and its replacement by the ACAGAG box of the U6 snRNA. This destabilization results in the release of the entire U1 snRNP. Multiple rearrangements in conformation and composition lead to the conversion of the B complex to the activated B complex (B^{act} complex) by releasing the U4 snRNP (Staley and Guthrie, 1999). This is regulated by the helicase Brr2, which unwinds the base-pairing of the U4/U6 duplex. U4 snRNA together with a fraction of di-snRNP proteins leaving the U6 snRNA and still required protein factors behind (Laggerbauer, Achsel and Lührmann, 1998). Due to the displacement of U4, the U6 snRNA is able to interact with the U2 snRNA, which brings the 5'SS and the BS in spatial proximity and makes the first splicing reaction possible.

The Prp2 helicase promotes the destabilization of SF3b from the BS to catalytically activate the B^{act} complex resulting in the B* complex (Madhani and Guthrie, 1992). This allows the first transesterification reaction to take place. Thereby, the BP adenosine attacks the 5'SS resulting in 5' exon release and formation of the 3' exon-lariat. Consequently, this leads to the C complex, which is remodeled by the Prp16 helicase, preparing the spliceosome for the second splicing step, including branch-site displacement (Schwer and Guthrie, 1991; Fica *et al.*, 2017). The second transesterification reaction is catalyzed by the resulting C* complex. The 3' hydroxyl group of the upstream exon attacks the 3' SS, ligating the exons and forming the intron lariat. The mature mRNA gets released from the spliceosome by the Prp22 helicase and exported to the cytoplasm. Prp43 disassembles the resulting intron lariat spliceosome (ILS), resulting in the release of the intron lariat. The intron lariat gets debranched and degraded. The spliceosome components get recycled and can then enter another round of splicing (Le Hir *et al.*, 2000).

1.2 Alternative pre-mRNA splicing

A regulatory mechanism prevalent in higher eukaryotes allows multiple unique mRNAs to be generated from a single gene (Baralle and Giudice, 2017). This mechanism is called alternative splicing (AS).

1.2.1 Mechanisms of alternative splicing

While splicing in general is absent in prokaryotes, simple eukaryotes use basic constitutive splicing. Higher eukaryotes on the other hand use alternative splicing to obtain more than one mRNA isoform from a single pre-mRNA transcript. In the human genome AS affects over 90 % of all multiexons (Pan *et al.*, 2008; Wang *et al.*, 2008). The mechanisms of alternative splicing include cassette exon skipping (SE), alternative 5' or 3'SS (A5SS/A3SS) selection, intron retention (IR) and mutually exclusive introns (MXE) (Pan *et al.*, 2008; Wang *et al.*, 2008) (Figure 4).

Flexible splicing of introns and ligation of exons creates a tremendous increase in proteome diversity compared to the relatively small human genome. Alternative splicing is responsible for most of the molecular and cellular complexity especially of elaborate organisms (Blencowe, 2006). For example, the proteome of a brain cell differs significantly of that of a liver cell despite they have an identical genome. In addition to the transcription of organ- or tissue-specific proteins, the generation of characteristic isoforms through alternative splicing plays an important role (Baralle and Giudice, 2017).

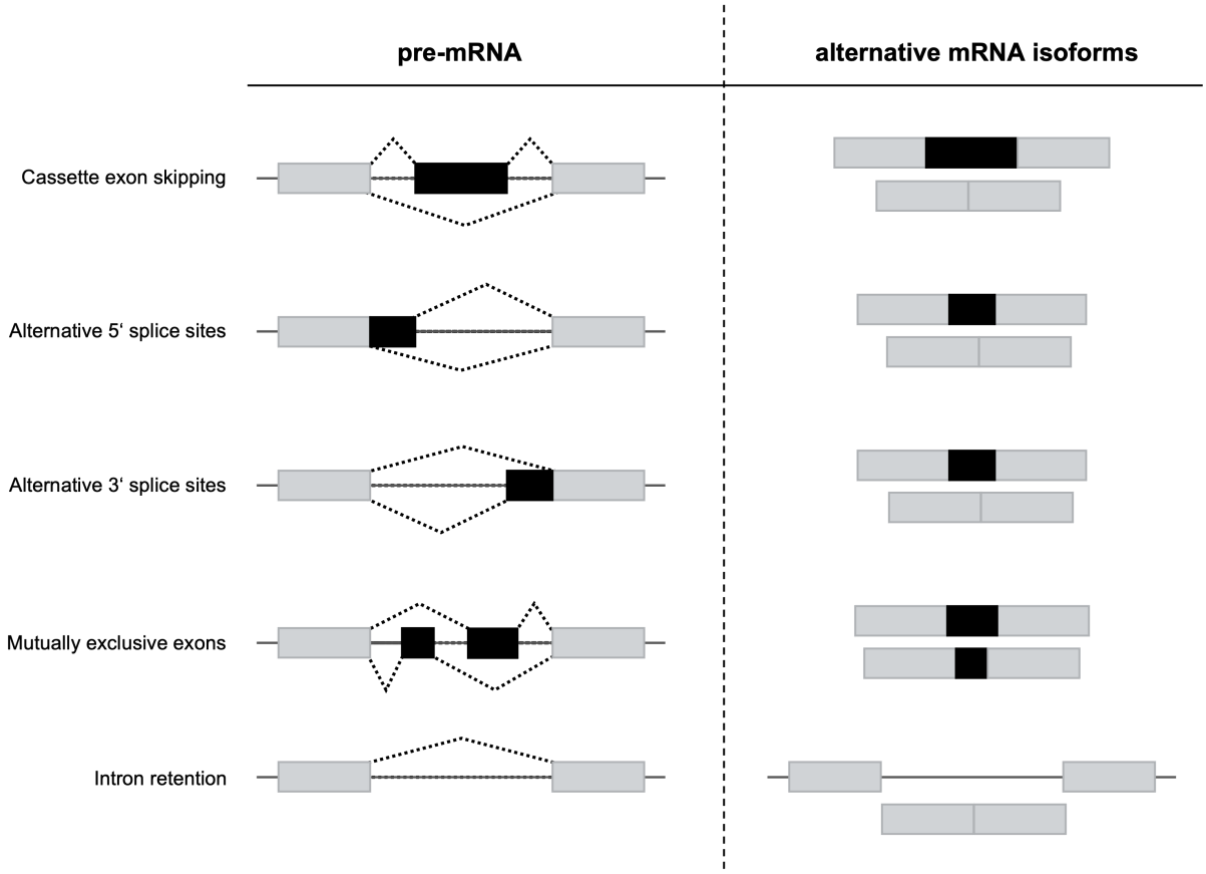

Figure 4. The different pre-mRNA splicing types
Schematic overview of the different pre-mRNA splicing types on the left and the different mRNA isoforms on the right. Exons are depicted by boxes, grey boxes indicate constitutive exons, black boxes indicate the alternative exon. Introns are depicted by continuous lines, while dotted lines mark the different splice options. Top to bottom: skipping or inclusion of alternative cassette exons represent most alternative splicing events. Exclusion or inclusion of partial exon segments into the mature mRNA by selection of an alternative 5’ or 3’ splice site. Only one of two exons gets included into the mRNA, if two exons are mutually exclusive. Inclusion of an entire intron into the spliced product is described by intron retention.

1.2.2 Alternative-splicing regulation

The regulation of the complex alternative splicing mechanism is known to be a complicated matter. Cis-acting elements and trans-acting factors influence the alternative splicing mechanism (Krämer, 1996). Especially the expression levels of trans-acting factors play a significant role in this regulation (Baralle and Giudice, 2017). SR proteins and heterogenous nuclear RNPs (hnRNPs) support or inhibit the binding of U1 and U2 to the mRNA.

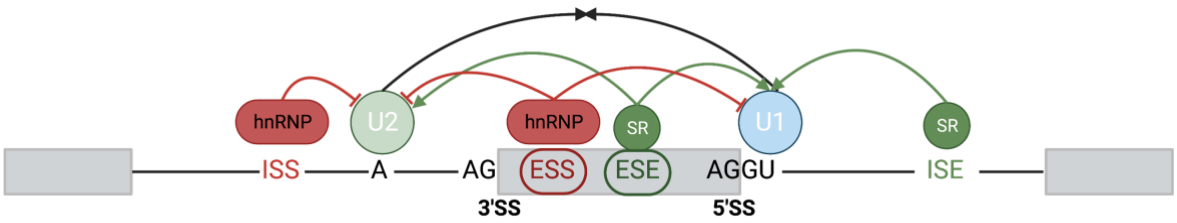

Figure 5. SR proteins and hnRNPs regulate alternative splicing
SR proteins and hnRNPs bind cis-regulatory elements to promote or inhibit splicing. Intronic splicing silencers (ISS) and exonic splicing silencers (ESS) inhibit splicing and are depicted by red lines, while intronic splicing enhancers (ISE) and exonic splicing enhancers (ESE) promote splicing and are depicted in green lines. Exons are marked by grey boxes and introns by black lines.

The repeated dipeptides of serine (S) and arginine (R), the RS domain, following one or two RNP binding domains, is a common characteristic of the family of SR proteins. With the RNP binding domain, they bind to pre-mRNAs (Black 2003). While most members of the SR protein family are generally

interchangeable, hnRNPs associate more specifically with RNA polymerase II primary transcripts, due to their higher structural diversity (Geuens, Bouhy and Timmerman, 2016).

Splicing factors like SR proteins and hnRNPs interact with cis-regulatory elements. These elements are located in the exon or intron of a pre-mRNA and are separated into different categories based on their regulation type and position. While SR proteins prefer the interaction with exonic splicing enhancers (ESE) or intronic splicing enhancers (ISE), which both promote SS usage, hnRNPS prefer exonic splicing silencers (ESS) and intronic splicing silencers (ISS), which repress the usage of a SS (Black, 2003) (Figure 5).

Several SR proteins and hnRNPs bind to a single pre-mRNA molecule and the ratio and interplay of these regulatory factors influences splice site selection determining the composition of the final transcript (Fu and Ares, 2014).

1.2.3 Temperature-dependent alternative splicing

As regulatory proteins can alter the open reading frame (ORF) of an mRNA, they play a crucial role in shaping the proteome. This flexibility in ORF definition is an important mechanism to allows cells to respond and adapt to changes in environmental condition, by alternative splicing (Heyd and Lynch, 2011). Changes in temperature are an environmental factor that affects all life activities at various levels in plants and animals, including alternative splicing. In comparison to mammals who are homeothermic animals, the cellular temperature in plants is directly coupled to the environmental temperature and therefore wider variations in their body temperature are considered (Shiina and Shimizu, 2020). Plants and animals follow a natural circadian 24-h rhythm which is stimulated by oscillating changes in light-dark and temperature conditions (Preußner and Heyd, 2016; Shiina and Shimizu, 2020). For homeothermic organisms, in particular humans, the core body temperature (CBT) is around 37 °C with oscillating changes between 36.5 °C and 37.5 °C during day and night rhythm (Refinetti, 2010). The influence of these rather subtle changes in body temperature on AS generate alternative splicing patterns in an oscillating manner and thereby allow the adjustment to the circadian rhythm (Preußner *et al.*, 2017). Additionally, two groups of protein families have been discovered that respond directly to larger temperature changes. These are transient receptor potential (TRP) channels and CDC-like kinases (CLKs), which also act as thermo-sensors within the cell (Wetsel, 2011; Haltenhof *et al.*, 2020). Maintaining the core body temperature is crucial for ongoing biochemical processes within the cells, to prevent the organism from tissue damage, morbidity, and mortality. An organism senses environmental changes via TRP channels in the skin and sensory nerves, leading to changes in local tissue function (Wetsel, 2011).

But not only environmental conditions influence changes in body temperature. In over 600 million years of evolution, vertebrates regardless of their thermoregulation, use the increase of 1 to 4 °C in CBT, termed fever, as a response to infection to improve the survival of the organism. It should be mentioned that fever is only beneficial in a certain temperature range, as uncontrolled fever in response to sepsis for example results in severe cellular damage or mortality (Evans, Repasky and Fisher, 2015). Changes in the physiological temperature range of an organism leads to structural rearrangements of the kinase activation segment in CLKs and thereby controls SR protein phosphorylation. This regulates AS and GE, as including premature termination codons (PTCs) into the mRNA transcript induces nonsense-mediated mRNA decay (NMD) (Haltenhof *et al.*, 2020; Neumann *et al.*, 2020).

Two examples of strongly temperature-regulated gene expression events are heat shock factors (HSFs) and cold-induced RNA-binding proteins (RBPs) (Liu *et al.*, 2022). The correlation between AS and GE in an extremely temperature-sensitive manner was observed for the RNA-binding motif protein 3 (RBM3) (Los *et al.*, 2022). For more than 30 years now, RBM3 and the cold-induced RNA-binding protein (CIRBP), which are both glycine-rich RNA binding proteins, have been identified as cold-induced genes (Danno *et al.*, 1997; Nishiyama *et al.*, 1997). For CIRBP, the alternative splicing event is coupled to NMD by the inclusion of a poison exon and thus regulating gene expression in response to temperature changes (Neumann *et al.*, 2020; Preußner *et al.*, 2023).

1.2.4 Alternative splicing affects the cellular proteome

Alternative splicing has the potential to modulate the proteome. In case where exons encode for a distinct protein domain, the in- and exclusion of exons modulates the protein structure (Jewer, Findlay and Postovit, 2012). At the beginning of research on mRNAs and their effects on the proteome, it was assumed that the correlation between mRNA and protein abundances was poor (Maier, Güell and Serrano, 2009). In contrast, recent studies show that mRNA levels explain approximately 40 % of the variability in protein levels (Schwanhäusser *et al.*, 2011). About 64 % of all frame-preserving splicing events are translated and present at the protein level (Sinitcyn *et al.*, 2023). In low abundance transcripts, the ribosome frequency is lower compared to high abundance transcripts. More often, low abundance transcripts are subject to intron retention (IR) events and thereby more likely reduce the ribosome engagement (Weatheritt, Sterne-Weiler and Blencowe, 2016). Additionally, transcripts including an IR events are more often retained in the nucleus, which suggests another explanation for its lower translation probability (Liu *et al.*, 2017).

1.3 Pathways of mRNA degradation

The changes in the ORF sequence caused by alternative splicing can alter mRNA stability, translational activity as well as the subcellular localization of the mRNA (Mockenhaupt and Makeyev, 2015). To ensure that no defective RNA molecules are translated into dysfunctional proteins, they get degraded by the surveillance machinery. Defects in processing, folding or protein assembly are precisely monitored and immediately degraded by the mRNA degradation machinery. mRNA processing and turnover are two mechanisms that control gene expression in mRNA metabolism (Houseley and Tollervey, 2009).

1.3.1 Co-translational mRNA surveillance

To protect cells from translating defective or potentially harmful transcripts, RNAs with errors in their sequence or structure get eliminated. This process is highly regulated, and the cell needs a mechanism to first asses and further ensure the quality of all classes of eukaryotic mRNA transcripts. Degradation of defective RNAs or more precisely RNPs, can occur via one of the three surveillance pathways (Houseley and Tollervey, 2009). The No-Go decay (NGD), Non-Stop decay (NSD) and nonsense-mediated mRNA decay (NMD) build the group of evolutionarily conserved mRNA degradation pathways (Figure 6). These pathways monitor the translation activity to detect unnormal progression of elongation (NGD/NSD) or early translation termination (NMD). NGD and NSD both follow the same mRNA decay trigger by scrutinizing the ribosome during elongation. Stalling of the ribosome during this step can occur due to a missing stop codon, resulting in the poly (A) read-through, which is a target of the NSD pathway. Here, the interaction of the nascent poly(Lysine) chain with the ribosomal exit tunnel slows down the translation and thereby induces NSD. Another triggers are large mRNA secondary structures or an unusable ribosomal A-site, which inhibit binding of the ribosome and thereby lead to NGD (Powers, Szeto and Schaffitzel, 2020). In contrast, NMD is triggered by PTCs within the mRNA in the presence of downstream exon junction complexes (EJCs) (Fatscher, Boehm and Gehring, 2015). Around 20 % of all genetic diseases are caused by mRNAs containing PTCs, as their encoded protein variants can be either unfunctional or harmful to the cell and are therefore eliminated (Holbrook *et al.*, 2004).

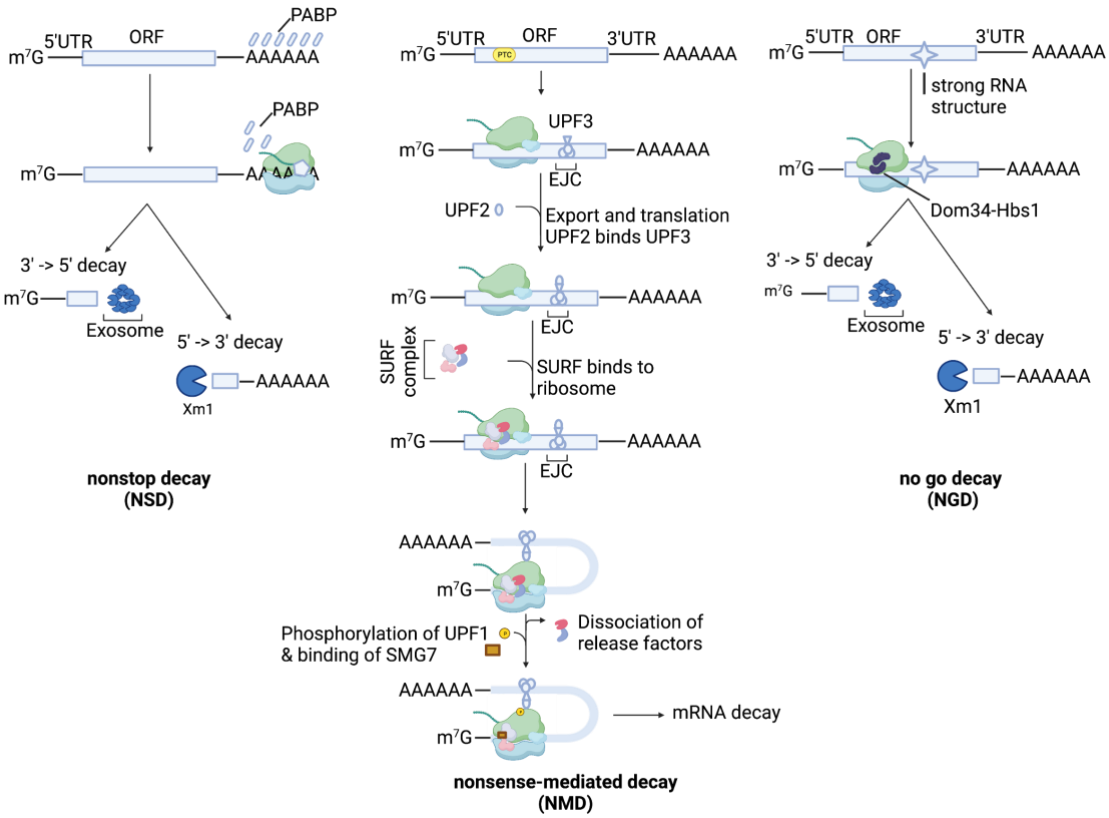

Figure 6. The mRNA surveillance pathways
Non-Stop decay (NSD) | Lacking a stop codon results in ribosomes traversing the poly(A)tail and stalling at the 3' end of the mRNA, which leads to the degradation of the mRNA by the exosome. Nonsense-mediated decay (NMD) | Ribosomes are stalled at the mRNA due to a PTC. The mRNA gets degraded by the NMD machinery. No-Go decay (NGD) | Strong secondary structures stall the ribosome within the ORF so that an endonucleolytic cleavage event is initiated near the stalling site, which releases the ribosome and two mRNA fragments which get targeted and degraded by the exosome. Modified from (Garneau, Wilusz and Wilusz, 2007)

1.3.2 The mRNA degradation machinery

After the surveillance machinery identified the defective RNA and triggered its degradation, an exonuclease accomplishes the actual degradation process. The exonuclease shortens the poly(A) tail, and the mRNA gets digested by the exosome either in 5' to 3' or in 3' to 5' orientation. This results in the suppression of gene expression. In eukaryotes, the carbon catabolite repression 4 (CCR4) – negative on TATA-less (NOT) complex, with its 3' to 5' exonuclease activity regulates the poly(A) tail degradation (Shirai *et al.*, 2014).

1.4 The RNA-binding motif protein 3

Falling temperatures are a real threat to endothermic species, as cell growth is paused by direct expression inhibition of certain genes and proteins. At the same time, other proteins, especially DNA/RNA-binding proteins, are upregulated to protect the cell from a cold shock or cell death (Ji *et al.*, 2020). The RNA-binding motif protein 3 (RBM3) is one of the most investigated cold shock proteins in human cells. Even a reduction of one degree in temperature leads to a significantly higher RBM3 expression (Los *et al.*, 2022). RBM3 shows a widespread involvement in various cellular processes such as cell stress, neuroprotection, metabolism, apoptosis, circadian rhythm (Peretti *et al.*, 2015; Preußner *et al.*, 2017; Yang *et al.*, 2018; Shi *et al.*, 2019). Thereby, RBM3 promotes transcription and translation to allow a fast adaptation to changes in cellular requirement (Dresios *et al.*, 2005). Especially the neuroprotective function of RBM3 in response to cold shock makes this gene a perfect target for clinical therapeutics to protect against neurodegeneration (Peretti *et al.*, 2015; Preußner *et al.*, 2023). The RBM3 gene contains 6 introns and 7 exons, additionally a poison exon (E3a) in intron 3 was recently identified (Figure 7). This exon is highly temperature responsive and controls RBM3 gene expression in

a temperature-dependent manner (Preußner *et al.*, 2023). This study recently showed the impact of temperature-dependent alternative splicing on RBM3 gene expression, which will be discussed in the following paragraph.

Figure 7. Schematic pre-mRNA structure of RBM3
The temperature-dependent splicing pattern of the RBM3 pre-mRNA is illustrated. The exons are depicted by grey and black boxes and the introns by lines. The numbers indicate the exons, and the black boxes mark the alternative splicing cassette. Red lines show the heat induced alternative splicing pattern, while the blue dotted line shows the cold induced alternative splicing pattern.

Preußner *et al.* performed an RNA sequencing analysis of mouse primary hepatocytes and identified the alternative exon E3a in the RBM3 transcript. They found that the evolutionarily conserved E3a contains seven PTCs, resulting in a poison exon inducing NMD. Thus, linking RBM3 expression to temperature-dependent AS-NMD. They furthermore showed that alternative splicing is regulated by surrounding cis-regulatory elements using a minigene containing exon 3a. Finally, the authors presented the use of antisense oligonucleotides (ASO) to clinically exploit neuroprotective effects via splicing modulators.

1.5 The eukaryotic translation initiation factor 4A2

DNA and RNA metabolism are processes within the cell that are heavily dependent on the correct function of helicases. For the different metabolic processes, helicases bind and precisely unwind DNA or RNA. A total of 6 helicase superfamilies (SFs) exists, which are distinguished based on their characteristic structures. Helicases that form a toroidal, predominantly hexameric structure are classified into SF3-6, whereas all helicases that do not form this structure are classified into SF1 and SF2 (Fairman-Williams, Guenther and Jankowsky, 2010).

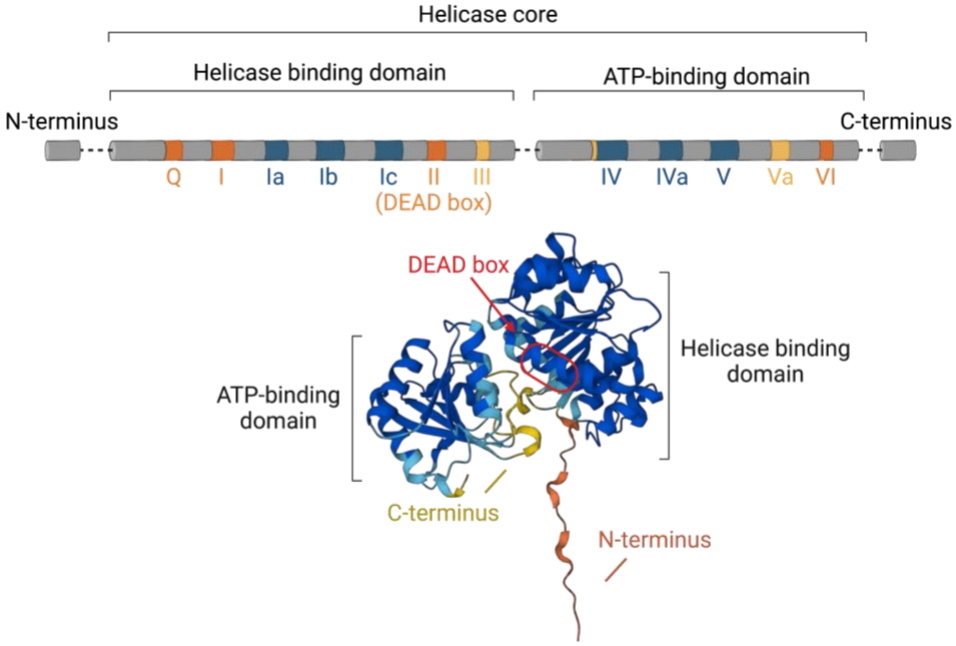

Figure 8. Architecture of DEAD-box RNA helicase eIF4A2
A Schematic illustration of the typical domain structure of DEAD-box RNA helicases on the example of eIF4A2. **B** Alphafold prediction of eIF4A2. Model confidence (0-100) is depicted in different colors (dark blue = very high > 90; light blue = confident > 70; yellow = low > 50; orange = very low < 50). Protein identifier: AF-Q14240-F1.

Introduction

The eukaryotic initiation factor 4A (eIF4A) is an ATP-dependent RNA helicase that can bind to mRNA and dissolve secondary structures via its helicase activity. It was among the first DEAD-box proteins, for which these functions were demonstrated (Ray *et al.*, 1985). eIF4A, with its two isoforms eIF4A1 and eIF4A2, is a typical DEAD-box RNA helicase, belonging to the helicase superfamily 2 (SF2). Typical for these helicases is the so-called DEAD-box, which features the eponymous amino acid sequence Asp-Glu-Ala-Asp, localized in motif II (Figure 8). In general, DEAD-box proteins contain two nearly identical recombinase A (RecA)-like helicase domains (helicase binding domain and ATP-binding domain) which build their conserved helicase core and N-terminal and C-terminal extensions, which are shorter in eIF4A compared to other DEAD-box proteins. As typical for ATP-dependent helicases, the ATP-binding site of eIF4A is located between the two (RecA)-like domains, allowing the helicase to undergo conformational changes to provide a cleft for the binding of RNA (Linder and Jankowsky, 2011).

1.5.1 The role of eIF4A in the cell

eIF4A functions with eIF4E and eIF4G in the eIF4F complex. eIF4A takes part in the initiation of translation by recognizing the 5' proximal secondary structure of mRNAs and supports binding of the ribosomal 40S subunit. The eIF4A family contains three members, termed eIF4A1, eIF4A2 eIF4A3 (Li *et al.*, 1999). eIF4A2 was identified in 1995 by the isolation of human cDNA and its localization in the human genome was identified (Sudo K., Yakahashi E., 1995). Its sequence is highly conserved over many species, from yeast (TIF1 and TIF2) to human (Linder and Slonimski, 1988). The amino acid sequences between the isoforms eIF4A1 and eIF4A2 show a similarity of 91% and are generally highly conserved (Nielsen and Trachsel, 1988). However, their N-terminal regions are not as highly conserved as the remaining part (Wilczynska *et al.*, 2019). A comparison of the amino acid sequences of the human eIF4A1, eIF4A2, and seIF4A3, generated by the PRALINE open-source alignment program, is shown below (Figure 9).

Due to the high sequence homology between eIF4A1 and eIF4A2, it has long been assumed that the two isoforms can functionally replace each other or are functionally indistinguishable (Li *et al.*, 1999). Both proteins are involved in translation initiation by providing the helicase activity of the eIF4F complex (Rogers, Komar and Merrick, 2002). Their expression is cell type-specific, as is the quantitative ratio between the two isoforms. While eIF4A1 is upregulated in dividing cells, especially malignant cells, eIF4A2 is highly expressed in low proliferating cells. An increased abundance of eIF4A2 in malignant cells was shown to lead to higher survival rates for the organism (Ji *et al.*, 2003; Shaoyan *et al.*, 2013). The ratio between expression levels of these isoforms is also evident in mouse tissues. While in most tissues eIF4A1 is significantly more expressed, in the brain, and kidney a fourfold higher eIF4A2 expression is shown compared to eIF4A1 (Nielsen and Trachsel, 1988). These results are consistent with recent findings that eIF4A2 transcript levels increase upon eIF4A1 suppression. However, it should be mentioned that in this case, eIF4A2 is unable to compensate for the translational inhibition caused by eIF4A1 loss (Galicia-Vázquez *et al.*, 2012). The role of the different eIF4A isoforms in the mRNA lifecycle is determined by their distinct protein interactions. The oncogenic protein MYC for example exclusively upregulates the transcription of eIF4A1 but not eIF4A2 (Lin *et al.*, 2008). The eIF4A1 protein level is regulated by programmed cell death 4 (PDCD4), which is directly regulated by mechanistic target of rapamycin (mTOR) (Asangani *et al.*, 2008). While the role of eIF4A1 in translation initiation has been extensively studied, the function of eIF4A2 remains unclear. However, it is evident, that eIF4A2 cannot functionally replace eIF4A1 and performs an opposite function in cancer cells.

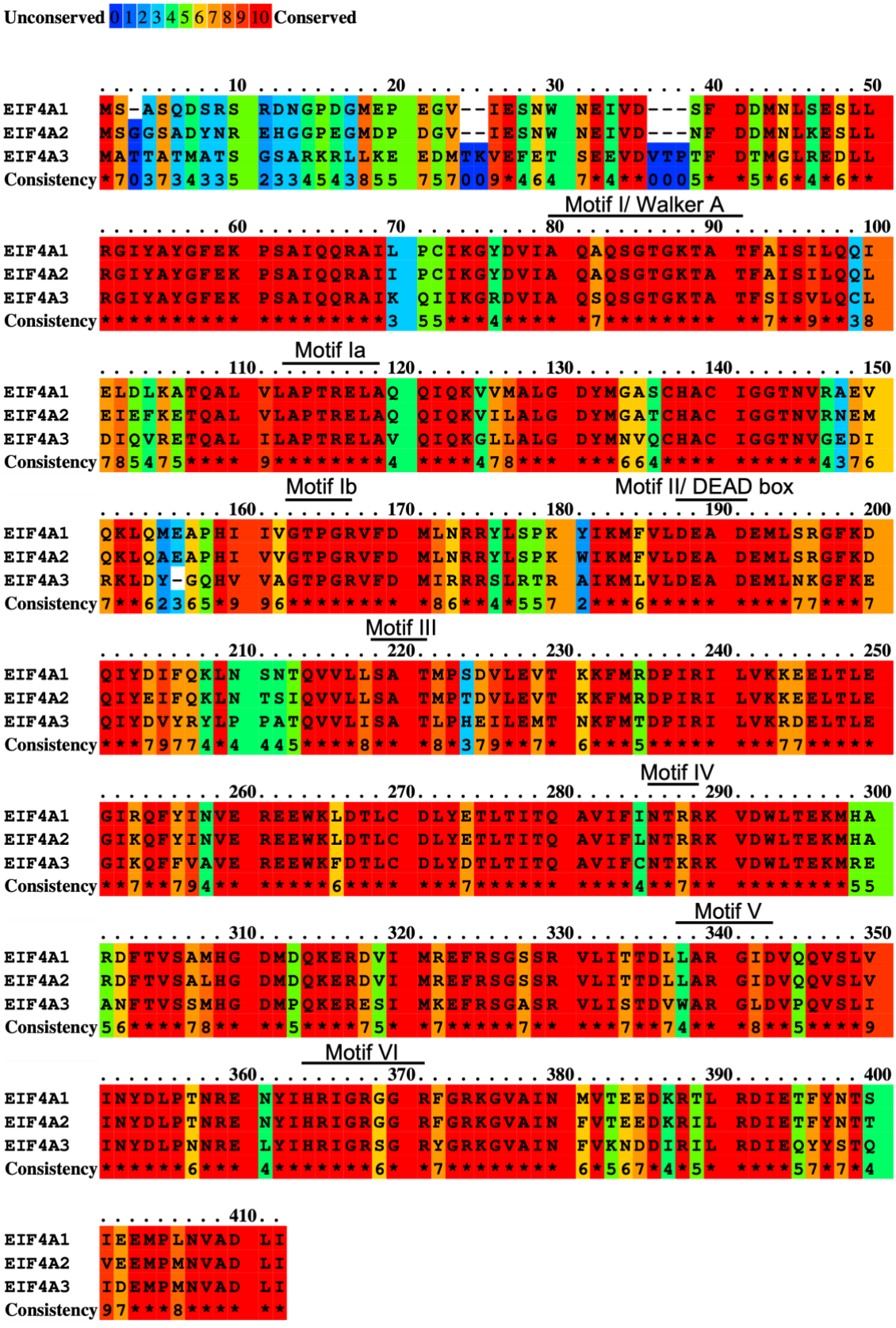

Figure 9. Amino acid sequence alignment of human eIF4A1, eIF4A2 and eIF4A3
A PSI-BLAST-based sequence alignment of eIF4A1 (NP_001407.1), eIF4A2 (NP_001958.2) and eIF4A3 (NP_055555.1) was generated by the open-source PRALINE multiple sequence alignment program. The residues are highlighted in different colors marking their conservation (blue = unconserved, red = conserved). eIF4A1 and eIF4A2 share over 90% identity. The sequence of eIF4A3 is 65% identical to those of eIF4A1 and eIF4A2. The motifs of eIF4A2 are depicted in black. Modified from (Lu *et al.*, 2014).

In comparison to eIF4A1 and eIF4A2, eIF4A3 shows only a sequence identity of 65 % on the amino acid level. Its RNA-dependent ATPase and ATP-dependent RNA helicase activity is comparable to eIF4A1 but is incapable of binding the 40S ribosome subunit and therefore is not capable of replacing eIF4A1 functionally (Li *et al.*, 1999).

While eIF4A1 and eIF4A2 are highly abundant and localized in the cytoplasm, their paralogue eIF4A3 located in the nucleus, where it participates in the exon junction complex (EJC) and RNA metabolism. eIF4A3 binds to the MAGOH-Y14 dimer in the nucleus (Lu *et al.*, 2014) and association of MLN51 then completes the key components of the EJC. The function of EJCs in NMD is to mark the exon junctions and trigger mRNA decay when the ribosome reaches a termination codon that is located prior to the EJC site (Palacios *et al.*, 2004). eIF4A3 uses ATP-dependent conformational changes to strongly bind ssRNA (Ballut *et al.*, 2005; Andersen *et al.*, 2006), which tethers the EJC to the mRNA, where it can now serve its function as a binding partner for NMD downstream effectors or prepare the spliced mRNA for nuclear export. Due to its lack of ATPase and helicase activity, eIF4A3 acts as an RNA clamp, which changes from its closed to open conformation as soon as binding to MAGOH-Y14 is released upon ATP hydrolysis (Lu *et al.*, 2014).

1.5.2 Eukaryotic protein synthesis

Protein biosynthesis is a biochemical process that occurs in prokaryotes and eukaryotes. In both domains, protein biosynthesis composes three major steps: initiation, elongation, and termination. While the synthesis of proteins in prokaryotes and eukaryotes has similarities, there are clear differences, especially in translation initiation. This starts with the number of initiation factors required. While bacterial translation initiation requires three factors (IF-1, IF-2, IF-3), eukaryotic initiation demands at least ten (Moldave, 1985).

Especially the initiation of the protein synthesis is crucial for the correct translation of mRNA into polypeptide chains and is therefore higher regulated than the following stages (Figure 10). The eukaryotic translation initiation begins with the formation of the 48S initiation complex, which subsequently binds to the mRNA together with the ribosomal 60S subunit after scanning, resulting in the mRNA bound 80S ribosome only once the AUG is bound (Jackson, Hellen and Pestova, 2010). The unification of the start codon (AUG) with an initiator methionyl-transfer RNA (Met-tRNA$_i$) results in the codon-anticodon interaction within the P site of the 80S ribosome and marks the beginning of the ORF. The binding of an aminoacyl-tRNA to the A site of the ribosome initiates the start of the translation elongation.

The eukaryotic initiation factors guide the ribosomal subunit and the Met-tRNA$_i$ to the respective start codon. An eIF2-GTP duplex binds the Met-tRNA$_i$, containing the anticodon complementary to the AUG initiation codon, thus resulting in the ternary complex (TC). The Met-tRNA$_i$ precisely binds to the ribosomal P site of the 40S ribosomal subunit and the preinitiation complex (PIC) is assembled (Jackson, Hellen and Pestova, 2010), which includes eIF1, eIF1A, eIF3 and eIF5. The pre-assembled eIF4F complex comprising eIF4A, eIF4E and eIF4G, and the poly(A) binding protein (PABP) bind the 5’ 7-methylguanosine cap (m7G cap) and the poly(A) tail respectively. These interactions activate the mRNA by inducing the alleged close loop conformation. eIF4A plays an important role in binding to the mRNA due to its helicase activity which is enhanced by eIF4B. Without the helicase activity of eIF4A1, the eIF4F complex is functionally inactive (Wilczynska *et al.*, 2019).

eIF4A1 binding to the MIF4G domain of eIF4G is crucial for the eIF4A unwinding activity (Virgili *et al.*, 2013). According to its helicase activity, eIF4A binds and unwinds the secondary structures of mRNAs to enable recruitment of the PIC complex in proximity to the 5' Cap, thus resulting in the mRNA-43S complex. In the next step, eIF1 and eIF1A facilitate the mRNA binding and scanning by binding the 40S subunit’s A and P sites, leading to a dynamic cleft formation. This complex is then stabilized by eIF3 and eIF4G. As eIF2 is only active in a complex with GFP, the AUG binding and thus eIF1 relocation induces changes in the eIF2 conformation resulting in the release of Pi, which immediately lowers eIF2’s affinity for Met-tRNA$_i$. The release of eIF2 and eIF5 are the results of these changes. In the last step of translation initiation, the 60S subunit binds the mRNA and re-arranges the Met-tRNA$_i$, via the recruitment

of eIF5B-GTP (Yamamoto *et al.*, 2014). Finally, the 80S ribosome binds to the mRNA, mediated by the release of eIF1A and eIF5B-GDP and the translation elongation is about to begin (Merrick and Pavitt, 2018).

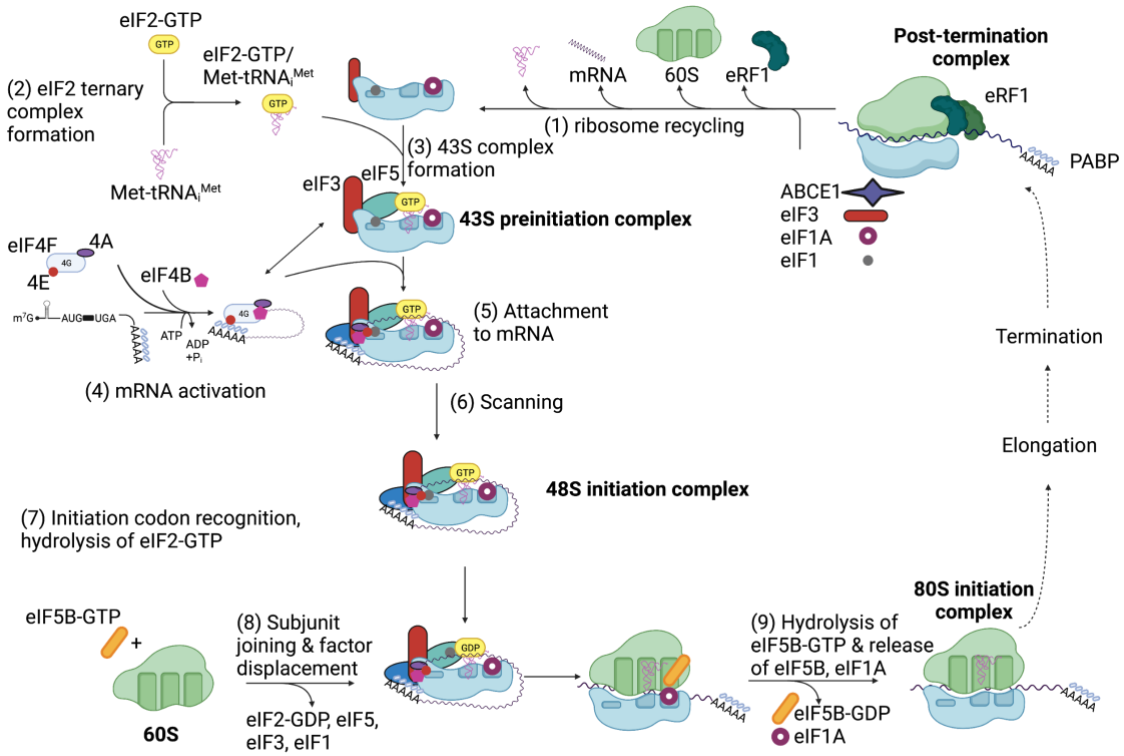

Figure 10. Model of eukaryotic translation initiation in a stepwise manner
Schematic illustration of the eukaryotic initiation pathway starting with the recycling of the post-termination complex followed by eight stages of translation initiation (1). Formation of the eIF2 ternary complex (2) is followed by the formation of the 43S preinitiation complex (3). The mRNA is activated by many eukaryotic initiation factors (4) and attached to the 43S preinitiation complex (5). This complex scans the mRNA for the start codon (6), whose recognition leads to the hydrolysis of eIF2-GTP (7). The 60S ribosome subunit joins the complex by the release of eIF2-GDP, eIF5, eIF3 and eIF1. The hydrolysis of eIF5B-GTP and the release of eIF5B-GDP and eIF1A lead to the formation of the 80S complex (9) as the final step of translation initiation. Modified from (Jackson, Hellen and Pestova, 2010).

1.5.3 The role of eIF4A2 in translation

While the role of eIF4A1 in the eukaryotic protein biosynthesis has been investigated and its importance in eIF4F activation proven, this is not the case for eIF4A2. At the outset of research on eIF4A1 and eIF4A2, it was assumed that the two paralogues can functionally substitute each other. eIF4A2 can interact with eIF4A1 binding partners at unphysiological levels (Wilczynska *et al.*, 2019). This complicates an accurate functional study of eIF4A2. However, a role in the regulation of translation inhibition by micro RNAs could be demonstrated (Meijer *et al.*, 2013).

Micro RNAs are non-coding RNAs with an average length of 22 nucleotides. The main site of action of miRNAs is the 3' UTR of mRNAs, the binding of which suppresses the translation of the target mRNA. In addition, miRNAs can also interact with the 5'UTR or gene promoters, suggesting that miRNAs can control translation rate at the translation initiation phase (Meijer *et al.*, 2013; Wilczynska and Bushell, 2015). Furthermore, eIF4A2 which binds only weakly to eIF4G was identified as the main factor for miRNA-mediated suppression of gene expression independently of its homologue eIF4A1 (Meijer *et al.*, 2013). As an assembly of many proteins, the CCR4-NOT complex regulates gene expression in the cell at different levels, which is why it is localized both in the nucleus and in the cytoplasm (Figure 11). The complex manages among other things the regulation of transcription initiation and the control of

transcription elongation, RNA export from the nucleus and nuclear RNA surveillance, as well as mRNA decay in the cytoplasm (Chalabi Hagkarim and Grand, 2020).

The scaffold protein CNOT1, the core component of the CCR4-NOT complex contains a MIF4G domain which is preferably bound by eIF4A2 and shows structural similarities to the PTRELA amino acid sequence of the binding domain of eIF4G.

Wilczynska and Bushell suggested a conformational change of eIF4A2 comparable with the one of eIF4A3 in the EJC. This prevents the scanning of the mRNA target's 5'UTRs by the 43S ribosome and consequently inhibits the translation initiation by the microRNA-induced RNA silencing complex (miRISC). Additionally, eIF4A2 preferentially binds to mRNAs with a high purine content in upstream proximity to the start codon (Wilczynska and Bushell, 2015).

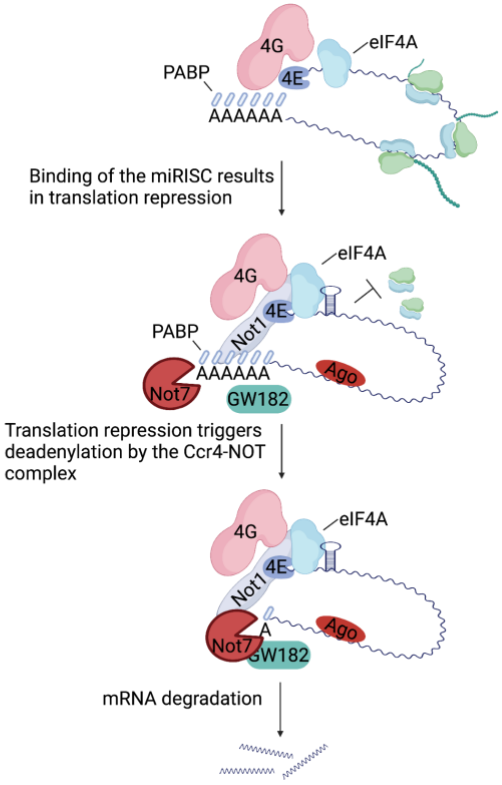

Figure 11. miRNA-mediated translation repression by the CCR4-NOT complex
Gene expression is controlled by miRNAs. Translational repression is initiated by the recruitment of RISC-bound miRNA to an mRNA. This is facilitated by eIF4A2 clamping to the 5'UTR thereby inhibiting the 40S scanning. Argonaute proteins (in humans Ago 1-4) directly bind the miRNA and interact with GW182, which binds to the poly(A) binding protein (PABP). The CCR4-NOT complex, comprising, eIF4G, eIF4E, eIF4A and Not1 deadenylates and immediately decaps the mRNA, causing its degradation by Not7. Modified from (Wilczynska and Bushell, 2015).

1.5.4 Impact of oxidative stress on eIF4A2

Phase separation gives the cell the ability to respond rapidly to changes in the environment. These changes arise, for example, from varying temperatures, oxidative stress, or in response to viruses and toxins. One example for the induction of oxidative stress is arsenite, which limits the translation rate by inhibition of the cap binding factor eIF4E in response to physiological stress (Othumpangat, Kashon and Joseph, 2005). During cellular stress, untranslated mRNAs are recruited to stress granules (SGs) and allow rapid resumption of translation when cellular conditions improve again (Mateju *et al.*, 2020). For this purpose, untranslated mRNAs are accumulated either in mRNP granules (P-bodies) or in SGs. These dynamic structures are localized in the cytosol of mammals (Kedersha *et al.*, 2005).

As a result of translation initiation inhibition, the ribosome stalls on the mRNA and needs to be further regulated. Together with RNA binding proteins and many translation initiation factors, these problematic mRNAs assemble into a granular structure, in which the different stress conditions determine the subset of assembled mRNAs and proteins. Structurally, SGs are separated into an outer layer and a core structure which has a higher density than the outer layer (Protter and Parker, 2016).

While mRNAs in P-bodies comprise the mRNA decay machinery, mRNAs in SGs are retained along with many translation initiation components. The oxidative stress response pathway inhibits the translation of most mRNAs by the phosphorylation of eIF2a, thus resulting in SG formation in the cytoplasm (Mateju *et al.*, 2020). Many translation initiation factors, especially those involved in early translation initiation, are localized in stress granules (Buchan and Parker, 2009). DEAD-box RNA-helicases such as eIF4A can unwind RNA-RNA interactions which seem to be involved in SG formation and thereby modulating the assembling of RNA in SGs (Tauber *et al.*, 2020). Although eIF4A1 is localized in SGs and DEAD-box proteins show a significant impact on the formation of SG, it remains unknown if eIF4A2 is also recruited into stress granules.

1.5.5 Regulation of eIF4A2 expression by alternative splicing

For the eIF4A2 gene, 10 introns and 12 exons haven been identified. One cassette exon, which is in intron 10 contains a PTC, located after the second base triplet in this exon (Figure 12). The PTC in this not yet annotated exon 10A is an NMD target. Additionally, the eIF4A2 gene expression is linked to this NMD target which seems to be evolutionarily conserved (Huth *et al.*, 2022). Accordingly, this exon is likely modulated by alternative splicing. Premature stop codons that are introduced into the mRNA by exon inclusion are part of a process named alternative splicing coupled to NMD (AS-NMD). This process allows precise regulation of gene expression, and approximately 30% of all alternatively spliced mRNAs in humans are targets of AS-NMD by introducing one or multiple PTCs (Lewis, Green and Brenner, 2003).

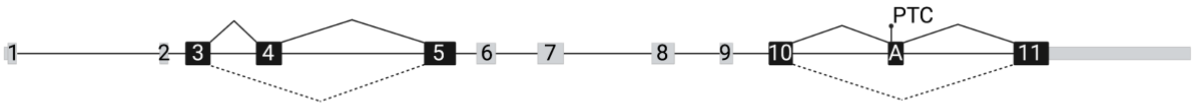

Figure 12. Schematic pre-mRNA structure of human eIF4A2
The alternative splicing pattern of the human eIF4A2 pre-mRNA is illustrated. The exons are depicted by grey and black boxes and the introns by lines. The numbers indicate the exons, and the black boxes mark the alternative splicing cassette. Solid and dotted lines mark the optional alternative splicing pattern.

eIF4A2 gene expression is highly tissue-specific in mice and impacts the ratio of eIF4A1 to eIF4A2, with eIF4A1 being more abundant than eIF4A2 in almost all tissues except for the brain and kidney (Nielsen and Trachsel, 1988). Since different organs in an organism have tissue-specific requirements for translation initiation and the ratio between eIF4A1 and eIF4A2 expression varies widely, there probably is a regulatory mechanism that is most likely alternative splicing (Nielsen and Trachsel, 1988).

While the mRNA sequences of eIF4A1 and eIF4A2 show strong similarities from the putative start codon (AUG) on, the short 5'UTR sequences of both genes are considered equal. Additionally, the 3'UTR shows no greater similarity, with a 310 nt long polyadenylation tail for eIF4A1 and a shorter 130 nt long polyadenylation tail for eIF4A2 (Nielsen and Trachsel, 1988).

1.5.6 The impact of eIF4A2 on the respiratory chain

The eIF4A2 helicase binds and unwinds various types of RNAs, among others also non-coding transcripts such as small non-coding RNAs (for example miRNAs) and long non-coding RNAs (lncRNAs). By triggering the RNA surveillance machinery, lncRNAs take part in the monitoring and direction of many functions within a cell (Nair, Chung and Basu, 2020). One of the lncRNAs bound by eIF4A2 was identified as lncRNA H19 (H19), which by its direct binding to the RNA helicase reduces its binding ability for the phosphatase and tensin homolog (PTEN)-induced kinase 1 (PINK1). The inhibition of PINK1 translation by eIF4A2 leads to a reduction of mitophagy which causes the loss of accurate

mitochondrial function, such as the maintenance of the respiratory chain (Wang *et al.*, 2021). It should be mentioned that the direct impact of eIF4A2 on the mitochondrial respiratory chain remains unclear.

As the 'powerhouses' of eukaryotic cells, mitochondria fulfil a fundamental role in producing energy. In contrast to the nuclear genome, the mitochondrial genomes contains neither introns nor histones, but both genomes need to work side by side to ensure correct mitochondrial biogenesis (Annesley and Fisher, 2019). The electron transport chain (ETC) is a coordinated concatenation of reactions, which serves the production of ATP, the universal energy currency. It contains four enzymatic complexes, termed complex I (NADH: ubiquinone oxidoreductase), complex II (succinate dehydrogenase), complex III (cytochrome bc_1 oxidoreductase), complex IV (cytochrome c oxidase) and two mobile electron carriers (the membrane-embedded hydrophobic ubiquinone and the soluble cytochrome c). Complexes I, II and IV pump protons through the reaction chain, which derive from the Krebs cycle where NADH and succinate are oxidated. Complex II, additionally provides electrons through the reduction of ubiquinone that can be used by complex III. In complex III cytochrome c gets reduced, which then is used by complex IV. The electron transfer is coupled to the reduction of molecular oxygen to hydrogen. In the final step of the ETC, energy is generated in form of ATP by phosphorylation of ADP by the ATP synthase (Vercellino and Sazanov, 2022).

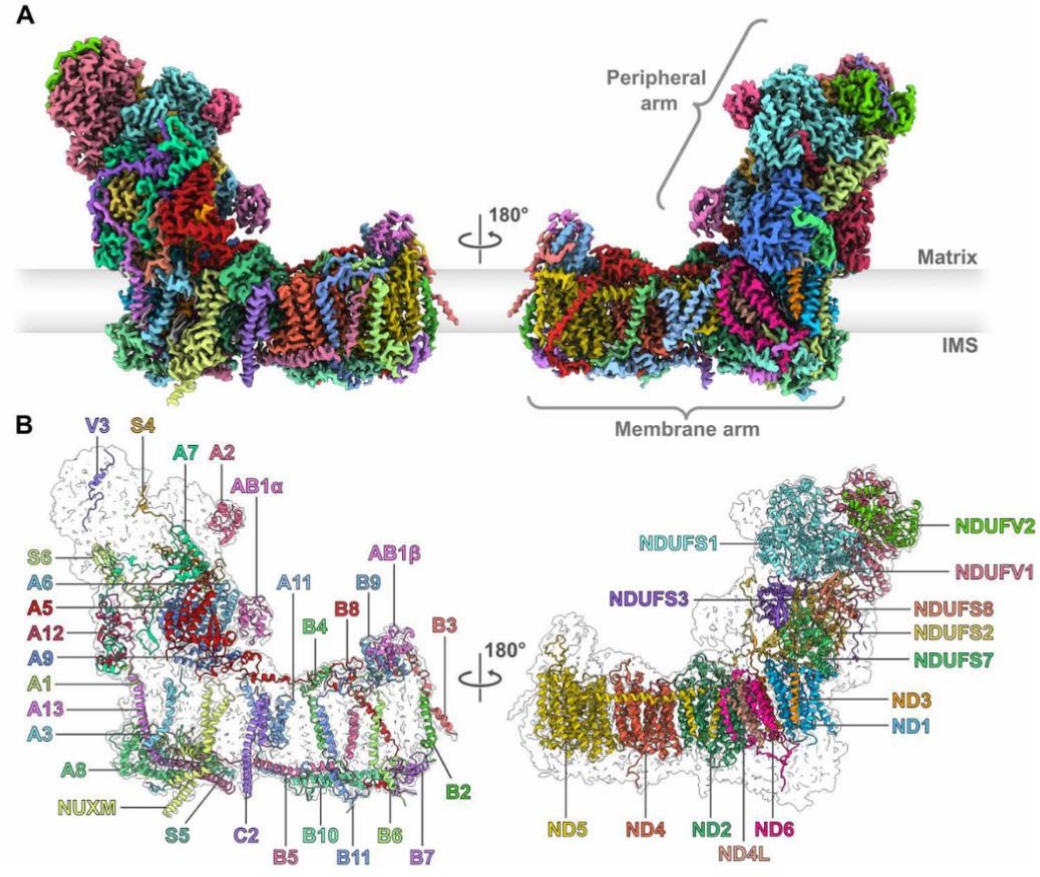

Figure 13. Model structure of mitochondrial complex I from *C. thermophilum*
A Ct-complex I CryoEM density map sorted by subunits shows the peripheral arm in the matrix and the membrane arm in the intermembrane space (IMS) **B** Ct-complex I subunits separated by the 29 accessory (left) and 14 core (right) subunits. The nomenclature is adapted from the human complex I (Laube *et al.*, 2022).

In complex I, the largest complex in the ETC, one group of genes play an important role, the NADH-ubiquinone reductase supernumerary subunits (NDUFs). 31 NDUF-proteins have been identified, and these build the ETC complex I together with the 14 conserved core subunits. While the conserved core subunits are necessary for energy transduction, the supernumerary subunits do not take part in catalysis

of redox reactions. NDUF-proteins are not conserved and only present in eucaryotic mitochondria. Additionally, their precise function remains unclear (Hirst, 2013). The seven hydrophilic subunits are encoded in the core genome and transported to the mitochondrion, where they form the redox domain which extends into the mitochondrial matrix (Figure 13). The seven hydrophobic core subunits, encoded by the mitochondrial genome, shape the membrane arm in the intermembrane space (IMS) (Chomyn *et al.*, 1986). In general, three reactions, oxidation of NADH, intramolecular electron transfer and quinone reduction, take place in complex I. During NADH oxidation, NADH is bound by the hydrophilic arm of complex I and due to the spatial proximity to the flavin mononucleotide, hydride transfer from the C4 of the nicotinamide ring to the N5 of the flavin can take place. This results in NAD+ formation and of flavin oxidation. Electrons are carried from the flavin to the ubiquinone by a FeS chain containing seven FeS clusters. Finally, complex I catalyzes the quinone reduction to quinol, via two semiquinone intermediates, a fast-relaxing and the slow-relaxing species (Hirst, 2013). The respiratory chain is then continued in complex II.

1.6 Aims

The cascade of transcription, pre-mRNA-processing, mRNA degradation, translation and protein degradation is controlled by gene regulatory processes. By themselves, these five fundamental cellular processes have been studied extensively however, it remains unclear how these individual processes are linked, especially alternative splicing and gene/protein expression. Temperature represents an indispensable factor in gene regulation. In this work, we addressed the question of how temperature-dependent alternative splicing affects the cellular proteome.

Many alternatively spliced exons are regulated by changes in temperature. While this process has been widely studied for cold-induced exons such as in RBM3 and CIRBP, heat-induced alternative splicing has only been studied in detail for some heat shock proteins (Neves-da-Rocha *et al.*, 2019). These temperature changes possibly generate mRNA transcripts, comprising pre-mature stop codons, which are targets of NMD or lead to truncated protein isoforms. Since body temperature increases above 37 °C during natural processes such as fever, heat-induced alternative exons and the resulting mRNA isoforms may be of critical importance for the survival of the organism.

Since eIF4A2 contains both, a heat- and a cold-induced alternative exon and takes part in translation as an initiation factor, it represents the perfect model system to study the function of temperature-dependent isoforms and their influence on protein translation under physiological conditions. In addition, RNA helicases play a major role in cellular RNA metabolism, so the potential impact of different eIF4A2 isoforms could be of great importance as they can affect many different cellular processes.

While the function of eIF4A1 and eIF4A3 has been investigated quite thoroughly to this date, the specific function of eIF4A2 remains unclear. Therefore, this thesis aims to investigate the role of eIF4A2 alternative splicing in gene and protein expression and further tries to understand its impact on various cellular processes like translation, stress response and stress granule formation as well as the respiratory chain in a temperature-dependent manner.

A combination of biochemical wet-lab and in-silico approaches was used, to resolve these questions. Initial investigations of splicing patterns or gene and protein expression were performed using wet-lab approaches.

To investigate the mechanism underlying these initial results, we generated CRISPR/Cas9-genome edited eIF4A2 human cell lines, that recapitulate specific alternative splicing events. This allowed us to examine the effects of distinct splicing isoforms on gene and protein expression under different temperature conditions. To globally analyze the effect of eIF4A2 and/or temperature on RNA and protein levels, we performed RNA-sequencing and mass spectrometry analysis, respectively. These findings were then used for further validations and investigations of molecular functions.

2. Materials and methods

2.1 Materials

2.1.1 Commercial kits and buffers

Kit	Supplier
BCA™ protein assay kit	Thermo Fisher Scientific, USA
Pierce™ECL Western Blotting Substrate	Thermo Fisher Scientific, USA
Lipofectamine™ 2000 Transfection Reagent	Thermo Fisher Scientific, USA
NucleoSpin® Gel and PCR Clean-up	Macherey-Nagel, Germany
ROTI®Fect Transfection Reagent	Carl Roth, Germany
iST Sample Preparation Kit	Preomics, Germany
iST-Fractionation Add-on	Preomics, Germany

Buffer	Supplier
Gel Loading Dye, Purple (2 X)	New England Biolabs, Germany
Phusion® HF Buffer Pack (5 X)	Mobidiag, Finland

2.1.2 Radiolabeled nucleotides

Nucleotide	Supplier
γ-^{32}P-dATP [10 µCI/µl, 6000 Ci/mmol]	Hartmann Analytic, Germany

2.1.3 Oligonucleotides

All oligonucleotides were set to a concentration of 100 ng/µL.

Name	Sequence (5' → 3')
CRISPR guides	
hEIF4A2_g1_F	CAC CGA AAA GGG AAA GTA ACC TCT G
hEIF4A2_g1_R	AAA CCA GAG GTT ACT TTC CCT TTT C
hEIF4A2_g2_F	CAC CGA ACA GGT GCT AGT CCC CCA G
hEIF4A2_g2_R	AAA CCT GGG GGA CTA GCA CCT GTT C
hEIF4A2_g3_F	CAC CGA TTA AAA GGA GGG ATC TGG T
hEIF4A2_g3_R	AAA CAC CAG ATC CCT CCT TTT AAT C
hEIF4A2_g4_F	CAC CGT AAG GCA CAA TAC CCT CTG G
hEIF4A2_g4_R	AAA CCC AGA GGG TAT TGT GCC TTA C

Name	Sequence (5' → 3')
hEIF4A2_g5_F	CAC CGA TTG CCC AGA TTG TGG ACA T
hEIF4A2_g5_R	AAA CAT GTC CAC AAT CTG GGC AAT C
hEIF4A2_g6_F	CAC CGA AGC CAC TAT AAC TAA ACC A
hEIF4A2_g6_R	AAA CTG GTT TAG TTA TAG TGG CTT C
hEIF4A2_g7_F	CAC CGT GTT TGA ATA AAG AGC GAG T
hEIF4A2_g7_R	AAA CAC TCG CTC TTT ATT CAA ACA C
hEIF4A2_g8_F	CAC CGA GAT GAC AGT ATC GTG TTT G
hEIF4A2_g8_R	AAA CCA AAC ACG ATA CTG TCA TCT C
RBM3_g1_F	CAC CGT GTG TCT GCT CGG GGC AGC G
RBM3_g1_R	AAA CCG CTG CCC CGA GCA GAC ACA C
RBM3_g2_F	CAC CGT CCT GTG AGT GGG CAC TGC G
RBM3_g2_R	AAA CCG CAG TGC CCA CTC ACA GGA C
RBM3_g3_F	CAC CGC TCC TGA TGA AGC CAT TCT G
RBM3_g3_R	AAA CCA GAA TGG CTT CAT CAG GAG C
RBM3_g4_F	CAC CGA GAG GCC AAA AAT TCC TGC T
RBM3_g4_R	AAA CAG CAG GAA TTT TTG GCC TCT C

Genotyping

hEIF4A2_I2_F	GTT CAT CTC ATT TAT GCG TGC A
hEIF4A2_I3_R	TGT CAA ACT TGG GAT GCT GC
hEIF4A2_I10_F	GGT TGA TGA GAA CAA AGT GGG A
hEIF4A2_I10_R	CTG TAA ACA AAT GCT GCA AAG GT
RBM3_genotype_F	ATC TGC AGA GGG ACC TTG TC
RBM3_genotype_R	CAG ACT TGC CTG CAT GAT CC

Cloning

hEIF4A2_XhoI_F	AAT TTC TCG AGA TGT CTG GTG GCT CCG CG
hEIF4A2_XhoI_F2	AAT TTC TCG AGA TGC TTA CGG TTT TGA GAA GCC TTC CGC TAT TCA GCA GAG AGC TAT TAT TCC CTG TAT TAA AGA TCC AAA AGG TAA TTC TGG CA
hEIF4A2_BamHI_R	AAT TTG GAT CCA ATA AGG TCA GCC ACA TTC ATG

Materials and Methods

Name	Sequence (5' → 3')
hEIF4A2_BamHI_R_NEW	AAT TTG GAT CCT CGA CTC CTG TGA ATA TAG TTT TCA CGA TTG G
hEIF4a2_KPN1_FWD	AAT TTG GTA CCA GTT GAG GTG GCC TGG AAG
hEIF4a2_XHO1_REV	AAT TTC TCG AGG AAG CAC AAT GCA CGT TGT G
hEIF4a2_E10_KPN1_FWD	AAT TTG GTA CCG TGG CCT ACA TGA CAG GTG
hEIF4a2_E5_XHO1_REV	AAT TTC TCG AGA AGA CAA TAC TTA CAA AGG TAT C
EIF4A2_E11_XHO1_REV	AAT TTC TCG AGG GCA TCT CCT CCA CTG TAG T
FL_Kpn1_Fwd_miniEIF4A2	GGT ACC AGT TGA GGT GGC CT
FL_XhoI_Rev_miniEIF4A2	CTC GAG GAA GCA CAA TGC AC
NDUFS4_5UTR_fwd	TCG AAT CCT GGC GTT TGC CTG CAG CAA G
NDUFS4_5UTR_rev	GAT CCT TGC TGC AGG CAA ACG CCA GGA T
NDUFS4_3UTR_fwd	TCG AGT TGG CAC TGA CTA TAT CTC TGC TTG ACT GTG AAT AAA GTC AGC TGT GCA GTA TTT ATA GTC CAT GTA TAA TAA ATA CAT CTC TTA ATC TCC TAA TAA ATT GGA CCT TTA AAC TAC
NDUFS4_3UTR_rev	GAT CTG TAG TTT AAA GGT CCA ATT TAT TAG GAG ATT AAG AGA TGT ATT TAT TAT ACA TGG ACT ATA AAT ACT GCA CAG CTG ACT TTA TTC ACA GTC AAG CAG AGA TAT AGT CAG TGC CAA
NDUFA11_5UTR_fwd	TCG AAA GTC TCG CGA TAG CCA GCC GCG GCT GCC CTT GCG CTT CCC GAG CTG GCG GGG TCC GTG GTG CGG GAT CGA GAT TGC GGG CT
NDUFA11_5UTR_rev	GAT CAG CCC GCA ATC TCG ATC CCG CAC CAC GGA CCC CGC CAG CTC GGG AAG CGC AAG GGC AGC CGC GGC TGG CTA TCG CGA GAC TT
NDUFA11_3UTR_fwd	TCG AGC CCT GTG CCT GCC GGG ACC TCC AGC CTG CAG AAT GCG TCC AGA AAT AAA TTC TGT GTC TGT GTG TG
NDUFA11_3UTR_rev	GAT CCA CAC ACA GAC ACA GAA TTT ATT TCT GGA CGC ATT CTG CAG GCT GGA GGT CCC GGC AGG CAC AGG GC
NDUFS8_5UTR_fwd	TCG AGC CTC CCG ATT GAC TGG CCT GCT TGG CAA GGC AAG TAG CGG CGG CGC TTC AAG
NDUFS8_5UTR_rev	GAT CCT TGA AGC GCC GCC GCT ACT TGC CTT GCC AAG CAG GCC AGT CAA TCG GGA GGC
NDUFS8_3UTR_fwd	TCG ACG CCC CAC CGG CCC GCA GCC CCT GCT GCC CAA TAA AAC CAC TCC GAC CCC A
NDUFS8_3UTR_rev	GAT CTG GGG TCG GAG TGG TTT TAT TGG GCA GCA GGG GCT GCG GGC CGG TGG GGC G

Name	Sequence (5' → 3')
PSMB10_5UTR_fwd	TCG AAG ACG TGA AGC CTA GCA GAG GAC TTT TTA GCT GCT CAC TGG CCC CGC TTG TCT GGC CGA CTC ATC CGC CCG CGA CCC CTA ATC CCC TCT GCC TGC CCC AAG
PSMB10_5UTR_rev	GAT CCT TGG GGC AGG CAG AGG GGA TTA GGG GTC GCG GGC GGA TGA GTC GGC CAG ACA AGC GGG GCC AGT GAG CAG CTA AAA AGT CCT CTG CTA GGC TTC ACG TCT
PSMB10_3UTR_fwd	TCG AGC TGA GGC TTA GAG CTT GGA ACA AGG GGG AAT AAA CCC AGA AAA TAC AGT TAA A
PSMB10_3UTR_rev	GAT CTT TAA CTG TAT TTT CTG GGT TTA TTC CCC CTT GTT CCA AGC TCT AAG CCT CAG C
Sequencing	
T7_fwd	TAA TAC GAC TCA CTA TAG GG
BGH_rev	TAG AAG GCA CAG TCG AGG
EGFP-C-for	GTC CTG CTG GAG TTC GTG
EGFP-C-rev	AGC TGC AAT AAA CAA GTT
EGFP-N-for	CAA CGG GAC TTT CCA AAAA TG
EGFP-N-rev	GCT TGC CGT AGG TGG CAT C
Splice PCR	
hEIF4A2_E2/3_F	GTG TCA TCG AGA GCA ACT GG
hEIF4A2_E5_R	TAT CAA ACA CTC TCC CGG GT
hEIF4A2_E10_F	CTC GCG GGA TTG ATG TGC
hEIF4A2_E11_R	GGC ATC TCC TCC ACT GTA GT
mEIF4A2_E2/3_F	GTG TCA TCG AGA GCA ACT GG
mEIF4A2_E5_R	TAT CAA ACA CTC TCC CTG GA
mEIF4a2_E10_F	CCC GTG GGA TTG ACG TGC
mEIF4a2_E11_R	GGC ATT TCC TCC ACT GTA GT
hRBM3_E3_F	TCA TCA CCT TCA CCA ACC CA
hRBM3_E5_R	TCT AGA GTA GCT GCG ACC AC
hGGCX_E1_F	GCA GAG CAA TGG CGG TGT CT
hGGCX_E3_R	ATC CAG TCA AGT GGC AGT GG
hGGCX_E9_F	GGA CAA ATG GGC TGT ATG GC

Materials and Methods

Name	Sequence (5’ → 3’)
hGGCX_E11_R	TGA AGA CCA CCT CAG TGT GG
hATXN2_E11_F	CCA GCG ACA TCC TCG AAA TC
hATXN2_E13_R	CTA GGT GAT GTT TCA TTG GG
hATXN2_E20_F	GCT AGA ATG ATG GCA CCA CC
hATXN2_E22_R	CTG GGT GCA GGA TGA CTT CC
hACSF2_E8_F	CCT GTA CCA TTG CCT GGG TT
hACSF2_E10_R	ATC AAC TCT GGA GGT GCA GG
hACSF2_E10_F	CCA GAG TTG ATC CGA GCC AT
hACSF2_E11_R	ATT CTG CCC ACG CTT TCT GC
hCD46_E6_F	GGT CAA ATG TCG ATT TCC AG
hCD46_E8_R	GAT AAT TTG AGA CTG GAG GC
hCD46_E11_F	GGA GTT GCA GTA ATT TGT GT
hCD46_E13_R	GGT TGT GGA ATC TAT TCA GC
qPCR	
hEIF4A2_qF	TGG CTG ACT GAG AAG ATG CA
hEIF4A2_qR	GCG AGC CAA CAA GTC AGT AG
mEIF4a2_qF	TGG CTC ACG GAG AAA ATG CA
mEIF4a2_qR	CAC GGG CCA ACA AGT CAG TAG
hRBM3_E2/3_qF	AAG GAA AGC TCT TCG TGG GA
hRBM3_E3_qR	GAC AAC GAC CAC CTC AGA GA
mRBM3_E2/3_qF	AAG GGA AAC TCT TCG TAG
mRBM3_E3_qR	GAC AAC AAC CAC CTC AGA GAT AG
hHprt_qFor	CCT GGC GTC GTG ATT AGT GA
hHprt_qRev	TCT CGA GCA AGA CGT TCA GT
EEF1A1_qPCR_F1	CGC TTT GCT GTT CGT GAT ATG
EEF1A1_qPCR_R1	TTA GCC TTC TGA GCT TTC TGG
EEF1A2_qPCR_F	ATC GTG GGC GTG AAC AAA
EEF1A2_qPCR_R	GGT TGT AGC CGA TCT TCT TGA T
GPNMB_qPCR_F	GCC TGA AAG CTC CCT AAT AGA C
GPNMB_qPCR_R	CAG ACA CAT CTC ATC CAC ATC C

Name	Sequence (5' → 3')
SPATS2L_qPCR_F1	CCA GGT TCA CTG GTT CTC TTC
SPATS2L_qPCR_R1	GAG CAA ACA TCC TCC TGT ACT T
ZNF_qPCR_F1	TCG GTG GAC ACT GGT ATT TAT TT
ZNF_qPCR_R1	GGG ATG GGA GGG TTT GTT T
hACSF_qPCR_F	CAG GCT ATG GAA CTG GAG TAT G
hACSF_qPCR_R	ATC TGC TTC AGG ACG TTG TAG

2.1.4 Plasmids

Name	Description	Reference
pSpCas9(BB)-2A-Puro (pX459)	Cas9 from S. pyogenes with 2A-Puro, and cloning backbone for sgRNA (V2.0)	Prof. Dr. Stefan Mundlos, MPI Berlin
pSpCas9(BB)-2A-GFP (pX458)	Cas9 from S. pyogenes with 2A-EGFP, and cloning backbone for sgRNA	Prof. Dr. Stefan Mundlos, MPI Berlin
hEIF4A2_FL_GFP	eIF4A2 full-length gene inserted via XhoI/BamHI; Kan^R	This study
hEIF4A2_SF_GFP	eIF4A2 delta exon 4 gene inserted via XhoI/BamHI; Kan^R	This study
hEIF4A2_FL+E10A_GFP	eIF4A2 full length plus exon 10A gene inserted via XhoI/BamHI; Kan^R	This study
hEIF4A2_SF+E10A_GFP	eIF4A2 delta exon 4 plus exon 10A gene inserted via XhoI/BamHI; Kan^R	This study
hEIF4A2_FL_FLAG	eIF4A2 full-length gene inserted via XhoI/BamHI; Amp^R	This study
hEIF4A2_SF_FLAG	eIF4A2 delta exon 4 gene inserted via XhoI/BamHI; Amp^R	This study
hEIF4A2_FL+E10A_FLAG	eIF4A2 full length plus exon 10A gene inserted via XhoI/BamHI; Amp^R	This study
hEIF4A2_SF+E10A_FLAG	eIF4A2 delta exon 4 plus exon 10A gene inserted via XhoI/BamHI; Amp^R	This study
pFLAG	Plasmid encoding C-terminal FLAG; Kan^R	Prof. Dr. Florian Heyd, FU Berlin
pEGFP-N3	Plasmid encoding C-terminal GFP; Kan^R	Prof. Dr. Florian Heyd, FU Berlin
pEGFP-C1	Plasmid encoding N-terminal GFP; Kan^R	Prof. Dr. Florian Heyd, FU Berlin
pcDNA3.1 $^{(+)}$	Plasmid encoding mammalian expression vector pcRNA3.1 $^{(+)}$; Amp^R	Prof. Dr. Florian Heyd, FU Berlin

Materials and Methods

Name	Description	Reference
EIF4A2 E4	eIF4A2 exon 2 to exon 5 gene inserted via XhoI/KpnI; Amp^R	This study
EIF4A2 E10A	eIF4A2 exon 10 to exon 11 gene inserted via XhoI/KpnI; Amp^R	This study
EIF4A2_FL	eIF4A2 exon 2 to exon 5 gene inserted via XhoI/KpnI; Amp^R	This study
NDUFS5_5'UTR_GFP	5'UTR of hNDUFS4 inserted via XhoI/BamHI; Kan^R	This study
NDUFA11_5'UTR_GFP	5'UTR of hNDUFA11 inserted via XhoI/BamHI; Kan^R	This study
NDUFS8_5'UTR_GFP	5'UTR of hNDUFS8 inserted via XhoI/BamHI; Kan^R	This study
PSMB10_5'UTR_GFP	5'UTR of hPSMB10 inserted via XhoI/BamHI; Kan^R	This study
NDUFS5_3'UTR_GFP	3'UTR of hNDUFS4 inserted via XhoI/BamHI; Kan^R	This study
NDUFA11_3'UTR_GFP	3'UTR of hNDUFA11 inserted via XhoI/BamHI; Kan^R	This study
NDUFS8_3'UTR_GFP	3'UTR of hNDUFS8 inserted via XhoI/BamHI; Kan^R	This study
PSMB10_3'UTR_GFP	3'UTR of hPSMB10 inserted via XhoI/BamHI; Kan^R	This study
tdTomato	Plasmid encoding N-terminal tandem-tomato; Amp^R	Dr. Andreas Franz, FU Berlin

2.1.5 Antibodies

Antibody	Supplier
mouse anti-EIF4A2	Santa Cruz Biotechnology, USA
rabbit anti-EIF4A2	Invitrogen I Thermo Fisher Scientific, USA
rabbit anti-RBM3	Proteintech, USA
mouse anti-GAPDH	Santa Cruz Biotechnology, USA
mouse anti-hnRNP L	Santa Cruz Biotechnology, USA
rabbit anti-FLAG	Cell Signaling Technology (CST), USA
mouse anti-GFP	Santa Cruz Biotechnology, USA
rabbit anti-G3BP1	Cell Signaling Technology (CST), USA
rabbit anti-peIF2a	Cell Signaling Technology (CST), USA

Antibody	Supplier
mouse anti-HSP70	Santa Cruz Biotechnology, USA
rabbit anti-CIRBP	Proteintech, USA
rabbit anti-NDUFS4	Bio-Techne; USA
mouse anti-Vinculin	Santa Cruz Biotechnology, USA
Goat-anti-rabbit (horseradish peroxidase coupled)	Cell Signaling Technology (CST), USA
Goat-anti-mouse (horseradish peroxidase coupled)	Cell Signaling Technology (CST), USA

2.1.6 Proteins, enzyme inhibitors and enzymes

Protein	Supplier
Bovine serum albumin (BSA)	Thermo Fisher Scientific, USA

Enzyme inhibitor	Supplier
PMSF – Protease Inhibitor	Carl Roth, Germany
Aprotinin – Protease Inhibitor	Carl Roth, Germany
Leupeptin – Protease Inhibitor	Carl Roth, Germany
Vanadate – Phosphatase inhibitor	Carl Roth, Germany

Enzyme	Supplier
Proteinase K (20 mg/mL)	Serva, Germany
Restriction endonucleases	Thermo Fisher Scientific, USA
T4 DNA Ligase	Thermo Fisher Scientific, USA
T4 PNK (Polynucleotide Kinase)	Thermo Fisher Scientific, USA
S7 Fusion Polymerase	Mobidiag, Finland
M-MuLV Reverse Transcriptase	Enzymatics Inc., USA
DNAse I, RNase-Free	Biosearch Tech, UK

2.1.7 Bacteria strains

Strain	Supplier
Escherichia coli TOP10 competent cells	Thermo Fisher Scientific, USA

2.1.8 Cell lines

HeLa and Hek293 cells were used for the generation of stable eIF4A2 CRISPR/Cas9 genome-edited cell lines, and all follow-up experiments. N2a, 3T3 and RPE1 cells were used for splice and gene expression analysis.

Cell line	Supplier
HeLa cells (human cervical cancer cells)	ATCC, USA
Hek293 cells (human embryonic kidney cells)	ATCC, USA
N2a cells (mouse neuroblastoma cell line)	Prof. Dr Gary Lewin, MDC, Berlin
3T3 cells (mouse embryonic fibroblasts)	ATCC, USA
RPE1 cells (human retinal pigment epithelial-1 cells)	ATCC, USA

2.1.9 Commercial media

Dulbecco's Modified Eagle Medium (DMEM) High Glucose	Biowest, France
Opti-MEM® I (1X) + GlutaMAX™-I - Reduced Serum Medium	Thermo Fisher Scientific, USA

2.1.10 Buffers, media and solutions

Media, buffers and solutions were prepared with deionized water (Millipore) and autoclaved if necessary (121 °C, 20 min, 3 bar). The pH was adjusted with 37 % HCl, 5 M NaOH or 5–10 M KCl.

Gel fixing solution

10 % (v/v)	Acetic acid
40 %	Ethanol or Methanol

5 X Hybridization buffer

1.5 M	NaCl
50 mM	Tris, pH 7.5
10 mM	EDTA

10 X Taq buffer

0.5 M	KCl
0.1 M	Tris, pH 8.3
15 mM	$MgCl_2$
0.01%	Gelatine

2 X SDS Loading Dye

20 %	Glycerol
4 %	SDS
125 mM	Tris-HCl, pH 6.8
10 % (w/v)	β-Mercaptoethanol
0.2 % (w/v)	Bromphenol blue

SDS-PAGE running buffer

25 mM	Tris-HCl, pH 6.8
192 mM	Glycine
1 % (w/v)	SDS
21.2 % (w/v)	Glycerol
0.12 % (w/v)	Bromphenol blue

2 X RIPA buffer

20 mM	Tris, pH 8.0
4 %	NP40
4 mg/ml	Sodium deoxycholate
4 mM	EDTA
200 mM	NaCl

1 X DNA extraction buffer

	10 X PCR buffer
1 %	Gelatine
10 %	Tween-20
10 %	NP-40

1 X PCR buffer

200 mM	Tris/HCl, pH 8.3
500 mM	KCl
500 mM	$MgCl_2$
0.1 %	Gelatine in H_2O

Materials and Methods

10 X T4 DNA ligase buffer

500 mM	Tris-HCl, pH 7.5
100 mM	$MgCl_2$
100 mM	DTT
10 mM	ATP
250 µg/mL	BSA

5 X HS TBS-T

250 mM	Tris-HCl, pH7.5
2 M	NaCl
1 %	Tween-20

1 X LS-TBS-T

50 mM	Tris-HCl, pH7.5
150 mM	NaCl
0.1 %	Tween-20

Western blot-blocking buffer

1 X	TBS-T
2 % (w/v)	BSA

10 X Western blot transfer buffer

500 mM	Tris-HCl, pH7.5
400 mM	Glycine
0.1 % (w/v)	SDS

10 X PCR buffer (for tissue or cell digest)

200 mM	Tris, pH8.3
500 mM KCl	KCL
5 mM	$MgCl_2$

1 X PNK buffer

70 mM	Tris-HCl, pH8.3
10 mM	$MgCl_2$
5 mM	DTT, pH 7.6

Formamide dye

21 mM	EDTA
0.02 (w/v)	Bromphenol blue
0.02 (w/v)	Xylene cyanol
80 % (w/v)	Formamide

1.25 X RT Mix

12.5 mM	DTT
12.5 mM	Tris, pH 8.0
7.5 mM	$MgCl_2$

2.2 Methods

2.2.1 Molecular biology standard methods

2.2.1.1 Cell culture and treatment

Hek293 cells, HeLa cells, 3T3 cells, RPE1 cells, and N2a cells were cultured in uncoated plastic flasks at 37 °C, 5 % CO_2 in a medium containing DMEM supplemented with 10 % fetal bovine (BIO&SELL, FCS.SAM-HI.0500) serum and 100 µg/ml penicillin-streptomycin (Lonza, DE17-602F). At around 80 % coverage from confluency, cells were split using a 0.25 % trypsin dilution (Gibco, 25200-056).

Transfection of immortalized cells

For transfection Hek239 or HeLa cells with expression constructs or minigenes, about $8x10^8$ cells were cultured in 12-well plates one day before transfection. Therefore, either Hek293 were transfected using the ROTI®Fect Transfection Reagent (Carl Roth) described in the user's manual or for HeLa cells, the Lipofectamine® 2000 Transfection Reagent (Thermo Fisher Scientific) used as described in the user's manual. After a transfection time of 48 hours, cells were washed once with ice-cold 1 X PBS and then harvested for RNA or protein extraction. If required, cells were shifted to different temperatures for 24 hours after transfection.

2.2.1.2 RNA extraction

For RNA extraction from cultured cells, the culture medium was removed, cells were washed with ice-cold PBS, RNA Tri-flüssig (BIO&CELL) was added directly to the wells and up taken in RNAse-free tubes. All further steps were performed at four degrees unless otherwise specified. Chloroform was added in a 1:5 ratio. By vortexing, the mixture was homogenized. The mixture was incubated at room temperature for 10 minutes. Afterwards, nucleic acids were extracted by phase separation through centrifugation, precipitated with isopropanol, resuspended in RNase-free H_2O, and digested with RNase-free DNase I if necessary.

Therefore, RNAs were subjected to a second phenol-chloroform-isoamyl alcohol extraction (PCI from Carl Roth) and subsequently precipitated with an excessive volume of 100 % ethanol with sodium acetate (final concentration: 150 mM). Finally, RNA pellets were washed with 70 % ethanol, left to air-drying followed by resuspension in nuclease-free H_2O.

Nucleic Acid quantification

Determining the nucleic acid concentration, its absorption at the two wavelengths of 260 nm and 280 nm was measured using a NanoDrop spectrophotometer according to the manufacturer's instructions. Sterile H_2O served as a reference for the measurement. The RNA was adjusted in sterile H_2O to a final concentration of 500 ng/µL.

2.2.1.3 RT-PCR

For splice PCR and SYBR green qPCR, cDNA was reverse-transcribed using MMuLV reverse transcriptase using gene-specific reverse primers, according to the following protocol.

Table 1. Composition of standard reverse transcription I

Component	Stock conc.	Final conc.
total RNA	500 ng/µL	1 µg
hybridization buffer	5 X	1 X
reverse primer	100 ng/µL	1 ng/µL

Table 2. Program of standard reverse transcription I

Temperature	Time	Cycles
90 °C…70 °C	20 sec	1
69 °C…51 °C	30 sec	1
50 °C…44 °C	40 sec	1
43 °C	∞	1

Table 3. Composition of standard reverse transcription II

Component	Stock conc.	Final conc.
RT annealing mix	500 ng/µL	1 µg
RT reaction buffer (+dNTPs)	1.25 X	1.25 X
MMuLV reverse transcriptase	100 ng/µL	1 ng/µL

Table 4. Program of standard reverse transcription II

Temperature	Time	Cycles
43 °C	30 min	1
94 °C	5 min	1
4 °C	∞	1

2.2.1.4 Quantitative real-time PCR

SYBR Green qPCR for all in this study used targets was performed on the Bioer Line Gene 9600 Plus, using the Biozym Blue S'Green qPCR Kit (Biozym®, 331416L). Reactions were set up according to the master mix protocol using the equivalent of <100 ng cDNA per reaction. Reactions were performed in technical duplicates. Biological replicates were indicated in the single experiments. hHPRT or hGAPDH served as reference genes depicted in the figures. Mean values of the expression levels of the target genes have been used to normalize the expression to mRNA of reference genes.

2.2.1.5 Splicing-sensitive PCR

Splicing-sensitive PCRs were performed using the Taq polymerase with reverse-transcribed RNA as a template. PCR components as shown below in a 25 µL reaction. After the run, the PCR product was mixed with 10 X orange loading dye and applied to a 2 % agarose gel (150 V). After 25 to 35 minutes, the desired degree of resolution was reached, and the gel was imaged with a GE AI600 RGB GEL Imaging System. The result was quantified using the GE ImageQuant TL 8.1 software.

Table 5. Composition of a standard splice PCR

Component	Stock conc.	Final conc.
Taq Buffer	10 X	1 X
Primer 1 (Fwd)	10 µM	100 nM
Primer 2 (Rev)	10 µM	100 nM
Template (cDNA)		1 µg
Taq DNA Pol.	5 U/µL	1.25 U/µL

Table 6. Program of a standard splice PCR

Step	Temperature	Time	Cylces
Initial denaturation	95 °C	5 min	1
Denaturation	95 °C	30 sec	35
Annealing	60 °C	30 sec	
Extension	72 °C	45 sec	
Final extension	72 °C	7 min	1
Hold	4 °C	∞	1

2.2.1.6 Radioactive splice-sensitive PCR

Radioactive labelling of splice-sensitive PCR primer

For the radioactive labelling of splice-sensitive Primers, 10 µL PNK buffer, 1 µL T4PNK, 2 µL forward primer, 2.5 µL ^{32}P-γ-ATP (Hartmann Analytic, SRP-501) and 84.5 µL H_2O were mixed and incubated in a water bath at 37 °C for 30-45 minutes. Afterwards, 23 µL 3 M NaOAc (pH 5), 1 µL glycogen, 76 µL H_2O and 200 µL phenol-chloroform-isoamyl alcohol-mix (Roti-Aqua P/C/I, Roth) was added to purify the primer mixture. The phase separation was obtained due to centrifugation and purified in ethanol afterwards. The primer pellet was resuspended in 80 µL H_2O. For a 20 µL PCR reaction, 1 µL radioactive labelled primer was used. pBR322-MspI Digest (NEB, N3032S) was used as a marker and labelled in the same way. The pellet was resuspended in 40 µL H_2O and the same volume of formamide loading dye.

Radioactive splicing-sensitive PCR

The PCR reaction is set up as described below. To prevent the approaches from evaporation, they were overlayed with mineral oil. After the run, the PCR products were mixed with formamide loading dye in a 1:1 ratio and denatured at 95 °C for 5 minutes alongside the marker. Up to 8 µL were applied to a denaturing polyacrylamide-urea gel. To ensure optimal product denaturation, the gel was pre-run in 1 X TBE buffer for 10 minutes at a current of 20 mA.

After the run, gels were fixated in fixation buffer and transferred to Whatman paper, vacuum-dried for up to 2 hours at 50 °C and assembled in photographic cassettes, together with a photostimulable phosphor plate. Exposure was performed for up to 24 hours depending on the strength of the luminous signal. Then, the phosphor plate was imaged with the GE Healthcare Typhoon 7000 FLA imager and the result was quantified using the GE ImageQuant TL 8.1 software.

Table 7. Composition of a standard radioactive splice PCR

Component	Stock conc.	Final conc.
Taq Buffer	10 X	1 X
Primer 1 (Fwd)	0.5 µM	2.5 nM
Primer 1 (Fwd) (^{32}P labelled)	0.5 µM	2.5 nM
Primer 2 (Rev)	1 µM	5 nM
Template (cDNA)		1 µg
Taq DNA Pol.	5 U/µL	1.25 U/µL

Table 8. Program of a standard radioactive splice PCR

Step	Temperature	Time	Cylces
Initial denaturation	95 °C	5 min	1
Denaturation	95 °C	30 sec	28
Annealing	60 °C	30 sec	
Extension	72 °C	45 sec	
Final extension	72 °C	7 min	1
Hold	4 °C	∞	1

2.2.1.7 Molecular cloning of Minigene, expression and reporter constructs

Cloning of ORFs for expression constructs

The pEGFP-N3 backbone was used for all expression constructs. Open reading frames of different potential eIF4A2 isoforms were incorporated in this backbone by PCR. Therefore, XhoI and BamHI restriction sites were spanned into the sequences. The DNA fragment was amplified by PCR from cDNA. Afterwards, the DNA fragment and the vector were cut with restriction enzymes. Subsequently, DNA fragments and vectors could be ligated and transformed into *E.coli* cells. Midi prep was performed afterwards according to the manufacturer's instructions using the NucleoBond Xtra Midi kit (Macherey&Nagel). Constructs were then sequenced to confirm correct insertion (Microsynth SEQLAB).

Cloning of minigenes

The pcDNA3.1(+) vector was used to generate eIF4A2 minigenes containing either the sequence for exon 2 to exon 5 or exon 10 to exon 11 by PCR from genomic DNA. As described for the expression constructs, XhoI and KpnI were used as restriction sites and human DNA as a template. The minigene constructs were purified and sequenced via Microsynth SEQLAB.

Generation of UTR reporter vectors

100 µM of each forward and reverse oligonucleotide containing either the 5'UTR or the 3'UTR region of Ndufs4, Ndufa11, Ndufs8 and Psmb10 were phosphorylated and annealed in presence of T4 PNK and 10 X T4 ligation buffer using the following parameters: 37 °C for 30 min, 95 °C for 5 min and then ramp down to 25 °C in 5° C/min steps.

The annealed oligos were diluted 1:200 in sterile H_2O and ligated into either pEGFP-N3 for the 3'UTRs or pEGFP-C1 for the 5'UTRs. The constructs were purified and sequenced as described above.

2.2.1.8 PCR amplification

For introducing the restriction sites into the constructs mentioned above the DNA fragments were amplified in a volume of 50 µL by PCR.

Table 9. Composition of standard cloning PCR

Component	Stock conc.	Final conc.
HF Buffer	5 X	1 X
dNTP mix	10 mM	200 µM
Primer 1 (Fwd)	10 µM	200 nM
Primer 2 (Rev)	10 µM	200 nM
Template (plasmid)		1 ng/µL
DNA Pol.	100 U/µL	0.02 U/µL

Table 10. Program of a standard cloning PCR

Step	Temperature	Time	Cycles
Initial denaturation	95 °C	3 min	1
Denaturation	95 °C	45 sec	
Annealing	Primer specific	40 sec	30
Extension	72 °C	1-2 min/kb	
Final extension	72 °C	15 min	1
Hold	4 °C	∞	1

2.2.1.9 Restriction digest of DNA

Restriction digests of PCR products and plasmids were performed in a reaction volume of 20 µL at 37 °C for 1 hour. Subsequently, the digested plasmids were resolved on a preparative 1 % agarose gel and the band of interest was cut, while digested PCR products were purified directly. Both products were purified by using the NucleoSpin® Gel and PCR Clean-up kit from Macherey-Nagel.

Table 11. Composition of a standard restriction digest

Component	Stock conc.	Final conc.
FastDigest Buffer	10 X	1 X
Enzyme 1	10 Units	10 U/µg DNA
Enzyme 2	10 Units	10 U/µg DNA
DNA		1–5 µg

2.2.1.10 Ligation of digested insert and vector

The ligation of the insert and plasmid was performed in 10 µL reaction volume at room temperature for 10 minutes. The ligation mixture was immediately transformed into competent *E.co*li cells. The composition of a standard ligation reaction is shown below.

Table 12. Composition of a standard ligation reaction

Component	Stock conc.	Final conc.
T4 DNA ligase buffer	10 X	1 X
T4 DNA ligase	1 U/µL	0.1 U/µL
Vector		50 ng
Insert		37.5 ng

2.2.2 Protein-biochemistry standard methods

2.2.2.1 Protein extraction

Cells were collected directly in RIPA buffer freshly mixed with protease and phosphatase inhibitors. 100 µL RIPA buffer with inhibitors was used per well of a 12-well plate. The cell suspension was vortexed on ice for 10 minutes and then centrifuged at maximal speed and 4 °C for 10 minutes. The cleared lysate was transferred to a fresh tube and stored on ice.

2.2.2.2 Protein quantification

For protein concentration measurement, the Roti®Nanoquant Bradford assay was used according to the manufacturer's protocol. The assay is based on Coomassie Brilliant Blue G250 for colourimetric detection. A BSA standard was prepared for calibration. To determine the protein concentration using a spectrophotometer absorbance for 450 nm and 590 nm was measured. The ratio between OD_{450}/OD_{590} was calculated and samples for western blotting were adjusted with RIPA buffer to achieve the same protein concentration. Protein samples were supplemented with 2 X SDS loading dye and denatured at 95 °C for 5 min.

2.2.2.3 Denaturing SDS polyacrylamide gel-electrophoresis (SDS-PAGE)

The same amount of total protein was applied on all lanes of the 12 % polyacrylamide gel, alongside the PageRuler Plus Pre-Stained protein ladder (Thermo Fisher, 26620). The separating gel included 12 % polyacrylamide (30 %, 37.5:1) and the stacking gel contained 4 % polyacrylamide. The gel was run in 1 X SDS running buffer at 80–140 V for up to 2 hours. Proteins were transferred to a nitrocellulose membrane (Amersham™ Protran® nitrocellulose 0.45 µm), for immunoblotting.

Table 13. Composition of SDS gels

Component	Stock conc.	Stacking gel	Separating gel
Acrylamide	30 %	4 %	12 %
Tris-HCl, pH 6.8	1 M	125 mM	-
Tris-HCl, pH 8.8	1 M	-	375 mM
SDS	10 % (w/v)	0.1 %	0.1 %
APS	20 % (w/w)	0.1 %	0.14 %
TEMED	100 %	0.1 %	0.07 %

2.2.2.4 Immunoblotting

For western blotting, denaturing SDS gels were transferred to a nitrocellulose membrane using the BioRad Mini Trans-Blot® wet/tank blotting system. For the transfer sandwich assembling, 6 Whatman paper and the membrane were saturated with pre-cooled 1 X transfer buffer including 20 % methanol. The sandwich was assembled as follows: sponge, three Whatman paper, denatured SDS page gel, nitrocellulose membrane, three Whatman paper, sponge. The electro transfer was conducted at 110 V for 1 h with the BioRad Mini Trans-Blot Electrophoretic Transfer cell system. A cooling unit was used to prevent overheating of the transfer buffer. Subsequently, the membrane was blocked in 2 % BSA in 1 X LS-TBS-T for one hour. The blocking solution served as an antibody solution and the immunoblotting was performed for either one hour at room temperature or overnight at 4 °C. Primary antibodies are listed in section 2.1.5. The immunoblotting was followed by 3 washing steps for 10 minutes each with 1 X HS-TBS-T. Afterwards, the membrane was incubated with the secondary antibody (horseradish-peroxidase-conjugated anti-mouse or anti-rabbit) for one hour at room temperature. After three washes with 1 X HS-TBS-T, proteins were detected by enhanced chemiluminescence using Pierce™ ECL Western Blotting Substrate (Thermo Fisher) according to manufacturer's instruction. Membranes were imaged with a GE Al600 RGB GEL Imaging System and the results were quantified using the GE ImageQuant TL 8.1 software.

2.2.3 Special methods

2.2.3.1 Generation of CRISPR/Cas9 edited cell lines

For genome engineering in Hek293 cells, sequences flanking either exon 3 and 5 of eIF4A2 or exon 10 and exon 11 were analyzed in silico for sgRNA candidates using the Benchling tool. Upstream and downstream a pair of oligonucleotides for the highest-ranked candidate sgRNA (Ran *et al.*, 2013) was synthesized and subcloned into the pX459 vector (kindly provided by Stefan Mundlos).

For genome engineering in HeLa cells, the same oligonucleotides were synthesized and subcloned into the pX458 vector. sgRNA sequences are listed in Section 2.1.3.

For Hek293 cells, cells were transfected in 6-well plates using ROTI®Fect following the manufacturer's protocol. 48 hours after transfection, the transfected cells were selected with 1 µg/ml puromycin and clonal cell lines were isolated by dilution (Ran *et al.*, 2013). For HeLa cells, cells were transfected in the same way and sorted for GFP signal into 96 well plates using a BD FACSMelody™ Cell Sorter 48 hours after transfection.

To confirm the exon knockout on the DNA level, genomic DNA was extracted, and a PCR was performed.

Table 14. Composition of a standard genotyping PCR

Component	Stock conc.	Final conc.
Taq buffer	10 X	1 X
dNTPs	10 mM	200 µM
$MgCl_2$	50 mM	5 mM
Primer 1 (Fwd)	10 µM	100 nM
Primer 2 (Rev)	10 µM	100 nM
Template (genomic DNA)	variable	<1000 ng
Taq DNA Pol.	5 U/µL	1.25 U/µL

Table 15. Program of a standard genotyping PCR

Step	Temperature	Time	Cylces
Initial denaturation	95 °C	5 min	1
Denaturation	95 °C	30 sec	
Annealing	60 °C	30 sec	28
Extension	72 °C	2 min	
Final extension	72 °C	7 min	1
Hold	4 °C	∞	1

To fully confirm the knockout, the RNA of promising clones was isolated, and a splice-sensitive PCR was performed by using one forward primer in exon 2/3 and one reverse primer in exon 5 for the exon 4 knockout. For exon 10A knockout a forward primer in exon 10 and a reverse primer in exon 11 was used. Independent positive clones for pX458, pX459, eIF4A2Δ4 and eIF4A2Δ10A were selected and used for all experiments shown in this study.

The same procedure was performed for RBM3 using sgRNAs flanking E3 and E4 to generate stable Hek293 RBM3Δ3a cell lines. Two independent clones were used for the experiments shown in this study.

2.2.3.2 Flow cytometry

For GFP reporter assays $1.0x10^5$ CRISPR/Cas9 edited HeLa cells were seeded into a 12-well plate and co-transfected with Lipofectamine® 2000 (Thermo Fisher) according to the manufacturer's instructions, using 1.6 µg of the different GFP reporter constructs and 1.6 µg of the red fluorescent control construct tdTomato. Forty-eight hours after transfection, cells were washed with ice-cold 1 X PBS using, trypsinized and transferred into tubes. GFP intensity and tdTomato intensity were measured in technical triplicates by BD FACSMelody™ Cell Sorter. Average GFP expression was normalized to averaged tdTomato expression.

2.2.3.3 Immunofluorescent staining

HeLa cells were cultured on coverslips coated with Poly(L)lysine at 37 °C. The coverslips with cells were then washed 3 X in PBS, fixated for 15 minutes at room temperature with 3.7 % PFA in PBS, and then washed two more times for 10 minutes in PBS. Coverslips were placed cell side up in a humid chamber and epitopes were blocked for 1 hour in 150 µL blocking solution (10 % horse goat serum, 0.1 % Triton X-100 in PBS). 150 µL primary antibody in blocking solution without Triton was used per 12 mm

coverslip for 1 hour. Subsequently, coverslips were washed 4 times with 1 X PBS. Fluorophore-conjugated secondary antibodies were applied in 150 µL blocking solution without Triton at room temperature for 2 hours. Coverslips were washed five times with 1 X PBS and then mounted with Roti®-Mount FluorCare DAPI (Carl Roth) on #1.5 cover glasses overnight. The following day, coverslips were sealed and stored at 4 °C until imaging. For oxidative stress conditions, 0.5 mM arsenite was added to the cells 1 hour before harvesting.

Image acquisition for immunofluorescence

Slides were imaged on a Leica Sp8 confocal laser scanning system with a DMI600C-SB microscope (BioSupraMol facility at Freie Universität Berlin).

Analysis of fluorescence micrographs

For quantitative analysis of stress granules using ImageJ, ROIs of the same size for the stress granules marker G3BP1 were used. To quantify the size and number of stress granules, individual cells were compared to the average number of stress granules.

2.2.3.4 RNA seq and data-processing

For RNA seq analysis, stable HeLa CRISPR/Cas 9 edited cells were harvested 24 hours after temperature shift to 32 °C, 37 °C or 40 °C and their total RNA was extracted. Two independent CRISPR clones of each cell line with an RNA amount ≥ 2 µg and a purity of $OD_{260/280}$ = 1.8-2.0 were selected for the RNA sequencing analysis. For library preparation, the RNA samples were filtered using the polyA+ selection method at BGI Genomics and sequenced using DNBSeq PE150 sequencing. This yielded approximately 50 to 60 million reads.

RNA sequencing data from Hek293 cells are listed under GSE143872 (Haltenhof *et al.*, 2020), RNA sequencing data from mouse primary hepatocytes are listed under GSE158882 (Neumann *et al.*, 2020), RNA sequencing data from human tissues are accessible under PRJEB4337 (Fagerberg *et al.*, 2014) and RNA seq data from mouse tissues are accessible under PRJEB4337 (Hu *et al.*, 2022). For the bioinformatics analysis, STAR version 2.4.3a (Dobin *et al.*, 2013) was used to map the reads to their reference genome. The reference genomes hg38 (human) and mm10 (mouse) were applied. To analyze the gene expression, Salmon version 0.11.3 transcript quantification (Patro *et al.*, 2017). This analysis was followed by a quantification using DESeq2 version 1.22.2 (Love, Huber and Anders, 2014). Splicing ratios and transcripts per million GE quantifications were obtained by Whippet version 0.11 (Sterne-Weiler *et al.*, 2018). As significantly different between the two investigated conditions, a $|\Delta PSI| > 15$ %, probability >85 % and on average more than 10 junction reads for a splice event were considered. Python3 scripts and GraphPad Prism 8 were used for further downstream analysis. Sashimi plots were generated using the IGV browser (Robinson *et al.*, 2011).

The minimum junction coverage was set to remove junction reads with low count numbers for clarity. The upstream analysis of the RNA sequencing data was performed by Dr. Marco Preußner (Freie Universität Berlin, Heyd lab).

2.2.3.5 Mass spectrometry

Sample preparation

Stable HeLa CRISPR/Cas9 edited cells were seeded and shifted to different temperatures. 24 hours after the temperature shift, cells were washed with ice-cold 1 X PBS and transferred into sterile tubes. For the proteomics sample preparation, the iST Kit (PREOMICS) was used according to the manufacturer's instructions. Briefly, the kit includes the lysis, digestion, and purification of the proteins. Subsequently, the samples were fractionated using the iST-Fraction Add-on (PREOMICS) to achieve 40-50 % more protein identifications compared to an unfractionated sample and therefore giving increased proteomic depth.

Mass spectrometry analysis

All measurements were performed on the Orbitrap Q Exactive HF mass spectrometer (Thermo Fisher Scientific) with a long LC-MS gradient (130 minutes in total) and 2 µL (200 ng) of each sample was applied to an Ultimate 3000 reversed-phase capillary nano liquid chromatography system. Samples were injected and concentrated on a PepMap100 C18 trap column (3 µm, 100 Å, 75 µm i.d. x 20 mm (Thermo Fisher Scientific #164535) equilibrated with 0.05 % (w/v) TFA in water. After switching the trap column inline, LC separations were performed on an Acclaim PepMap100 RSL C18 capillary column (2 µm, 100 Å, 75 µm i.d. x500 mm, NanoViper (Thermo Fisher Scientific #164942) at an eluent flow rate of 300 nL/min. Mobile phase A contained 0.1 % (v/v) formic acid in the water, and mobile phase B contained 0.1 % (v/v) formic acid in 80 % (v/v) acetonitrile 20 % H_2O. The column was pre-equilibrated with 5 % mobile phase B followed by an increase to 44 % mobile phase B over 100 min. Mass spectra were acquired in a data-dependent mode, utilizing a single MS survey scan (350–1650 m/z) with a resolution of 60,000 in the Orbitrap, and MS/MS scans of the 15 most intense precursor ions with a resolution of 15,000. The dynamic exclusion time was set to 20.0 seconds, and the automatic gain control was set to $3x10^6$ and $1x10^5$ for MS and MS/MS scans, respectively (Bergfort *et al.*, 2022).

Search engine and quantitation of the MS raw data was performed with the label-free quantification by MaxQuant version 2.0.3.0. Data were searched against the human reference proteome, which was downloaded from SwissProt (79052 protein entries: 03.23.2022) and the match between runs option was enabled. As a significantly different between the two investigated conditions, a log_2 foldchange >0.5 (<-0.5) and a q-value FDR < 0.05 was considered.

The mass spectrometry analysis was performed by Dr. Benno Kuropka (Core Facility BioSupraMol facility at Freie Universität Berlin).

2.2.3.6 Statistical analysis

GraphPad Prism 8 software was used to perform all statistical analyses, using the tests as indicated in the respective experiments.

3. Results

Alternative splicing and intron retention lead through exon or intron inclusion and skipping to many more mRNA isoforms and thereby to a much higher number of possible translated proteins. Temperature seems to be an important factor in the regulation of alternative splicing (Shiina and Shimizu, 2020). However, little is known about the expression, stability and functionality of the proteins deriving from the different mRNA isoforms. This study aims to provide evidence on how two temperature-dependent alternative splicing events in a transcript affect mRNA levels and protein expression. To investigate this, global bioinformatics analyses were combined with *in vitro* and cell culture approaches for individual targets.

3.1 Global analysis on the effect of temperature on alternative splicing

To globally evaluate the impact of temperature-dependent alternative splicing, we performed RNA-sequencing using the human immortalized cell line HeLa and the derivate human cell line Hek293. HeLa, cells were incubated for 24 hours at 32 °C, 37 °C and 40 °C and RNA-seq was performed in duplicates for two independent clones per condition. For Hek293, RNA-seq data were analyzed by Haltenhof *et al.* 2020 (GSE143872).

3.1.1 Alternative splicing of a specific exon-set is affected by temperature

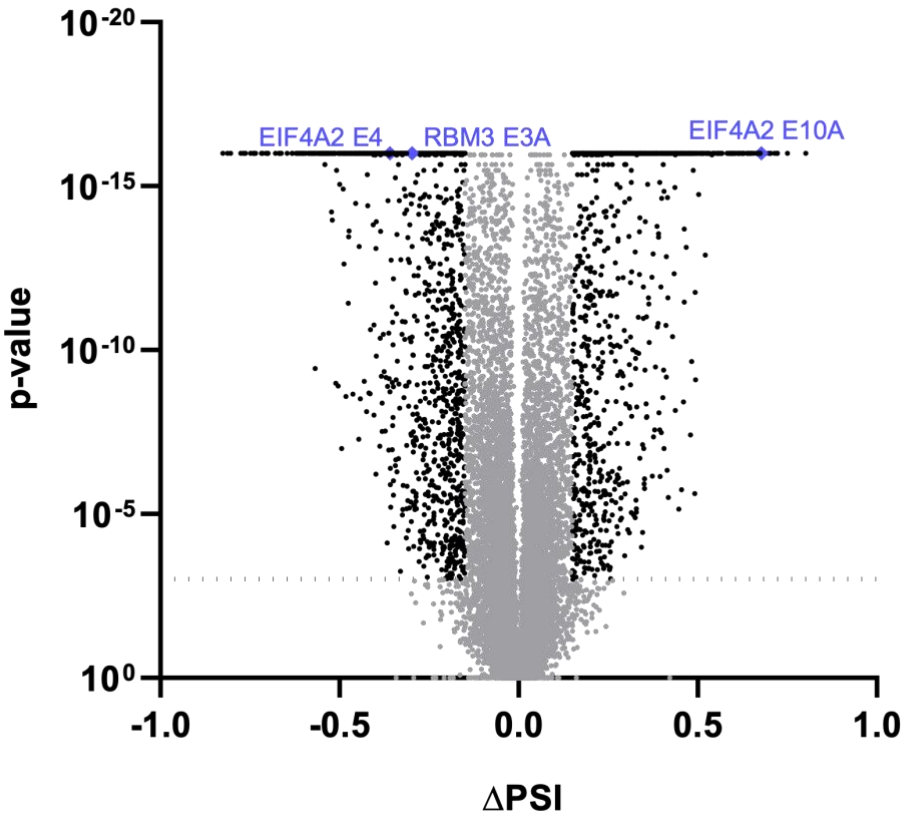

Figure 14. eIF4A2 and RBM3 each contain one of the strongest temperature-dependent alternative exons in HeLa cells
Global splicing analysis was performed using RNA-sequencing data obtained from HeLa cells. Volcano plot shows the ΔPSI between HeLa cells incubated at 32 °C or 40 °C (for 24 hours). In total, 85,099 exons were identified. With the usage of stringent filtering conditions, 4629 exons with a temperature-dependent change in ΔPSI |0.15 %| and a p-value < 0.001 were identified. PSI values were determined using rMATS. p-values = 0 were set to $1x10^{-16}$. Downstream analysis was performed using GraphPad Prism 8.0. Each non-significant splicing event is depicted as a grey dot; each significant splicing event is illustrated as a black dot. eIF4A2 alternative exons 4 and 10A and RBM3 alternative exon 3a are highlighted as purple diamond.

Results

We globally analyzed the differences in alternative splicing between 32 °C and 40 °C in HeLa cells using the |ΔPSI| <15 % and p < 0.001 as cut-offs (Figure 14). We found around 80,000 alternatively spliced exons in total, whereby 4,629 significant changes in exon inclusion were linked to changes in temperature. We could not observe significant differences in the number of exons that were included at a higher or lower temperature, exon inclusion was slightly increased at 40 °C. Exon 3a of RBM3 was identified as one of the strongest heat-induced exon inclusion events (ΔPSI = -0.297 + p-value = $1x10^{-16}$), which is consistent with recently published data from Preußner *et al.* (2023). Another strongly regulated splicing event specific for higher temperatures was identified as exon 4 of eIF4A2 (ΔPSI = -0.359 + p-value = $1x10^{-16}$). In cold, we could establish exon 10A of eIF4A2 as one of the most included exons (ΔPSI = 0.678 + p-value = $1x10^{-16}$). Thus, eIF4A2 contains two alternatively spliced exons that are regulated in an antagonistic manner.

3.1.2 Alternative splicing in Hek293 and HeLa cells reveals strong similarities in temperature-dependent splicing

From previous experiences with temperature-dependent alternative splicing events we wondered, if there are cell type-specific events in AS. We, therefore, compared the RNA-sequencing dataset of Hek239 cells from Haltenhof *et al.* (2020) with our HeLa RNA-sequencing dataset (Figure 15). It is important to point out, that we did not apply the same experimental approach. HeLa cells were incubated for 24 hours at 32 °C, 37 °C and 40 °C, respectively. Haltenhof *et al.* (2020) performed RNA-sequencing with Hek293 cells, that were shifted to 35 °C for 6 hours after a 12-hour incubation at 39 °C. Our bioinformatic analysis identified 276 exons that were spliced differently between 32 °C and 37 °C as well as 37 °C and 40 °C. Despite their different experimental approaches, the two datasets show a great similarity suggesting a high conservation of alternative splicing in these two cell lines.

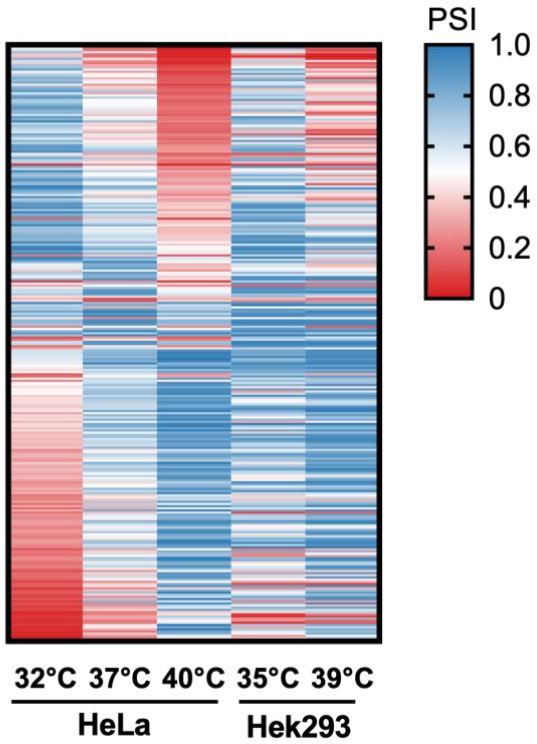

Figure 15. Global RNA-seq analysis of alternative exons shows similarities between HeLa and Hek293 cells
A heatmap of the percentage spliced in (PSI) of all exon-skipping events (276) that are temperature-dependent in HeLa at 32 °C versus 37 °C and 37 °C versus 40 °C is shown. We considered a temperature-dependent change in PSI > 15 % and p > 0.001 as significant. The first three columns show the RNA-seq data obtained in this study, while the last two columns show the RNA-seq data from Hek293 cells at 35 °C versus 39 °C obtained by Haltenhof *et al.* (2020). Exon skipping events were determined by whippet 0.11 (Sterne-Weiler *et al.*, 2018) and a downstream analysis was performed using GraphPad Prism 8.0. Events are classified based on their PSI foldchange in HeLa.

3.1.3 Identification and validation of temperature-dependent alternative splicing events

As our global analysis revealed many targets containing splicing events that are regulated in a temperature-controlled manner, we started looking for specific genes, that have more than one temperature-dependent alternative exon. We found 250 genes, that contain two alternatively spliced exons and found eIF4A2 for both HeLa and Hek239 cells under the top 20 most regulated genes (Figure 16A, B). This appoints eIF4A2 an interesting target for further investigations. For HeLa cells, eIF4A2 was the most temperature-sensitive gene containing two alternative exons, while for Hek293 cells eIF4A2 was the 7th most regulated. The global RNA-sequencing analysis in Hek293 and HeLa cells suggested that alternative splicing of the eIF4A2 exons 4 and 10A, respectively is similar in responses to temperature. We then decided to validate GGCX and CD46 (Figure 16D-G), as both genes include two alternative splicing events responsive to higher or lower temperature, respectively. Furthermore we, verified the alternative splicing of ACSF2 and ATXN2, which both comprise one heat- and one cold-induced alternative exon, comparable to eIF4A2. To confirm, whether the temperature-dependent alternative splicing of two exons results in temperature-dependent gene expression, we plotted the transcripts per million (tpm) values against the indicated temperatures (Figure 16C).

For ATXN2 and CD46 we did not observe the gene expression to be temperature dependent while ACSF2 and GGCX expression was upregulated in heat. This shows that not all temperature-sensitive splicing events do directly correlate with gene expression. To further analyze these alternative splicing events, RNA-sequencing data were mapped to the corresponding human genome (GRCh38/hg38) and sashimi plots were generated using the IGV browser (Figure 16D-G). To validate the identified splicing events, we used radioactive PCR primers flanking the alternative splicing cassettes. The heat-induced exon 9 and exon 12 in ACSF2 and ATXN2, respectively were more included at 40 °C, while the exon 10A and exon 21, respectively were predominantly included at 32 °C. In GGCX, inclusion of exon 2 and exon 10 was increased at 40 °C, while in CD46 exon 7 and exon 12 are more included at 32 °C. Thus, the validation of the alternative exons confirmed the identified splicing events (Figure 17).

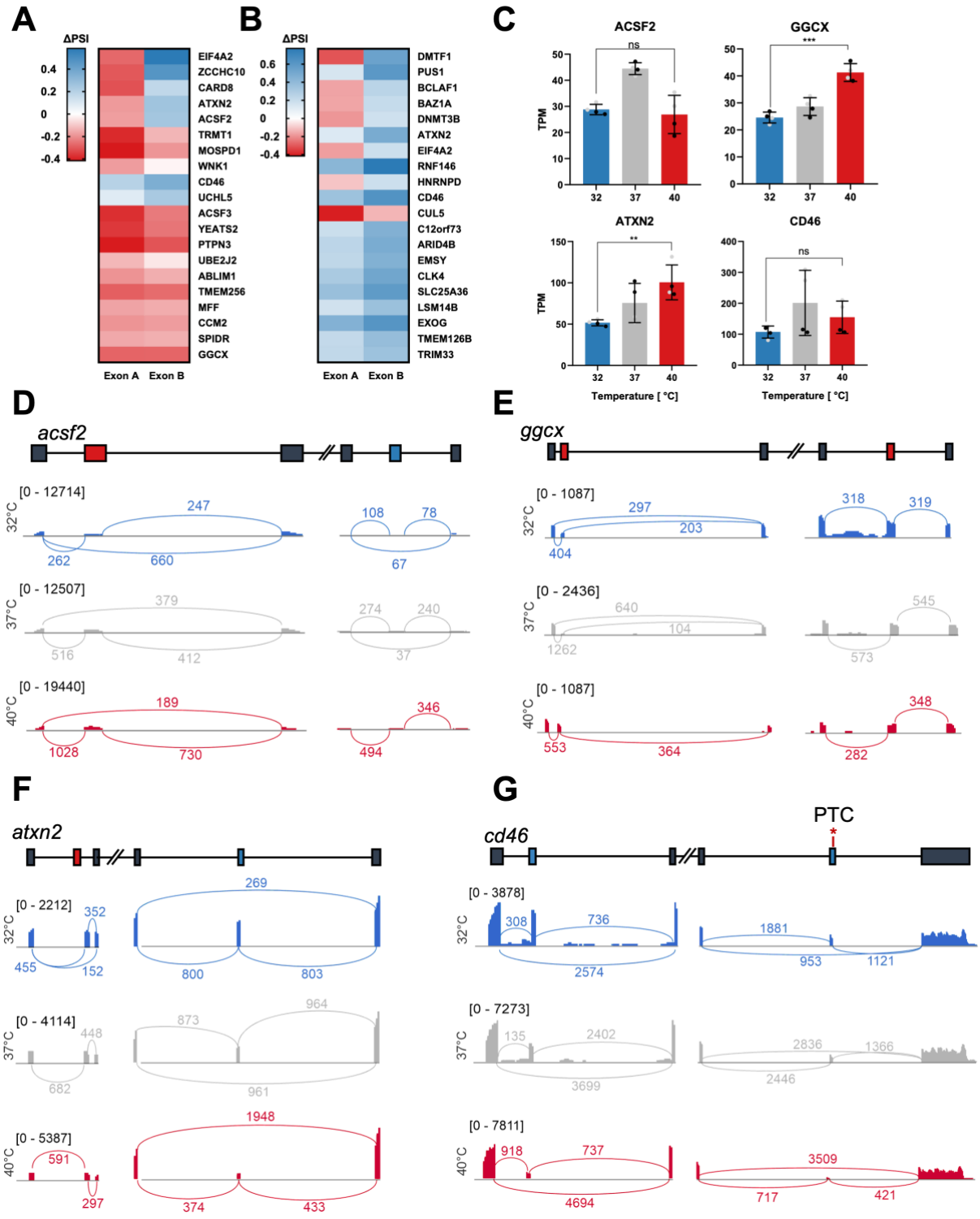

Figure 16. RNA-seq analysis of RNAs containing two temperature-dependent alternative exons
HeLa cells were incubated at 32 °C, 37 °C or 40 °C for 24 hours. Afterwards, RNA was extracted and analyzed by RNA-seq. **A** A heatmap of ΔPSI values of two temperature-dependent exon skipping events in one transcript in HeLa cells at 32 °C versus 40 °C is shown. Top 20 events were classified by the ΔPSI of the individual exons. **B** Same analysis of Hek293 cells at 35 °C versus 39 °C as shown in (A) with the RNA-seq data from Haltenhof *et al.* (2020). **C** Temperature-dependent gene expression does not correlate with the alternative splicing pattern of the selected targets from (A). Transcripts per million (tpm) values are plotted on the y-axis. Statistical significance was determined by an unpaired t-test. **p < 0.01, ***p < 0.001. n = 4 (mean ± SD). All individual data points from two independent samples (grey/black) are shown. Sashimi blots created using IGV genome browser for **D** ACSF2 **E** GCCX **F** ATXN2 **G** CD46 are shown. Above the sashimi blot exon/intron structures of each respective mRNA are shown. Red boxes show heat-induced exons, blue boxes illustrate cold-induced exons. Lines depict introns.

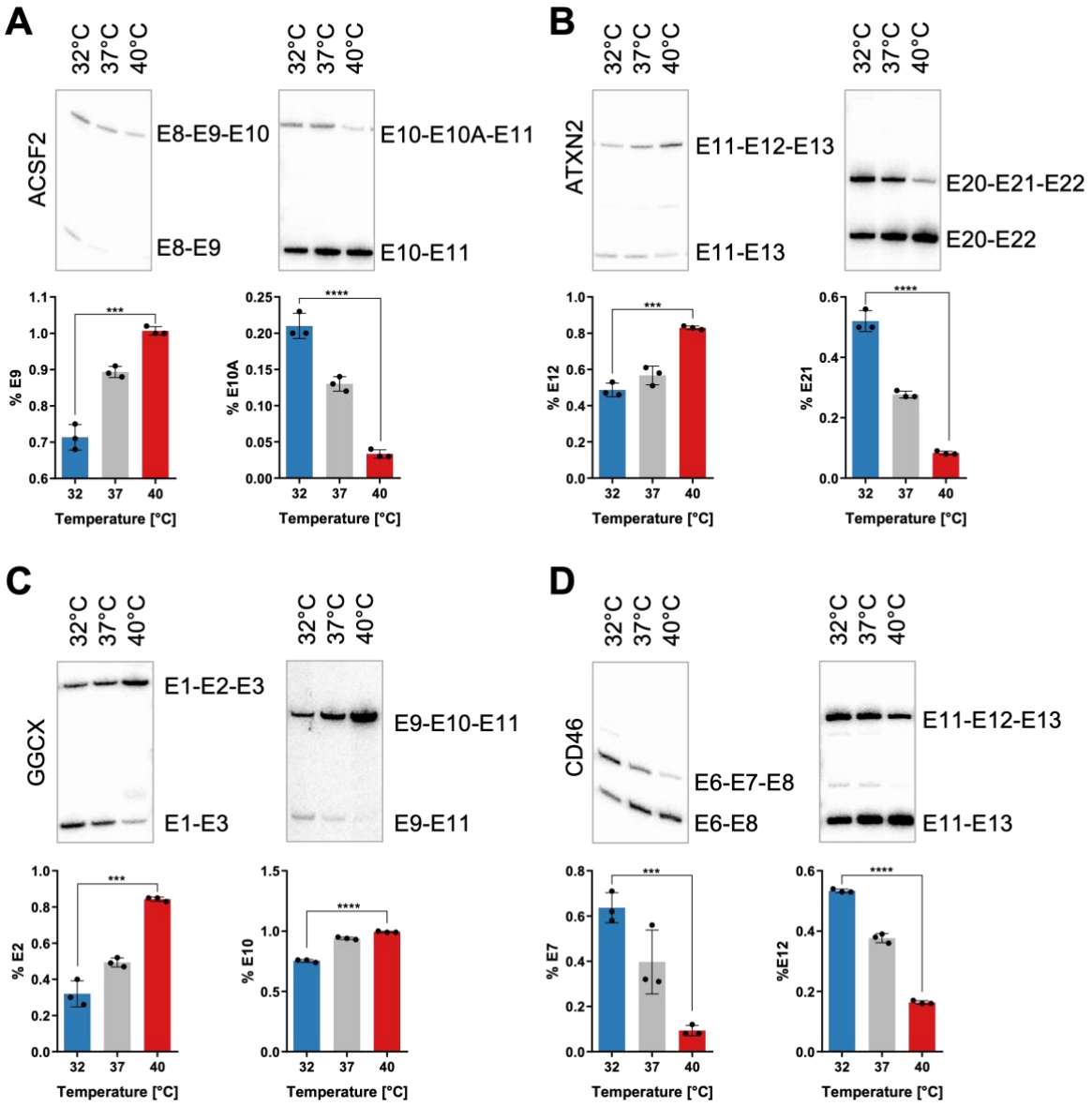

Figure 17. Validation of the temperature-dependent splicing of 2 alternative exons in one mRNA transcript
Validation of the selected genes from Figure 16. Radioactive splice-sensitive RT-PCR of HeLa cells cultured at the indicated temperatures is shown and quantified (n = 3, plotted are single replicate values). PCRs were performed with radioactively labeled forward and unlabeled reverse primers. The primers annealed to the respective upstream (forward) or downstream (reverse) exons of the alternatively spliced exons. **A**-**D** Upper panels show the representative splice PCRs. Lower panels show the quantifications of the splice PCRs, which confirm the alternative splicing in response to changes in temperature. Unpaired t-tests determined statistical significances which is indicated by asterisks: ***p < 0.001, ****p < 0.0001. All data points are shown.

Results

3.1.4 eIF4A2 AS is highly conserved across different species, cell lines and tissues

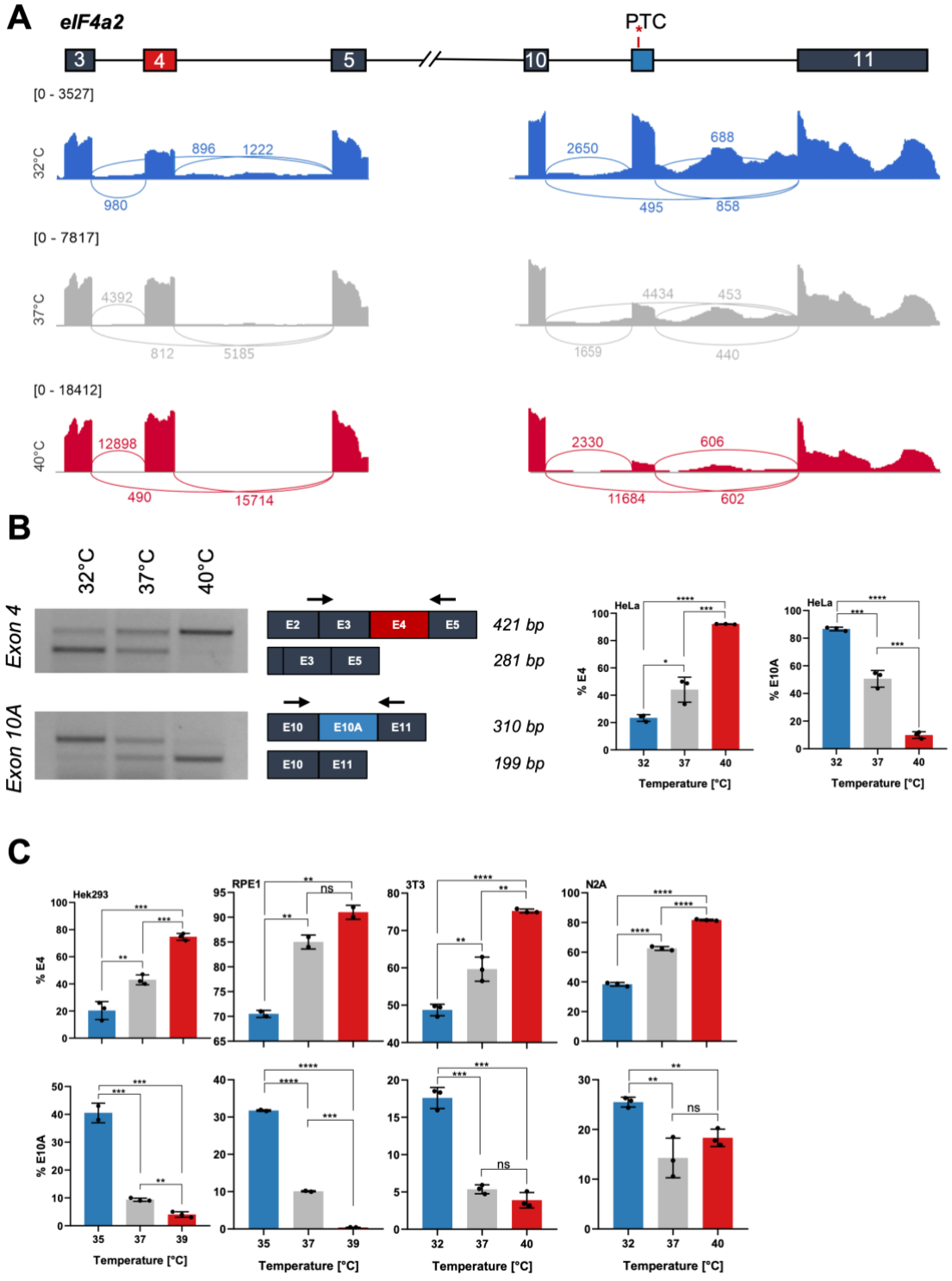

Figure 18. eIF4A2 contains two evolutionarily conserved alternative exons that are spliced in a temperature-dependent manner

A Sashimi plot illustrates two temperature-dependent alternatively spliced exons in eIF4a2. HeLa cells were incubated at 32 °C (blue), 37 °C (grey) or 40 °C (red) for 24 hours, analyzed by RNA sequencing, mapped to the human reference genome GRCh38/hg38 and visualized by IGV browser. The minimum junction coverage was set to 100. Above the simplified exon-intron structure is shown. The red box shows the heat-induced alternative exon 4, the blue box shows the cold-induced alternative exon 10A. The numbers connecting the exons indicate the exon-exon junction reads. **B** Splice-sensitive RT-PCR analysis of eIF4A2 exon 4 and 10A in HeLa cells. HeLa cells were incubated for 24 h at the indicated temperatures. RNA was isolated and analyzed by RT-PCR. Arrows mark sequence specific forward and reverse primers annealing to the upstream or downstream exons of alternative exon 4 or 10A, respectively. The right panel shows the quantification of the splice-sensitive RT-PCR for exon 4 (top) and exon 10A (bottom), which confirm the temperature response in eIF4A2 AS. **C** Quantification of eIF4A2 AS splicing by RT-PCR in indicated human and mouse cell lines using primers from (B). In (B) and (C), (mean ± SD) n = 3, unpaired t-test and significance is indicated by asterisks: *p < 0.05, **p < 0.01, ***p < 0.001, ****p < 0.0001. all individual data points are shown.

Since eIF4A2 contains two of the most strongly regulated exons, one heat- and one cold-induced exon, we wanted to take a closer look at these splicing events. Therefore, we plotted the RNA-sequencing data against the human reference genome GRCh38/hg38 and found a significant increase in inclusion reads with raising temperature for exon 4 (Figure 18A). The opposite effect could be observed for exon 10A. Here we see a significant decrease in inclusion reads with increasing temperature. To confirm these findings, a splice-sensitive RT-PCR on total RNA was performed (Figure 18B). Using sequence-specific primers flanking the alternative exons, we could reproduce the splicing pattern predicted in the sashimi plots for both exons.

For both alternative exons, we observed, a change in splicing levels from almost 0 to 100 % in response to increasing or decreasing temperatures, respectively. Exon 4 is almost 100 % included at 40 °C while it is almost completely skipped at 32 °C. For exon 10A we determined almost 100 % inclusion at 32 °C while it was almost completely skipped at 40 °C. These significant changes in splicing were observed in different human cell lines including HeLa, Hek293 and RPE1 (Figure 18C). Also, in the mouse fibroblast cell line 3T3 and the mouse neuronal cell line N2a, exon 4 and exon 10A were spliced in response to temperature. While splicing of exon 4 was similar in all observed cell lines and species, alternative splicing of exon 10A in N2a cell line differed somewhat from the other cell lines we examined. In N2a cells, the ΔPSI between 32 °C and 40 °C was lower compared to other cell lines. The data from our global RNA sequencing analysis of Hek293 and HeLa cells together with the splicing analysis in different human and mouse cell lines suggest ubiquitous and evolutionary conserved eIF4A2 alternative splicing in a temperature-dependent manner.

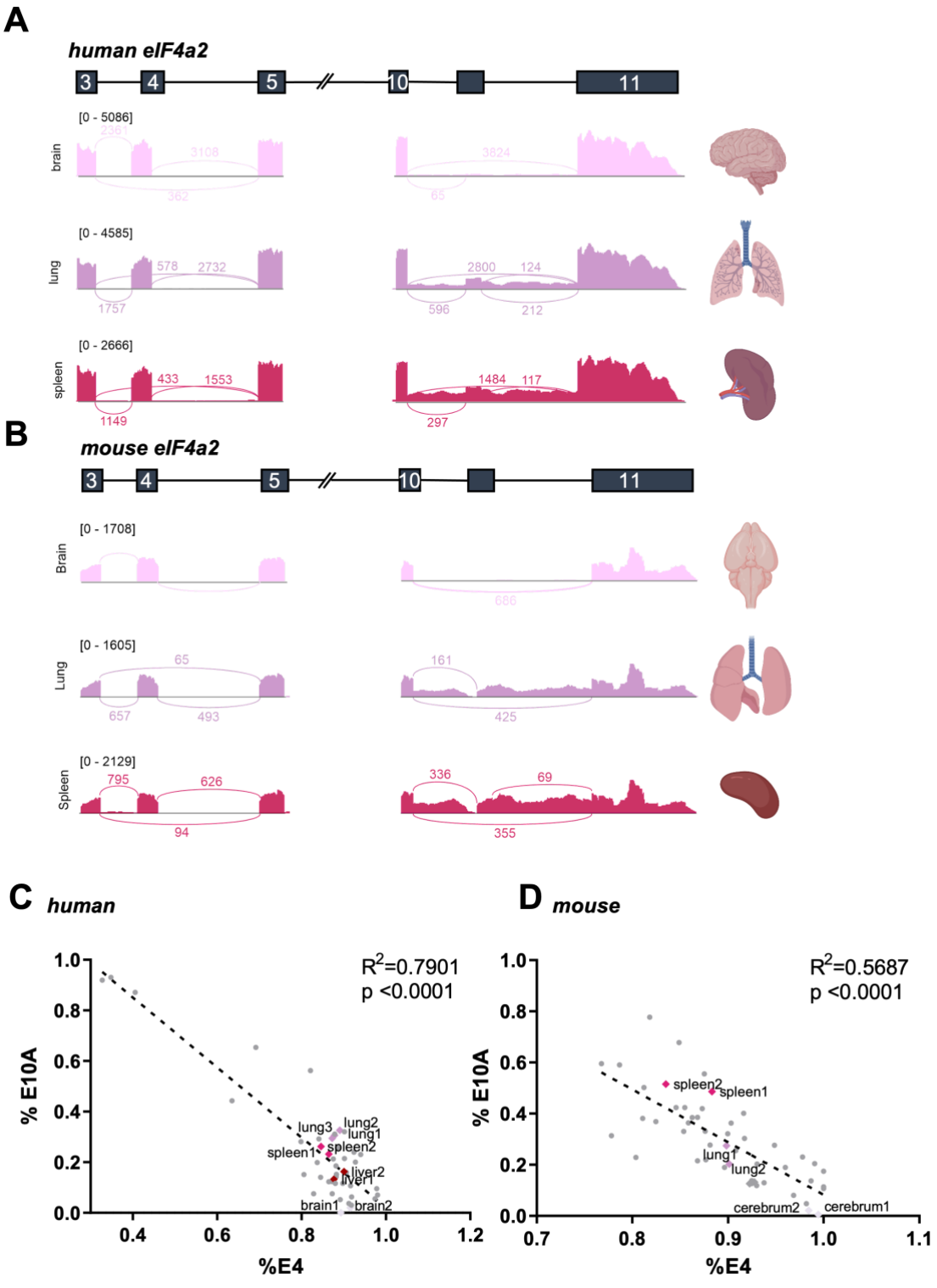

Figure 19. eIF4A2 alternative splicing of exon 4 and 10A is tissue specific
A, **B** Schematic exon/intron structure of the human (A) or mouse (B) eIF4A2 mRNA at the top. Boxes show exons; lines show introns. Below, Sashimi plots were visualized by the IGV browser and show the raw sequencing distribution. Minimum junction coverage was set to 50. **C**, **D** Correlation of exon 4 and exon 10A inclusion. The dashed line shows the linear regression, and the goodness of fits is indicated by R^2. In (C), human tissues are shown in two biological duplicates. In (D), mouse tissues are shown in two biological replicates. Human RNA-seq data were obtained from Fagerberg L *et al.* (2014) (PRJEB4337) and mouse RNA-seq data from Tanikawa *et al.* (2017) (PRJDB5738).

To test whether exon 4 and 10A of eIF4A2 are also regulated in a tissue-specific manner, we analyzed the splicing pattern of these two exons throughout publicly available RNA-sequencing data from different mouse and human tissues independent from temperature. The sashimi plots illustrate the splicing of

eIF4A2 exons 4 and 10A in three different (brain, lung and spleen) human and mouse tissues, respectively (Figure 19A, B). Indeed, we could observe that higher inclusion of exon 4 was accompanied by a lower inclusion of exon 10A, while exon 4 exclusion was associated with a higher exon 10A incorporation rate. Due to these findings, we wondered, if there is a connection between exon 4 and exon 10A splicing. We compared the PSI of exon 4 with the PSI of exon 10A over many human and mouse tissues and observed a significant linear correlation between the PSI of the two exons (Figure 19C, D). If exon 4 is more included, we observe less inclusion of exon 10A and the other way around. This could be found in divers human and mouse tissues.

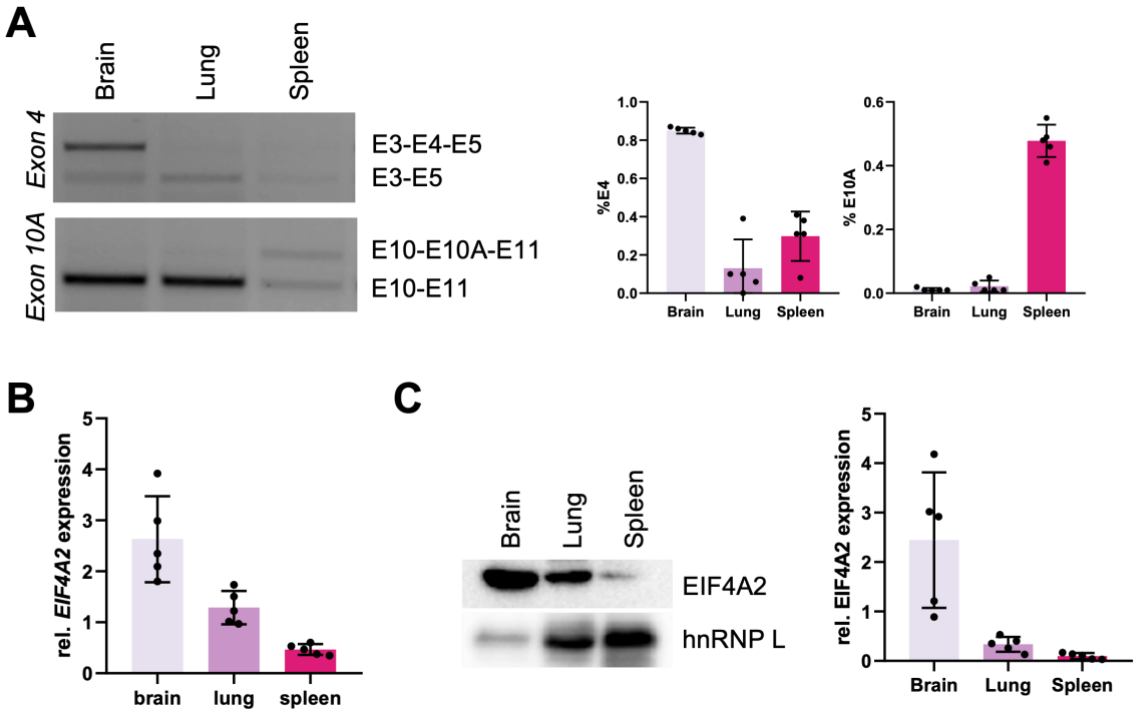

Figure 20. Validation of tissue-specific eIF4A2 exon 4 and 10A alternative splicing
Mouse tissues were homogenized, and RNA or total protein was extracted. **A** A splice-sensitive RT-PCR was performed with sequence specific forward and reverse primers annealing in the exons up- and downstream of either exon 4 or exon 10A and visualized on a 2 % agarose gel. The quantification is shown on the right. **B**, **C** RT-qPCR (B) and Western blot (C) analysis of eIF4A2 RNA and protein levels in different mouse tissues. In (B), RNA was isolated and subsequently analyzed by qPCR. eIF4A2 is shown relative to mHPRT levels. In (C), total protein lysates from five independent animals were investigated for eIF4A2 protein expression. hnRNP L served as a loading control. A representative blot is shown on the left and a quantification is shown on the right. All panels: mean ± SD; n = 5.

We then validated these findings by splice-sensitive RT-PCR and subsequently investigated eIF4A2 RNA and protein levels by RT-qPCR, and immunoblotting for the three different mouse tissues (Figure 20). In the brain, eIF4A2 showed almost 90 % exon 4 inclusion and exon 10A exclusion. In the lung, the inclusion levels of exon 4 and exon 10A were both at around 10 to 20 %. In the spleen, we observed a PSI of approximately 30 for exon 4 and 50 for exon 10A.

The eIF4A2 expression on RNA level was much higher in the brain, with an almost two-fold increase compared to the lung and a three-fold increase compared the spleen. These data suggest that alternative splicing of eIF4A2 produces differences in eIF4A2 expression levels in a tissue-specific manner.

Results

3.1.5 eIF4A2 is temperature dependent on genomic and proteomic level

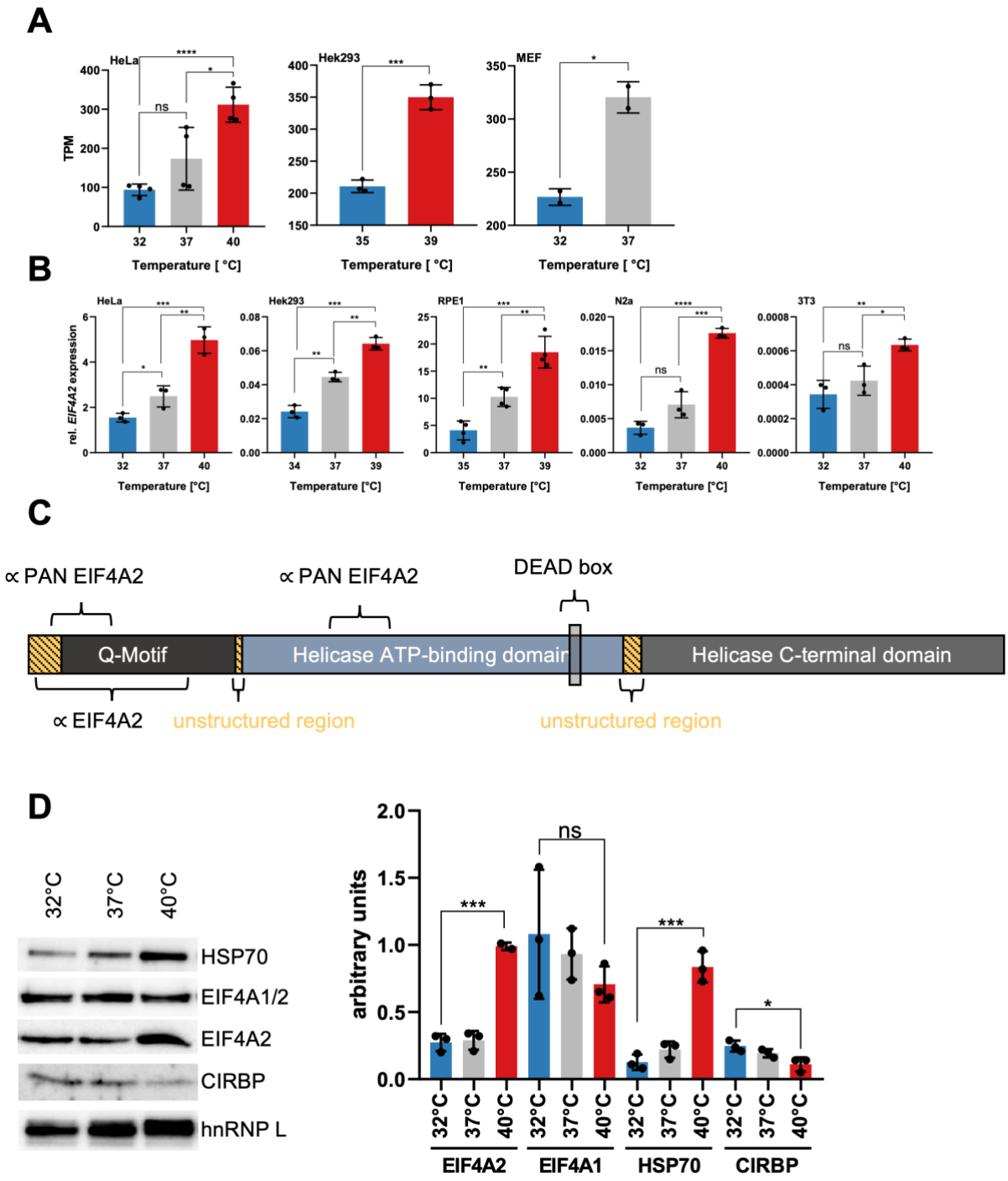

Figure 21. Temperature controls eIF4A2 mRNA and protein expression
A RNA-seq analysis of eIF4A2 mRNA expression in human and mouse cell lines at different temperatures. RNA-seq data for Hek293 cells were obtained from Haltenhof *et al.* (2020). RNA-seq data from mouse embryonic fibroblasts (MEF) were acquired from Liu *et al.* (2013). Transcript per million (tpm) values were calculated using Whippet 0.11 (Sterne-Weiler *et al.*, 2018). **B** RT-qPCR confirmed changes in eIF4A2 mRNA expression levels in response to temperature in human and mouse cell lines. eIF4A2 expression is in relation to Hprt levels. **C** Schematic representation of the eIF4A2 helicase structure comprising the Q-motif, the helicase ATP binding domain, and the helicase C-terminal domain. The isotopes recognized by the eIF4A2 and the pan eIF4A2 antibody are depicted. **D** Western blot analysis of eIF4A2 protein expression levels. HeLa cells were incubated at the indicated temperatures for 24 hours and the lysates were separated by 12 % SDS-PAGE. Proteins were subsequently blotted onto a nitrocellulose membrane and visualized using antibodies specific for the indicated proteins. For the quantification the intensities of the individual proteins were related to the hnRNP L signal, which is depicted on the right.

Due to the strong impact of temperature on the splicing of eIF4A2, we hypothesized that the eIF4A2 mRNA and protein expression follows the splicing pattern in the same temperature-dependent manner. Analysis of different publicly available RNA-sequencing datasets showed that eIF4A2 is strongly temperature dependent in mRNA expression throughout different cell lines and species (Figure 21A). mRNA levels significantly increased with temperatures above 37 °C and significantly decreased with temperatures below 37 °C. To validate these predictions, we performed RT-qPCRs with sequence-specific primers in human and mouse cell lines and could confirm the heat-induced upregulation of eIF4A2 in all tested cell lines (Figure 21B). Since the total amount of protein partly depends on the transcript levels, we wanted to test whether the response in eIF4A2 mRNA expression to temperature changes, observed in RNA-seq and RT-qPCR, also translated to the protein level. Indeed, immunoblotting of HeLa total protein lysates from 24-hour temperature shifts, revealed similar changes in eIF4A2 protein levels (Figure 21D). We detected an accumulation of eIF4A2 at 40 °C and a reduction at 32 °C. Due to the proteins high sequence similarity with eIF4A1, we tested different eIF4A2 antibodies to ensure the exclusive detection of the eIF4A2 protein. The eIF4A2 antibody from Santa Cruz reflected the temperature-dependent changes in eIF4A2 protein levels leading to the conclusion of a high antibody specificity (Figure 21C). The eIF4A2 antibody from Thermo Fisher did not reflect the response in temperature of eIF4A2. This suggests that this antibody detects eIF4A1 as well eIF4A2, evoking the impression that the eIF4A2 protein levels remain constant regardless of the temperature. As a control, we investigated the expression of the cold-inducible RNA binding protein CIRBP and the heat shock protein HSP70. The expression of these proteins was in line with our RNA-seq predictions and the results we obtained from RT-PCR and RT-qPCR. Taken together these data support our observation that eIF4A2 protein expression is strongly temperature dependent.

3.1.6 eIF4A2 is the only eIF4A paralogues regulated by alternative splicing

eIF4A belongs to the family of ATP-dependent RNA helicases and three paralogues (A1, A2 and A3) exist in mammals. 91 % of the amino acid sequences of eIF4A1 and eIF4A2 are identical and both function in translation initiation (Lu *et al.*, 2014). In comparison, eIF4A3 only shares 65 % identity on the amino acid level with eIF4A1 and eIF4A2 (Figure 9). We then analyzed the gene expression patterns of all three paralogues and observed temperature-dependent changes in mRNA expression in for eIF4A1, eIF4A2 and eIF4A3 (Figure 22A). While eIF4A1 shows a slightly higher mRNA expression at higher temperatures than its homologue eIF4A2, eIF4A3 is indicated to be more expressed at 32 °C compared to 40 °C. Furthermore, neither eIF4A1 nor eIF4A3 show a dramatic change in temperature, compared to eIF42A2. While eIF4A2 and eIF4A1 both show a heat-induced increase in their tpm values, eIF4A3 is significantly cold induced. This suggests that eIF4A1 and eIF4A2 are required under more similar conditions in contrast to eIF4A3.

We further wanted to investigate whether the eIF4A2 paralogues show similar splicing patterns in response to temperature as eIF4A2. For this purpose, we visualized the RNA-sequencing data from HeLa cells by generating Sashimi plots for eIF4A1 and eIF4A3 (Figure 22B, C). Both plots show no changes in inclusion or exclusion reads at different temperature conditions, suggesting that only eIF4A2 expression is regulated by temperature-dependent alternative splicing.

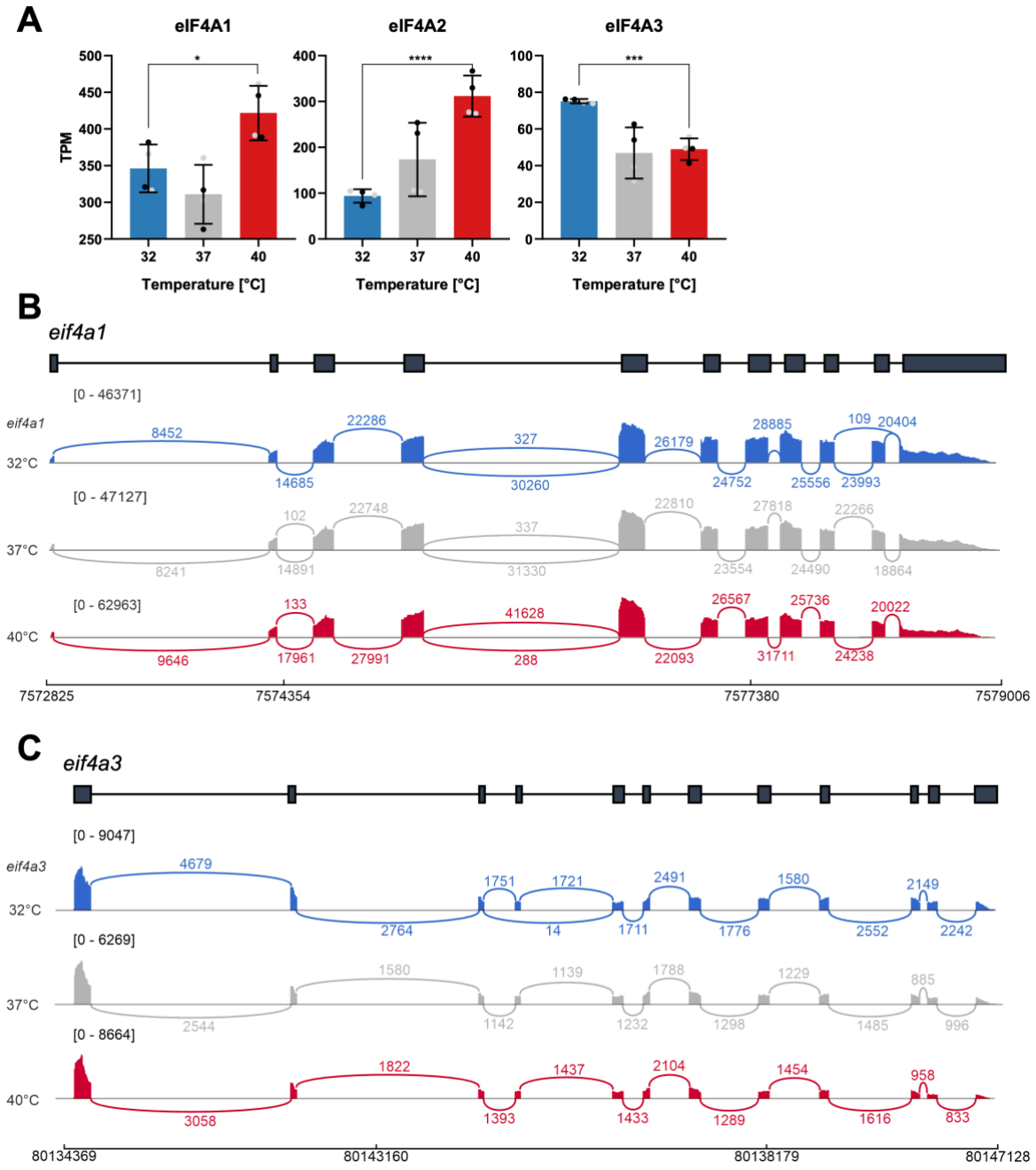

Figure 22. The eIF4A2 paralogues eIF4A1 and eIF4A3 are not regulated by alternative splicing in response to temperature

A The tpm values from RNA-seq data deriving from HeLa cells incubated at 32 °C, 37 °C and 40 °C for 24 hours were plotted for eIF4A1, eIF4A2 (as shown in Figure 16A) and eIF4A3. **B**, **C** For sashimi plots of eIF4A1 (B) and eIF4A3 (C) minimum junction coverage was set to 100 and the raw sequencing read distribution is shown. For each target, the exon/intron structure is shown above. The numbers connecting the exons indicate exon-exon junction reads. The different temperatures are represented by different colors: 32 °C (blue), 37 °C (grey) or 40 °C (red). The numbers below show the chromosomal coordinates of the respective gene.

3.2 Functional analysis of temperature-dependent splicing events in RBM3 and eIF4A2

To further investigate and understand the effects of temperature on alternative splicing, stable cell lines lacking the temperature-dependent exons were generated by a highly efficient CRISPR/Cas9 genome-editing system. Hek293 and HeLa cells were used as model systems for this purpose. As a first example, we analyzed the alternative splicing event in RBM3, which comprises the heat-induced exon 3a. In our global analysis we identified this exon as one of the strongest targets of temperature-dependent AS. Interestingly, this splicing event shows a great similarity to the splicing regulation of CIRBP, which has been thoroughly investigated by Haltenhof *et al.* (2020) and Neumann *et al.* (2020). These studies established CIRBP as an excellent representative for temperature-regulated AS-NMD and based on the parallels we observed between the two proteins, we expected similarly interesting findings for RBM3.

The analysis of RBM3-AS is followed by a large-scale transcriptomic and proteomic analysis of AS in eIF4A2. As this factor not only comprises one temperature-sensitive alternative exon, but two oppositely regulated temperature-dependent splicing events, we expect the underlying mechanism to be even more complex and the resulting data to be highly informative. Furthermore, we expanded previous research approaches by investigating the effect of these splicing events at protein level.

3.2.1 Temperature dependent RBM3 gene expression is regulated by exon 3a alternative splicing

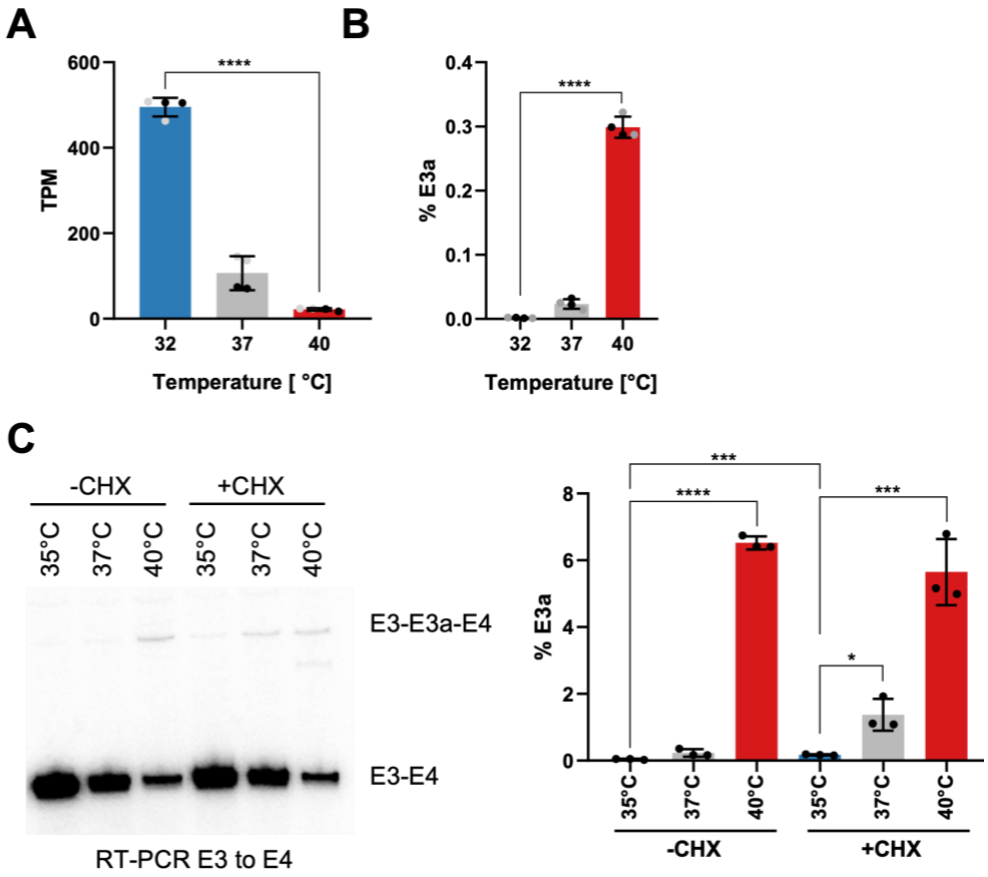

Figure 23. RBM3 contains an evolutionarily conserved uncharacterized alternative exon 3a, which is responsive to temperature
A RBM3 mRNA expression is shown by its tpm values at the indicated temperatures. RNA-sequencing data were obtained from HeLa cells incubated at 32 °C, 37 °C and 40 °C for 24 hours and analyzed with whippet 0.11 (Sterne-Weiler *et al.*, 2018). **B** The temperature-dependent splicing of RBM3 alternative exon 3a is shown. RNA-sequencing data from (A) were obtained and the exon 3a percentage spliced in (PSI) is shown on the y-axis. **C** Radioactive RT-PCR confirmed alternative splicing of E3a in response to temperature. Hek293 cells were incubated at the indicated temperatures and the translation inhibitor cycloheximide (CHX) was added for 4 hours. RNA was extracted and sequence specific splice primers mapping to the up- and downstream exon of E3a were used to analyze E3a alternative splicing. A quantification is shown on the right (n = 3, mean ± SD), unpaired t-test ruled out significance (indicated by asterisks): *p < 0.05, ***p < 0.001, ****p < 0.0001 all individual data points are shown.

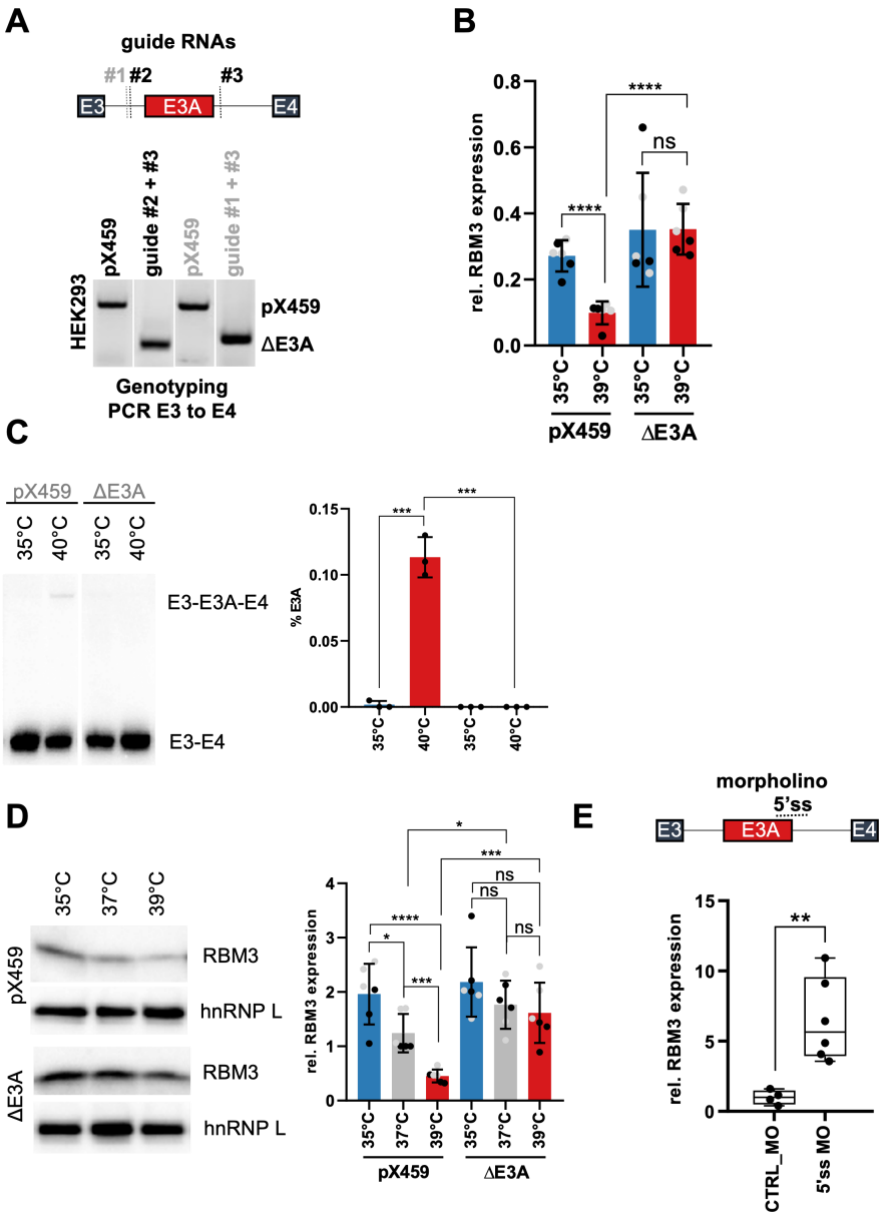

Figure 24. Temperature-dependent RBM3 mRNA and protein expression is controlled by exon 3a
A Top: schematic exon/intron structure of RBM3 exon 3 to exon 4. Intron specific guide RNAs lead to CRISPR/Cas9-mediated removal of RBM3 alternative exon 3a. Therefore, either guide RNA #1 or #2 (targeting upstream intron sequences) were co-transfected with the downstream targeting guide RNA #3 in Hek293 cells. Bottom: confirming positive clones by genotyping PCR. pX459 transfected cells serve as negative control. **B** RBM3 expression levels in Hek293 CRISPR/Cas9-edited cells were analyzed by RT-qPCR using sequence-specific primers. Total RNA was extracted from clonal cell lines incubated at the indicated temperatures for 24 hours and RBM3 mRNA expression levels are shown in relation to GAPDH levels. **C** To confirm RBM3 exon 3a removal by radioactive RT-PCR, cells from (A) were incubated at 35 °C and 40 °C and alternative splicing was analyzed using sequence-specific primers annealing to the up- and downstream exons of E3a. A quantification is shown on the right, n = 3 (mean ± SD) unpaired t test indicates significance: ***p < 0.001. **D** For western blot analysis of cells from (A), lysates were blotted onto a nitrocellulose membrane and RBM3 expression levels were detected in control and exon 3a knockout cells. The cells were incubated at 35 °C, 37 °C or 39 °C and total protein was extracted. The quantification is shown on the right (mean ± SD, n = 6 (3 per clone, indicated in black/grey)), all individual data points are shown). The statistical significance was determined by unpaired t-tests and is indicated by asterisks *p < 0.05, ***p < 0.001, ****p < 0.0001 **E** The exon/intron structure of RBM3 exon 3 to exon 4 indicates the location of a 5'SS blocking morpholino (MO) (top). 48 hours after MO transfection, RNA was extracted from Hek293 cells and analyzed by RT-qPCR. RBM3 expression is shown relative to GAPDH levels and normalized to a non-targeting MO control (bottom). The statistical significance was determined by unpaired t-test and is indicated by asterisks: **p < 0.01 (n = 4-6).

RBM3 contains an alternative exon between the two constitutively spliced exons 3 and 4. In a global analysis, RBM3 exon 3a was predicted as to be one of the strongest heat-induced alternative splicing events in the human HeLa cell line. RNA-seq analysis showed a significant increase in RBM3 mRNA expression at 32 °C compared to 37 °C and 40 °C after 24 hours of incubation at the mentioned temperatures (Figure 23A). In contrast, exon 3a has a significantly higher PSI at 40 °C compared to

lower temperatures such as 37 °C or 32 °C (Figure 23B). RBM3 responds to temperature on splicing and transcriptomic level. A splicing-sensitive radioactive RT-PCR confirmed the inclusion of exon 3a at higher temperatures and the stabilization of this mRNA isoform after four hours of incubation with CHX (Figure 23C). The increase of the exon 3a inclusion isoform was mainly visible at 32 °C. As exon 3a was almost 100 % excluded at lower temperatures, a significant increase or additional stabilization of the exon 3a isoform is possible at 32 °C. The strong increase in the exon 3a inclusion levels upon addition of CHX suggest an NMD-mediated degradation of the exon 3a isoform. Taken together, we confirmed exon 3a as a direct target for the mRNA surveillance pathway.

CRISPR/Cas9-mediated genome editing was used to generate two stable Hek293 cell lines lacking RBM3 exon 3a (Figure 24A). We used two different guide RNAs complementary to the upstream intron and one which binds to the downstream intron of exon 3a to cause permanent exon skipping. A genotyping PCR was performed to confirm the absence of exon 3a on genomic level, using primers in the exon 3a flanking introns. To confirm exon 3a as the main factor in the temperature-dependent control of RBM3 mRNA expression, we performed RT-qPCRs comparing the transcript levels in the control cell lines pX459 with the exon 3a knockout cell lines (Figure 24B). We investigated two independent exon 3a knockout cell lines to reduce CRISPR/Cas9-mediated artefacts. While the control cell lines still showed RBM3 expression in a temperature-dependent manner, this was abrogated in the exon 3a knockout cell lines. Instead, these cell lines showed a constantly high RBM3 mRNA expression level, which resembled the level at lower temperatures in the control cell lines. To further validate this, we performed a radioactive splice-sensitive RT-PCR with the same primers as used in the previous experiment (Figure 24C). We observed a similar splicing pattern in the control cell lines as we did in Hek293 wild-type cells. A weak exon 3a inclusion band at its predicted height was observed at 40 °C but not at 35 °C. The exon 3a knockout cell line showed no exon 3a inclusion band regardless of the temperature or the presence of CHX. This proves the successful knockout of exon 3a via the CRISPR/Cas9 system.

3.2.2 Generation of RBM3 CRISPR/Cas9-edited cell line could be validated on protein level

As we already confirmed the RBM3 exon 3a knockout in the CRISPR/Cas9-genome edited cell lines on DNA and RNA level, we also wanted to investigate the effect of exon skipping on protein expression. Immunoblotting of total Hek293 protein lysates with an RBM3-specific antibody showed similar changes to those seen for RBM3 mRNA expression (Figure 24D). An accumulation of RBM3 protein in the cell lines lacking exon 3a was observed regardless of temperature. As a proof of principle, we further transfected a splice-site blocking morpholino (MO), directed against the 5'SS of RBM3 exon 3a, into Hek293 cells (Figure 24E), which increased RBM3 mRNA levels substantially. This confirmed that the expression of RBM3 can be controlled in trans by targeting exon 3a splicing.

Taken together, these data provide strong evidence for splicing-controlled RBM3 expression by its temperature-responsive exon 3a.

3.2.3 The alternative splicing of the eIF4A2 exons 4 and 10A is regulated by temperature

To address the involvement of the eIF4A2 exons 4 and 10A in temperature-controlled eIF4A2 mRNA expression, we performed CRISPR/Cas9-mediated genome editing to generate Hek293 and HeLa cell lines lacking exon 4 or exon 10A (Figure 25A). We used two different guide RNAs complementary to the upstream and downstream intron of exon 4 and exon 10A, respectively, to cause permanent exon skipping. In HeLa cells, we created two independent homozygous cell lines lacking exon 4 or exon 10A respectively. Additionally, two control HeLa cell lines were obtained from empty vector-transfected (pX458) cells (Figure 25B). In Hek293 we generated four homozygous cell lines lacking exon 4 or exon 10A respectively and two control cell lines generated via transfection of the empty vector (pX459).

The absence of exon 4 or 10A, respectively, was confirmed by genotyping PCR (Figure 25B). To further investigate temperature-sensitive AS in our HeLa CRISPR/Cas9-generated cell lines, we performed an RNA-sequencing analysis (Figure 25C). We obtained RNA-seq data from two independent clones of the exon 4 knockout, the exon 10A knockout, and the control cell line, respectively.

Results

Technical duplicates of each CRISPR cell line were analyzed. Therefore, cells were incubated at 32 °C, 37 °C or 40 °C for 24 hours and total RNA was extracted and subsequently DNAse I digested. The obtained RNA sequencing data confirmed the absence of either exon 4 or exon 10A in the respective cell lines. The control cell lines showed a temperature response similar to HeLa and Hek293 wild-type cells. The temperature-responsive splicing pattern of exon 4 was almost abolished in the absence of exon 10A. While exon 4 inclusion levels were between 90 and 100 %, regardless of the temperature in the exon 10A knockout cell line, the exon 4 inclusion level in the control cell line at 32 °C was only around 60 %. The PSI of exon 10A in the absence of exon 4 decreased about 50 % from 32 °C to 40 °C. This suggests a co-regulation of these two alternatively spliced exons which is consistent with our previous findings in human and mouse tissues (Figure 19).

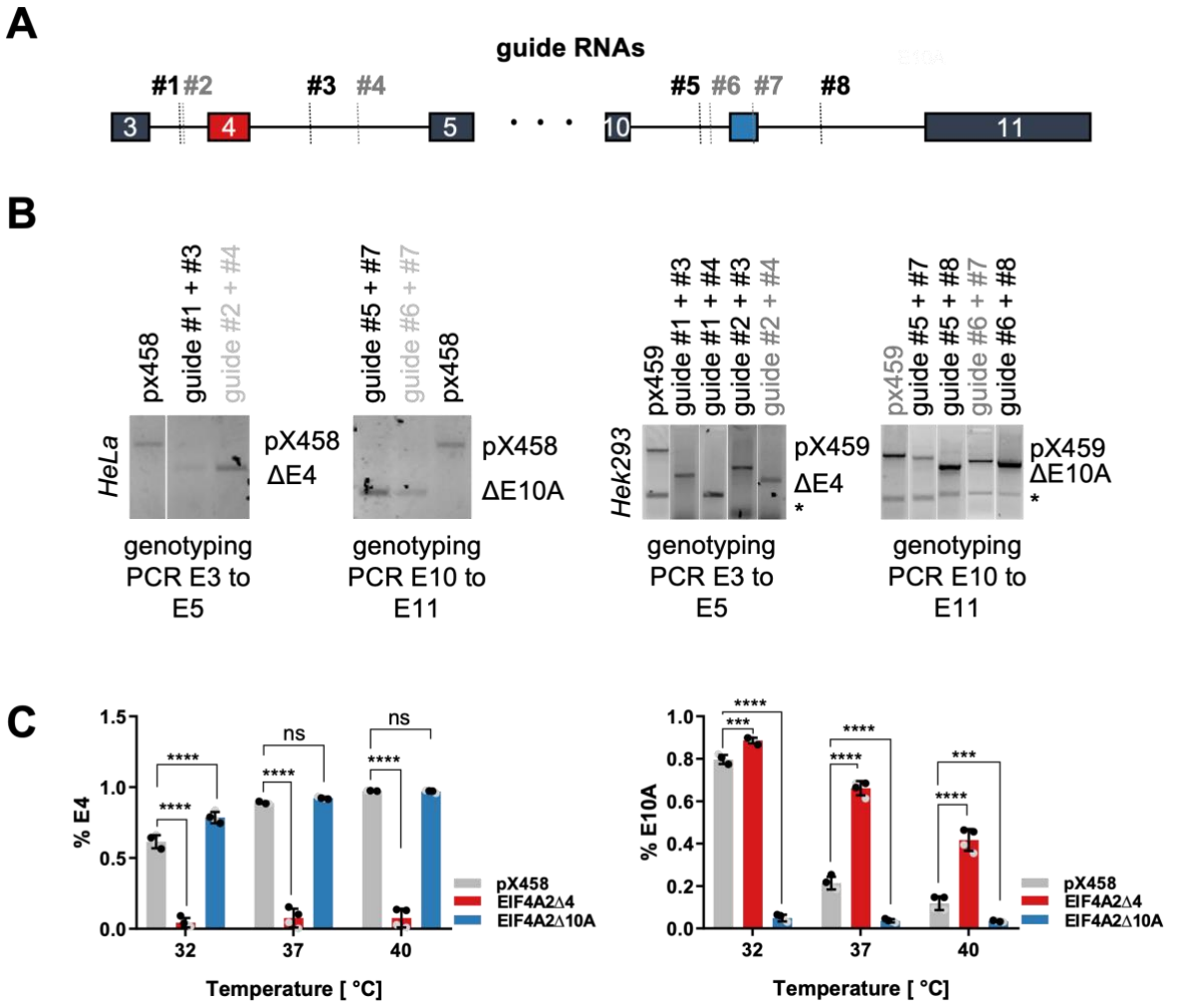

Figure 25. Generation of CRISPR/Cas9-edited HeLa and Hek293 cell lines lacking either alternative exon 4 or 10A

A Schematic exon/intron structure of eIF4A2. The red box highlights heat-induced alternative exon 4; the blue box illustrates cold-induced exon 10A. Each combination of one sequence-specific guide RNA targeting the upstream intron of either exon 4 or exon 10A (#1, #2 or #5, #6) was co-transfected with one of the two guide RNAs (#3, #4 or #7, #8) targeting the downstream intron. **B** The genotyping PCR after clonal selection confirmed successful exon knockout. pX458 transfected HeLa cells (left) or pX459 transfected Hek293 cells (right) served as negative controls. **C** The clonal cell lines from (B) were incubated at 32 °C, 37 °C or 40 °C for 24 hours. The RNA was extracted and further analyzed by RNA-seq confirming the complete removal of exon 4 or exon 10A. **C** The PSI values of exon 4 (left) and exon 10A (right) are shown for the two clonal cell lines (n = 4, mean ± SD, 2 per clone). An unpaired t-test was performed, and the calculated significance is indicated by asterisks: *p < 0.05, **p < 0.01, ***p < 0.001, ****p < 0.0001. All individual data points are shown by clone specific colors (black/grey).

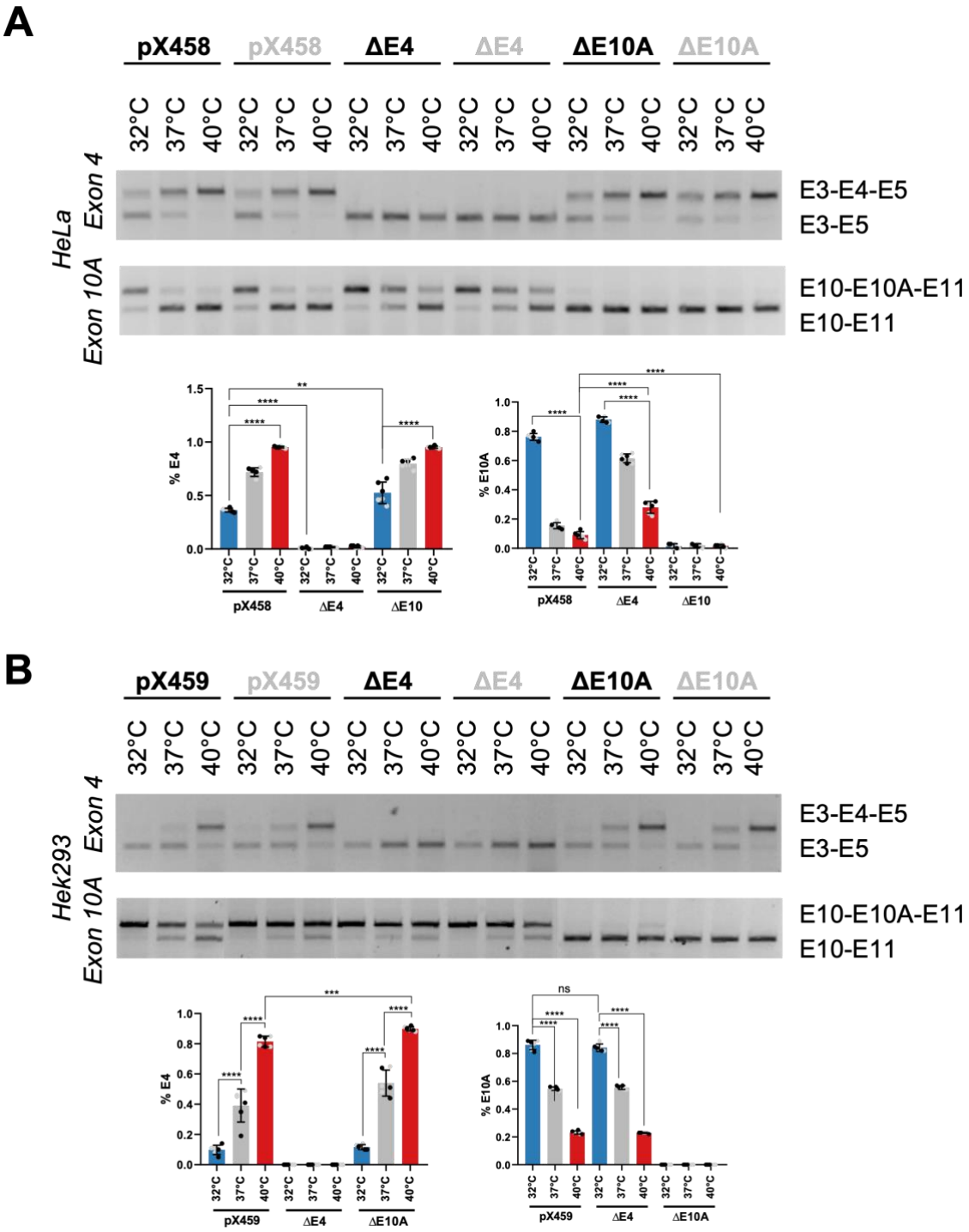

Figure 26. Validation of CRISPR/Cas9-edited eIF4A2 exon 4 and exon 10A knockout cell lines
To confirm CRISPR/Cas9-mediated removal of either eIF4A2 exon 4 or exon 10A, the clonal cell lines from Figure 25 were incubated at the indicated temperatures and RNA was extracted and analyzed by a splice-sensitive RT-PCR using exon-specific primers. **A**, **B** Top: The representative RT-PCR analysis of eIF4A2-edited HeLa (A) and Hek293 (B) cell lines was visualized on a 2 % agarose gel. Individual clonal cell lines are shown. Bottom: Quantification of percentage spliced in (PSI) for exon 4 (left) and exon 10A (right). (n = 6, mean ± SD, 3 per clone), unpaired t-test and significance is indicated by asterisks: *p < 0.05, **p < 0.01, ***p < 0.001, ****p < 0.0001 all individual data points are shown.

Further validation of the CRISPR/Cas 9-edited cell lines was performed by splicing sensitive RT-PCR on total RNA. We incubated the HeLa and Hek293 CRISPR/Cas9-edited cell lines at 32 °C, 37 °C or 40 °C for 24 hours and extracted the total RNA. For the splice PCR, sequence-specific primers binding in the constitutive exons upstream and downstream of the respective alternative exon were used (Figure 26). In both, HeLa and Hek293 control cell lines, expression of the exon 4 containing isoform was

increased at higher temperatures, concomitant with a decrease of the variant lacking exon 10A. In the exon 4 knockout cell lines, we could only detect the isoform containing exon 3 and exon 5. This proves the complete absence of exon 4 in this knockout cell lines on RNA level. In the exon 10A knockout cell lines, the same exon 4 splicing pattern as in the control cell lines was observed.

Analysis of exon 10A splicing in the control cell lines showed a decrease of the isoform containing exon 10, 10A and 11, concomitant with an increase of the isoform lacking exon 10A in response to increasing temperatures. The exon 10A inclusion levels at 37 °C and 40 °C were significantly increased in the exon 4 knockout cell lines compared to the control. These findings suggest that exon 10A splicing is co-regulated with that of exon 4. As the exon 10A inclusion level was nearly 100 % at 32 °C, this temperature appears to mark the thermoregulatory limit of exon 10A splicing. Therefore, the co-regulatory effect of exon 4 on 10A is visible only at higher temperatures (37 °C & 40 °C). In the exon 10A knockout cell lines, we observed only the isoform containing exon 10 and exon 11, regardless of temperature, which proves the absence of exon 10A on the RNA level.

3.2.4 The two alternative exons in eIF4A2 are co-regulated

The RNA-sequencing data suggest that exon 4 and exon 10A alternative splicing is co-regulated or coupled. Therefore, we designed minigene constructs containing the region from exon 2 to exon 5 or exon 10 to exon 11, respectively (Figure 27A). Minigenes contain the genomic sequence of interest, including surrounding constitutive and alternatively spliced exons and the flanking introns and are cloned to eukaryotic expression constructs (Cooper, 2005). Because minigenes contain intronic sequences, they undergo splicing. The minigenes were transfected into HeLa and Hek293 cells, respectively and incubated at 32 °C and 40 °C for 24 hours. Additionally, both minigenes were co-transfected to investigate the impact of one alternative splice event on the other. Radioactive splice-sensitive RT-PCR was performed to determine the minigene splicing products (Figure 27B, C). Overall lower PSI values were obtained compared to the endogenous splicing analysis, suggesting an artificial effect of the minigene constructs. In HeLa cells, the results demonstrated that the PSI of exon 4 increased from 5 % to 20 % in response to the temperature shift from 32 °C to 40 °C, while the PSI of exon 10A decreased from 30 % to almost 0 %. Similar effects could be obtained in Hek293 cells. In the presence of exon 10A, the temperature-dependent alternative splicing of exon 4 remained unaltered. In the presence of exon 4 however, the PSI of exon 10A was reduced from 30 % to 20 % at the lower temperature. The difference in exon 10A inclusion efficiency suggests that exon 4 impacts exon 10A splicing, while exon 10A only marginally effects the PSI of exon 4. The fact that we could observe differences in splicing of exon 10A upon co-transfection of the two minigenes suggests that a competition for trans-acting factors is involved in the coupling of exon 4 and 10A splicing.

Taken together, our data indicate a potential coupling of exon 4 and exon 10A splicing in human and mouse tissues and cell lines, respectively. However, it is not entirely clear whether this coupling is uni- or bidirectional, but the influence of exon 4 on splicing of exon 10A appears to be more significant than the other way around. Furthermore, that fact that our minigenes could recapitulate the impact of temperature on splicing of exon 4 and 10A individually as well as cooperatively, proves that the previously observed effects were not cell type or tissue-specific, but universally abundant.

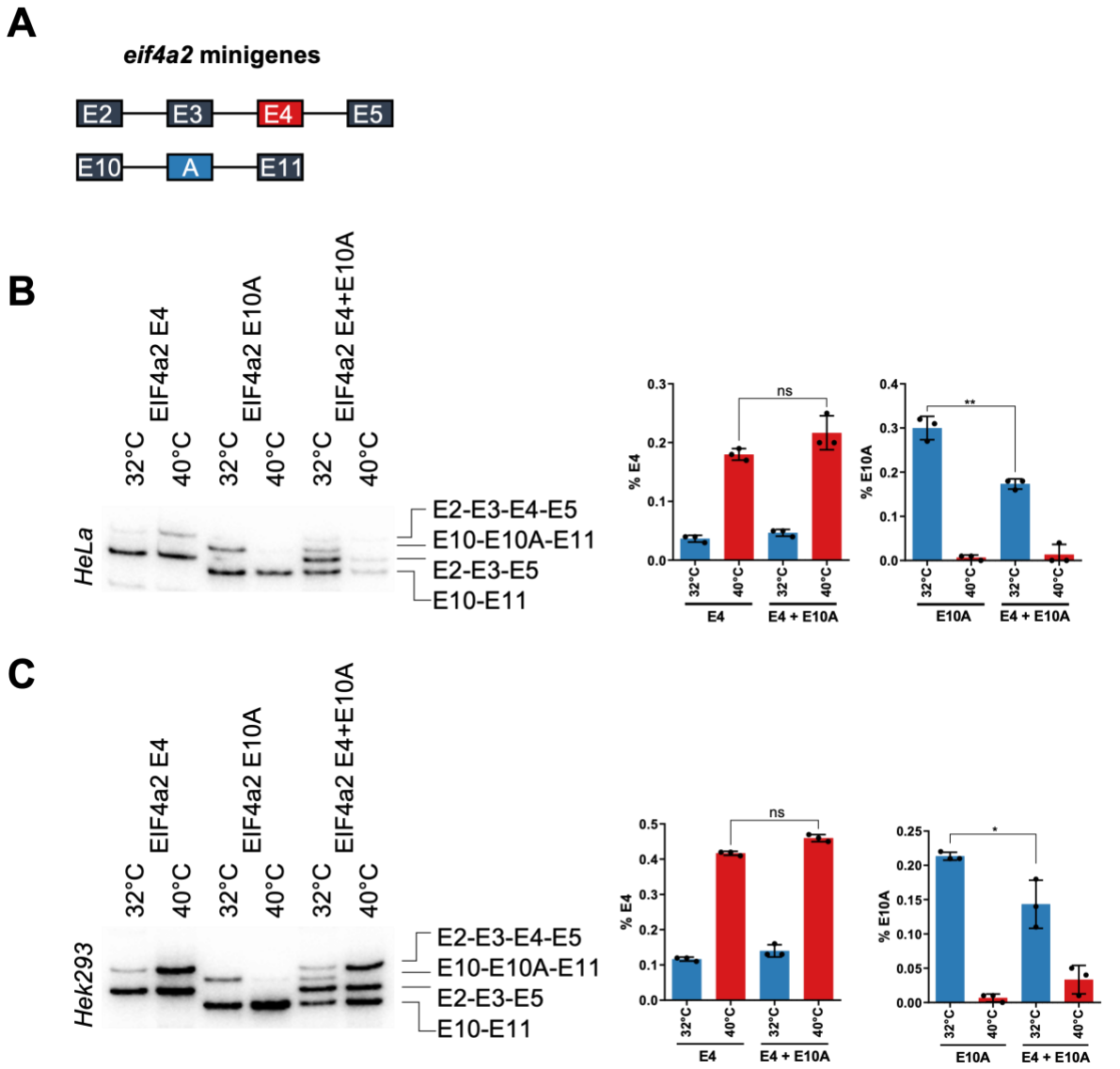

Figure 27. eIF4A2 alternative exon 4 impacts splicing of exon 10A
A A schematic exon/intron structure of an eIF4A2 minigene including either one of the two alternative exons is depicted. Highlighted in red is the heat-induced alternative exon 4 and in blue is the cold-induced alternative exon 10A. The minigene for exon 4 contains the whole unmodified sequence form exon 2 to exon 5 and the minigene for exon 10A from exon 10 to exon 11. **B**, **C** The eIF4A2 exon 4 and exon 10A minigenes recapitulate alternative splicing regulated by temperature. HeLa (B) and Hek293 (C) cells were transfected with eIF4A2 exon 4, exon 10A or co-transfected exon 4 and exon 10A minigenes and incubated at the indicated temperatures for 24 hours. RNA was extracted and radioactive exon-specific primers were used to analyze alternative splicing by RT-PCR (left). The quantification is shown on the right (n = 3, mean ± SD); unpaired t-test and significance is indicated by asterisks: *p < 0.05, **p < 0.01, all individual data points are shown.

3.2.5 eIF4A2 mRNA expression is coupled to nonsense-mediated decay

To see what effect the investigated splicing events, have on mRNA abundance, we studied our RNA-sequencing data in more detail. As previously observed for diverse untreated cell lines, our RNA-seq data indicated a substantial increase in eIF4A2 mRNA expression with increasing temperatures in the control cell lines. This suggests that the CRISPR/Cas9 genome editing did not evoke significant artificial effects (Figure 28).

The cell lines lacking exon 4 showed no response to temperature and the eIF4A2 mRNA level was overall reduced and resembled that of the control cell lines at 32 °C. The opposite was observed for the cell lines lacking exon 10A, where we observed a constantly high eIF4A2 expression level, which was even higher than that found in the control cell lines at 40 °C. Additionally, the absence of exon 10A caused the loss of temperature sensitivity in eIF4A2 mRNA expression. This suggests a direct effect of exon 4 and exon 10A splicing on the eIF4A2 mRNA levels.

Results

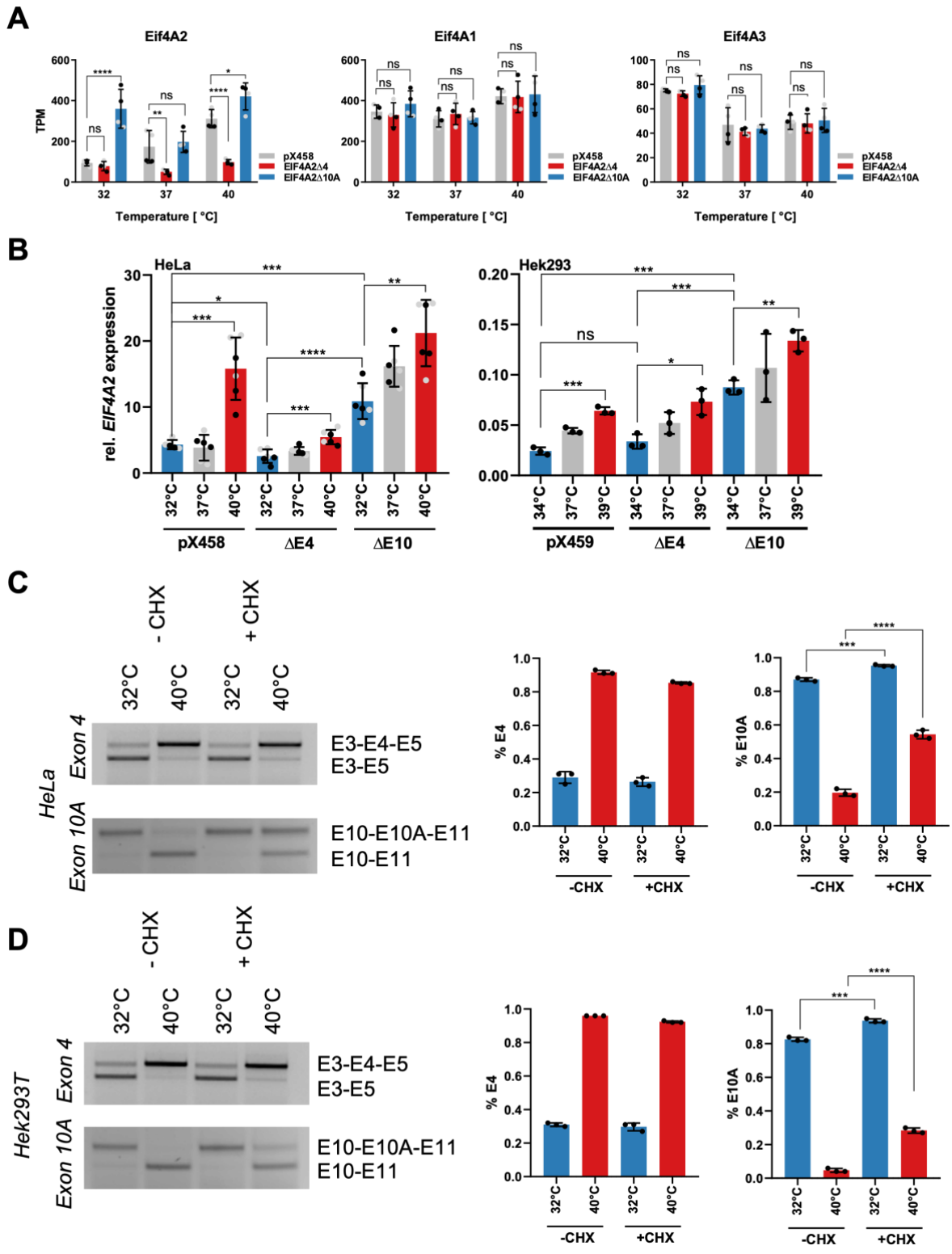

Figure 28. The eIF4A2 poison exon 10A controls eIF4A2 mRNA expression in HeLa and Hek293 cells
A RNA-sequencing analysis of eIF4A2 (left), eIF4A1 (middle) and eIF4A3 (right) gene expression in CRISPR/Cas9-edited eIF4A2 HeLa cells. For each target, transcripts per million values are shown. (n = 4, mean ± SD, 2 per clone) **B** eIF4A2 expression is investigated by RT-qPCR. Therefore, clonal cells from Fig 25 were incubated at the indicated temperatures for 24 hours and total RNA was extracted. eIF4A2 expression in HeLa (left) and Hek293 (right) cells is shown relative to HPRT levels. **C**, **D** Splice sensitive RT-PCR analysis of HeLa (C) and Hek293 (D) cells incubated at the indicated temperatures with DMSO or the translation inhibitor cycloheximide (CHX) for 4 hours. Upper panel shows exon 4 splicing, lower panel shows exon 10A splicing, which was visualized on a 2 % agarose gel. The quantification on the right shows the PSI of exon 4 (left) and exon 10A (right). For all panels an unpaired t-test was performed, and the calculated significance is indicated by asterisks: *p < 0.05, **p < 0.01, ***p < 0.001, ****p < 0.0001 all individual data points are shown.

As it remains unclear whether eIF4A2 can be functionally replaced by its paralogues (eIF4A1 and eIF4A3), we investigated mRNA expression of eIF4A1 and eIF4A3, upon loss of exon 4 or exon 10A, respectively. Our RNA-seq data did not indicate differential expression of eIF4A1 or eIF4A3 mRNA in the exon 4 or exon 10A knockout cell lines compared to the control cell lines, suggesting that the absence of exon 4 or exon 10A in eIF4A2, respectively do not alter the eIF4A1 and eIF4A3 mRNA expression.

To further validate these predictions, we performed RT-qPCR on HeLa and Hek293 mRNA. In both cell lines, the eIF4A2 mRNA expression was increased in response to the raising temperature (Figure 28B). In HeLa cells, the absence of exon 4 resulted in a reduced eIF4A2 expression compared to the control cells. This was not the case in Hek293 cells, suggesting cell type-specific effects on the eIF4A2 gene expression. In both, the HeLa and Hek293 exon 10A knockout cell lines, the eIF4A2 mRNA expression was significantly higher than in the control cell lines. Taken together, these findings were in line with what we observed in the RNA-sequencing data.

Analysis of the two alternative exons of eIF4A2 revealed a PTC in exon 10A. Inclusion of exon 10A leads to the inclusion of the PTC into the mRNA sequence. The concomitant exclusion of exon 4 leads to a frameshift, resulting in the inclusion of another PTC in exon 5. Therefore, exon 4 and 10A could be identified as potential NMD targets. To investigate whether these splicing events are indeed coupled to NMD, we treated the cells with CHX, which is an established translation inhibitor. In both, HeLa and Hek293 cells, inclusion of exon 4 was not altered in the presence of CHX compared to the DMSO treated cells (Figure 28C). In contrast, we observed a minor increase of the exon 10A isoform at 32 °C and a substantial accumulation at 40 °C in the presence of CHX. As exon 10A is almost to 100 % included at lower temperatures, an increase or additional stabilization of this isoform is barely possible under this condition. Nevertheless, these findings suggest that the exon 10A isoform is most likely degraded via the NMD pathway, irrespective of the temperature.

Taken together, we confirmed exon 10A but not exon 4 as a direct target for the mRNA surveillance pathway.

3.2.6 Temperature-dependent splicing of the alternative exons 4 and 10A impacts eIF4A2 protein expression

Since transcript levels are a major factor influencing the final amount of expressed protein, we wanted to test, whether the knockout of exon 4 or exon 10A affects the abundance of the eIF4A2 protein. By immunoblotting protein lysates from HeLa and Hek293 eIF4A2 CRISPR/Cas9-edited cells, we could observe similar changes to those seen in previous experiments on mRNA level (Figure 29). The two control cell lines both showed a strong temperature-controlled eIF4A2 expression. Detection of eIF4A2 with a paralogue-specific antibody in the exon 4 knockout lysates, showed that the eIF4A2 protein was not detectable at any temperature condition, suggesting that protein expression could not be induced by heat in the absence of exon 4. These data suggest that the absence of exon 4 does not allow formation of a protein. In contrast, the eIF4A2 protein was highly expressed in all exon 10A knockout cell lines, reaching levels that even exceeded those in the control cells at 40°C. As protein levels were nearly identical at 32 °C and 40 °C, eIF4A2 expression in these cell lines appeared to be only marginally temperature dependent.

While eIF4A2 protein expression in Hek293 control and exon 4 knockout cells was nearly indistinguishable from that in HeLa cells, temperature sensitivity was not only drastically reduced, but completely lost in the exon 10A knockout cell line. This deviation could be an artefact of the CRISPR/Cas9 system or a characteristic of HeLa or Hek293 cells, respectively.

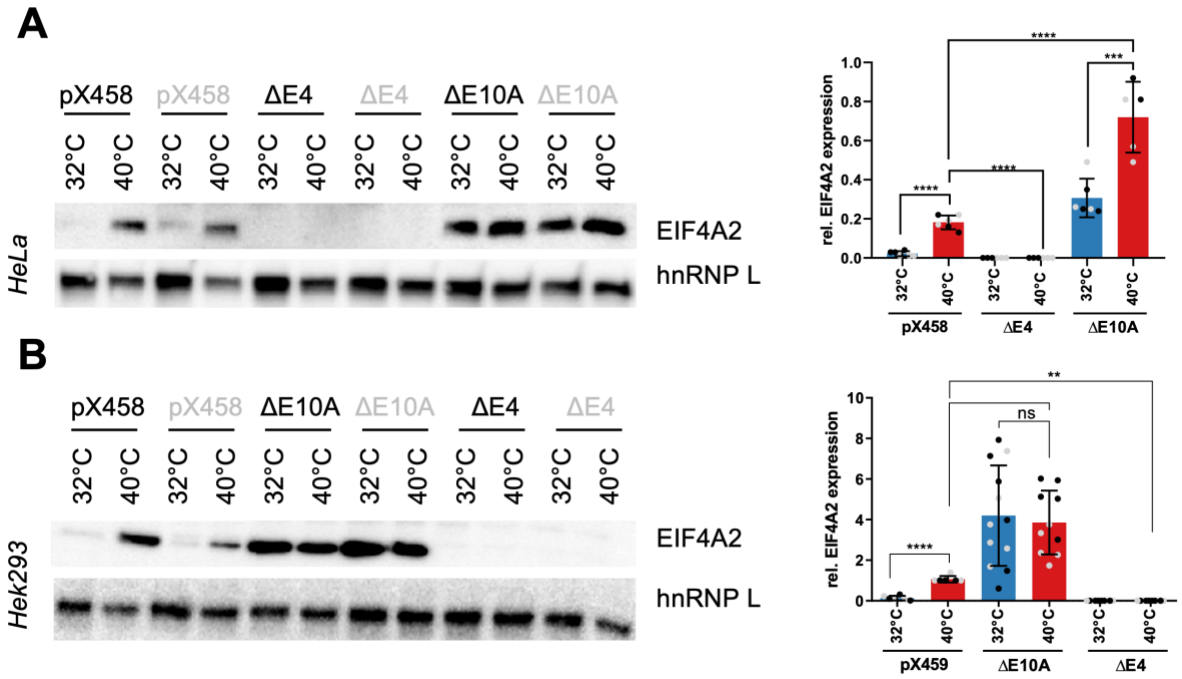

Figure 29. Exon 4 controls eIF4A2 protein expression in HeLa and Hek293 cells
A A western blot analysis of eIF4A2 levels in CRISPR/Cas9-edited HeLa and Hek293 cell lines is shown. Clonal cell lines from Fig. 25 were incubated for 24 hours at the indicated temperatures. The respective lysates from independent experiments were investigated for eIF4A2 protein expression and hnRNP L served as a loading control. The quantification is shown on the right. mean ± SD, n = 6 (3 per clone; individual clones indicated in black/grey), **B** Same experimental setup as in (A) for Hek293 cells. mean ± SD, n = 10 (5 per clone; individual clones indicated in black/grey). For all panels: all individual data points are shown. Unpaired t-tests were performed to determine the statistical significance, which is indicated by asterisks: **p < 0.01, ***p < 0.001, ****p < 0.0001.

To further investigate the intracellular localization of eIF4A2, we performed immunofluorescence staining of HeLa cells incubated at 37 °C using the eIF4A2-specific antibody previously applied in immunoblotting. As can be seen in the fluorescence micrographs, in the control cells eIF4A2 showed an opposite distribution to DAPI and co-localized with the cytoplasmatic marker G3BP1, suggesting that the protein is predominantly localized in the cytoplasm (Figure 30). In the absence of exon 4, we did not perform a G3BP1 staining, as we wanted to detect the low intensity of the eIF4A2 signal. The observed cytoplasmic localization of eIF4A2 is consistent with the findings of a previous study (Kyono, Miyashiro and Taguchi, 2002). In exon 10A knockout cells, we observed an increase in the eIF4A2-specific signal in the cytoplasm compared to the control cell line, consistent with a higher eIF4A2 protein expression. The elimination of exon 4 resulted in a strongly reduced eIF4A2 signal, suggesting that the absence of exon 4 led to a total knockdown of eIF4A2 protein expression, confirming our previous findings from immunoblotting.

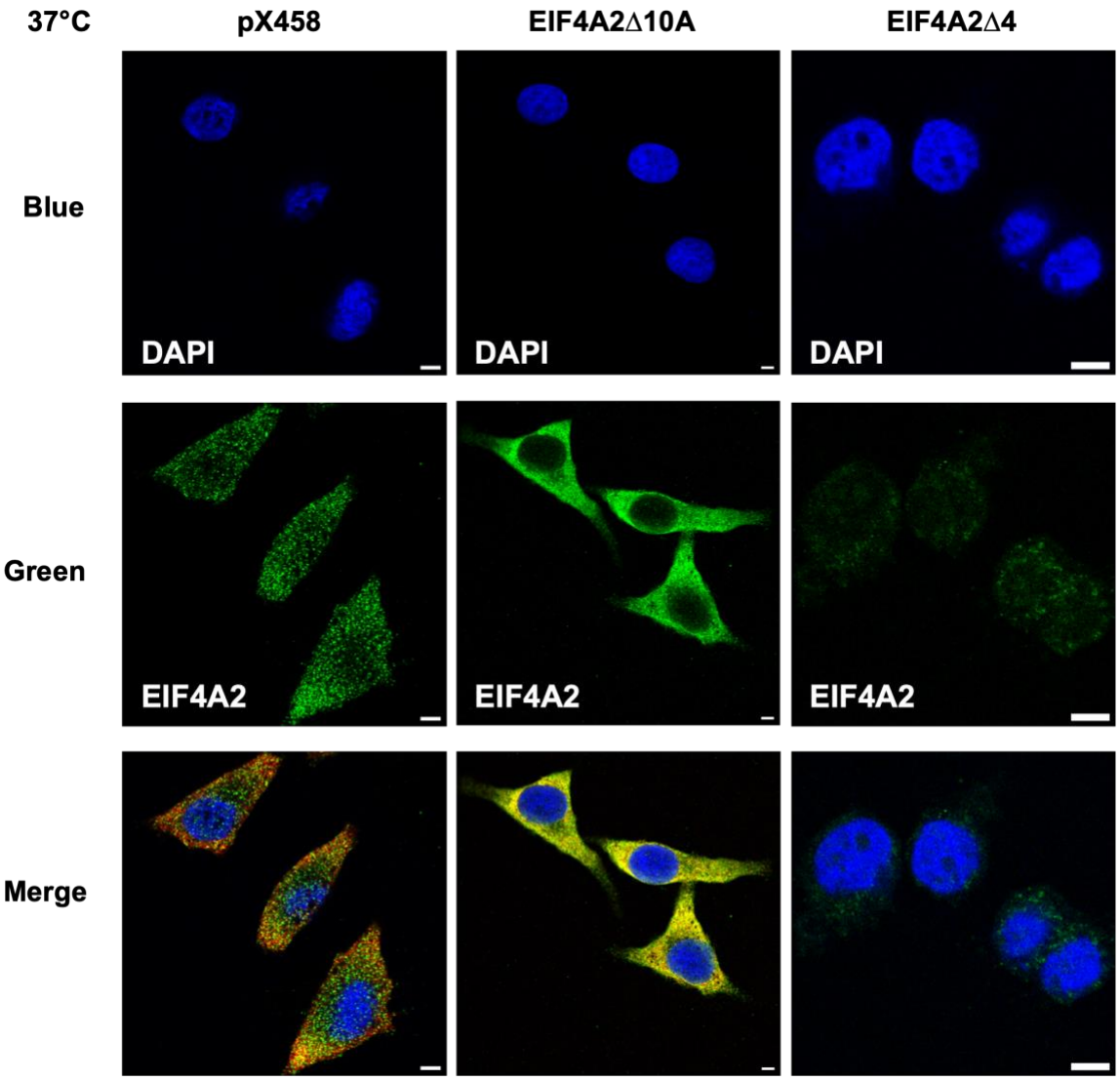

Figure 30. eIF4A2 is predominantly localized in the cytoplasm of HeLa cells
DAPI (blue), eIF4A2 (green) and G3BP1 (red) fluorescence staining for the detection of eIF4A2 in CRISPR/Cas9-edited HeLa cells (data for G3BP1 not shown). The fluorescence signals of DAPI and eIF4A2 were examined under a confocal laser scanning microscope. Unless otherwise noted all scale bars are 5 µm.

To further investigate whether the localization of eIF4A2 depends on the quantity of eIF4A2 protein present in the cell, we performed immunofluorescence staining of our CRISPR/Cas9-edited HeLa cells as previously described. eIF4A2 distribution was investigated in the control and exon 10A knockout cell lines after 24 hours incubation at 32 °C and 40 °C, respectively. In the control cell line, the eIF4A2 protein appeared less restricted to the cytoplasm at 32 °C compared to 40 °C. Furthermore, we observed a generally stronger eIF4A2 signal in the exon 10A knockout cell line compared to the control cell line at both temperatures, suggesting that this overexpression is temperature independent (Figure 31). Taken together, our findings indicate that eIF4A2 is predominantly localized in the cytoplasm irrespective of its abundance in the cell.

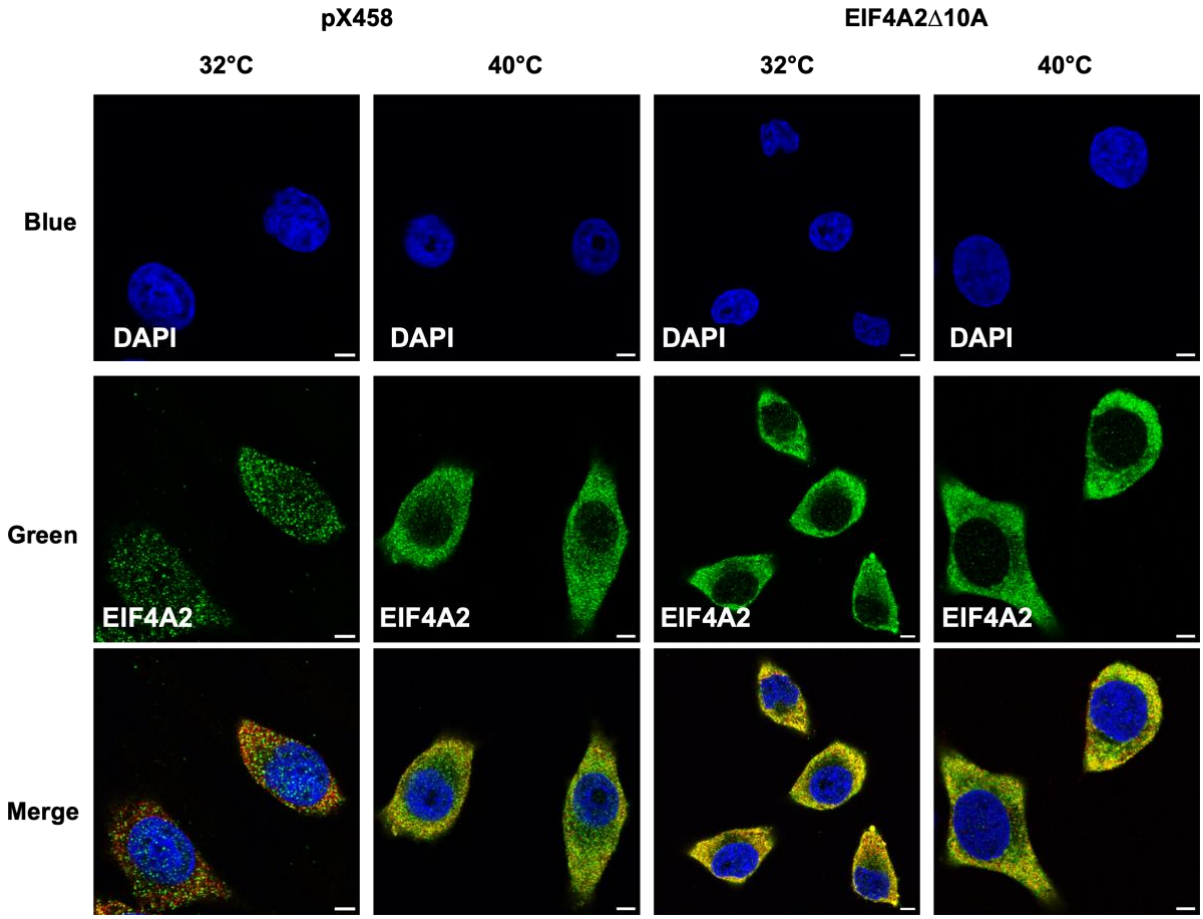

Figure 31. eIF4A2 is predominantly cytoplasmic independent of its protein quantity in HeLa
DAPI (blue), eIF4A2 (green) and G3BP1 (red) fluorescence staining for the detection of eIF4A2 in CRISPR/Cas9-edited HeLa cells (data for G3BP1 not shown). Cells were incubated at 32 °C and 40 °C for 24 hours. The fluorescence signals of DAPI and eIF4A2 were examined under a confocal laser scanning microscope. Unless otherwise noted all scale bars are 5 µm.

3.2.7 The absence of exon 4 or exon 10A, respectively does not lead to truncated eIF4A2 isoforms

The evidence gathered up to this point from the eIF4A2 immunoblotting and immunofluorescence staining indicates a complete loss of the eIF4A2 protein in response to the absence of exon 4. Based on the RNA sequence of eIF4A2 we could identify an additional start codon in exon 3 and a PTC in exon 5, resulting from a frame shift caused by exon 4 skipping. This suggests that in the exon 4 knockout cell line two potential open reading frames exist, which could result a hypothetical bicistronic transcript (Figure 32A); one covering the exons 1 - 5 and second including the exons 3 - 11 (both excluding exon 4).

To investigate whether the absence of exon 4 leads to the formation of any eIF4A2 protein isoform or to confirm the total loss of protein, we investigated protein levels by global quantitative proteome analysis. Additionally, the PTC in exon 10A suggests the possible translation of a C-terminally truncated eIF4A2 protein, which should be detectable via mass spectrometry. The mass spectrometric analysis of different HeLa cell lines was performed by Dr. Benno Kuropka (Core Facility BioSupraMol) in the laboratory of Prof. Dr Christian Freund, Freie Universität Berlin. For the control cell line, we obtained data from four independent samples incubated at 32 °C or 40 °C and two independent samples incubated at 37 °C. To investigate the abundance of potential eIF4A2 protein isoforms, we designed an experimental setup with a temperature-dependent linear increase in eIF4A2 protein levels similar to the ascending protein levels in the control. Therefore, four separate samples incubated at 32 °C and two from 37 °C were investigated from the exon 4 knockout cell line as well as four individual exon 10A knockout protein samples from 40 °C. Remarkably, 4,000 to 5,000 proteins were identified for each sample.

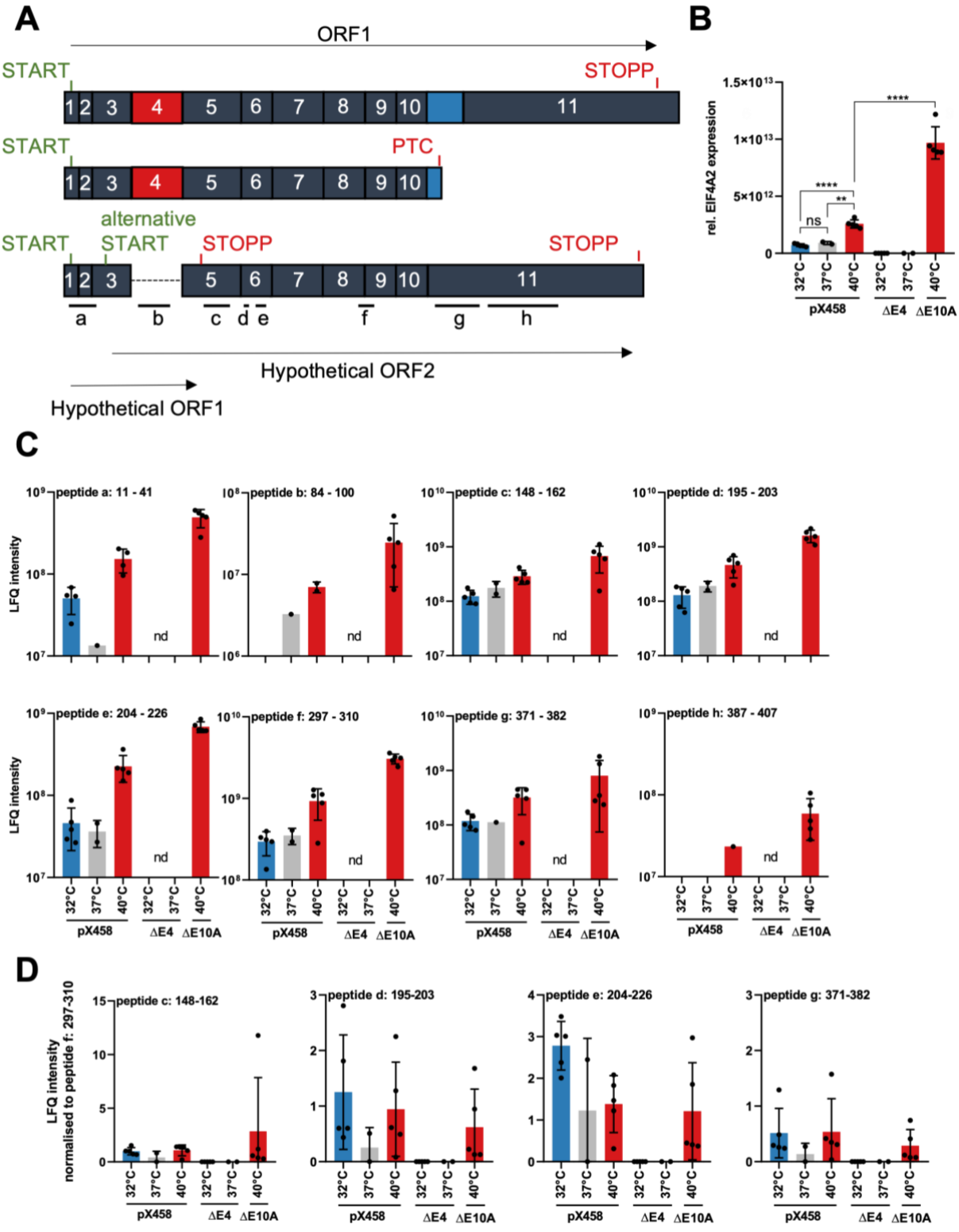

Figure 32. eIF4A2 protein expression is controlled by alternative splicing of exon 4 and 10A
A The schematic exon structures of hypothetical eIF4A2 mRNA isoforms are shown, including a potential bicistronic exon 4 knockout transcript. The heat-induced alternative exon 4 is highlighted in red, the cold-induced alternative exon 10A in blue. The black lines below indicate unique peptides, identified by a global proteomics analysis. The arrows show the hypothetical open reading frames (ORFs) of eIF4A2. The depicted line indicates the skipped exon 4. **B** A quantification of eIF4A2 expression levels obtained from mass spectrometry data is depicted. HeLa CRISPR/Cas9-edited cells were incubated at the indicated temperatures for 24 hours. The extracted proteins were purified using the preomics kit and subsequently fractionized (n = 4, mean ± SD/ n = 2 for 37 °C samples) An unpaired t-test was performed, and the calculated significance is indicated by asterisks: **p < 0.01, ****p < 0.0001 all individual data points are shown. **C** In total 15 unique peptides mapping to the amino acid sequence of eIF4A2 were identified by mass spectrometry analysis. 8 representative peptides are shown, and the label-free quantification (LFQ) intensity is plotted for all indicated conditions. The numbers above the quantification show the exact position of the respective peptide. **D** The LFQ intensity of the respective peptide normalized to peptide f is plotted. For panel B-D, all individual data points are shown.

The analysis of the data generated by mass spectrometry revealed a gradual increase in eIF4A2 protein levels in the control cell line equivalent to the increasing temperature (Figure 32B), as a higher peptide count was detected at 40 °C compared to 37 °C and 32 °C. By mapping to different parts of the eIF4A2 amino acid sequence, we found in total 15 unique peptides at the different temperatures in the control cells as well as well as the exon 10A knockout cell line. As observed before also the mass spectrometry showed a constitutive overexpression of eIF4A2 in the absence of exon 10A, with a tremendous increase in expression even in comparison to the control cell line at 40 °C.

As our previous results suggested a complete loss of the eIFA2 protein in the absence of exon 4, we performed an in-depth bioinformatical analysis of the peptides identified via mass spectrometry, specifically looking for peptides corresponding to potential truncated isoforms of eIF4A2. To verify the utilization of the first hypothetical open reading frame, we examined whether there is a peptide mapping to the amino acid sequence of eIF4A2 between exon 1 and exon 3. To identify the second hypothetical ORF, we inspected whether there are peptides corresponding to the region between exon 5 and exon 11. We further searched for peptides specific for the exon 10A inclusion isoform, to determine the presence of a truncated protein ending in exon 10A. However, regardless of the temperature, we could not find a single peptide in any sample deriving from the exon 4 knockout cell line that could be unambiguously assigned to eIF4A2 (Figure 32C). This strongly suggests a complete loss of the protein in this cell line. Referring to the immunofluorescence images, we can now be confident that the faint green-fluorescent signal in the eIF4A2 channel corresponds to nonspecific autofluorescence.

Additionally, we calculated the ratio between the peptides coding for the C-terminal region in eIF4A2 and a peptide specifically coding for the region of the constitutive exons 8 to 9 (Figure 32D). We did not observe any changes in the peptide counts for all tested peptides. Specifically, the peptides covering the region coding for the C-terminus showed no change in peptide counts. This proves that there is no truncated eIF4A2 protein ending with the PTC located in exon 10A in any of our investigated cell lines.

3.2.8 Changes in eIF4A2 alternative splicing have no global impact on the mRNA expression and alternative splicing in HeLa cells

Up to this point, we have established that the absence of exon 4 leads to a complete loss of eIF4A2 protein. Additionally, we could not identify a truncated protein isoform resulting from the PTC in exon 10A. Taken together our findings confirm only the presence of the full-length eIF4A2 protein according to our western blots and proteomic analysis. Due to the drastic effects of eliminating exon 4 or exon 10A, respectively, on eIF4A2 protein abundance, we wondered if a knockout or overexpression could lead to global changes in mRNA expression and/or AS patterns – although eIF4A2 most likely directly effects only protein levels i.e., by direct control of translation initiation or via miRNA-mediated translation repression.

To answer this question, we analyzed our RNA sequencing dataset and compared the mRNA expression (Figure 33A) and AS (Figure 33B) in all cell lines at all temperatures. Analysis of the mRNA levels of 927 temperature-dependent genes showed significant changes in response to a shift in temperature from 32 °C to 40 °C in the control cell line. Similarly, we observed no global differences between the control and the exon 4 or exon 10A knockout cell lines.

While investigating the alternative splicing in control cells at 32 °C and 40 °C, we identified 244 alternatively spliced exons with a temperature-dependent change in PSI > 15. Analysis of these identified alternative splicing events in exon 4 and exon 10A knockout cells did not indicate significant differences in splicing patterns, suggesting that eIF4A2 levels have no significant effect on AS on a global level.

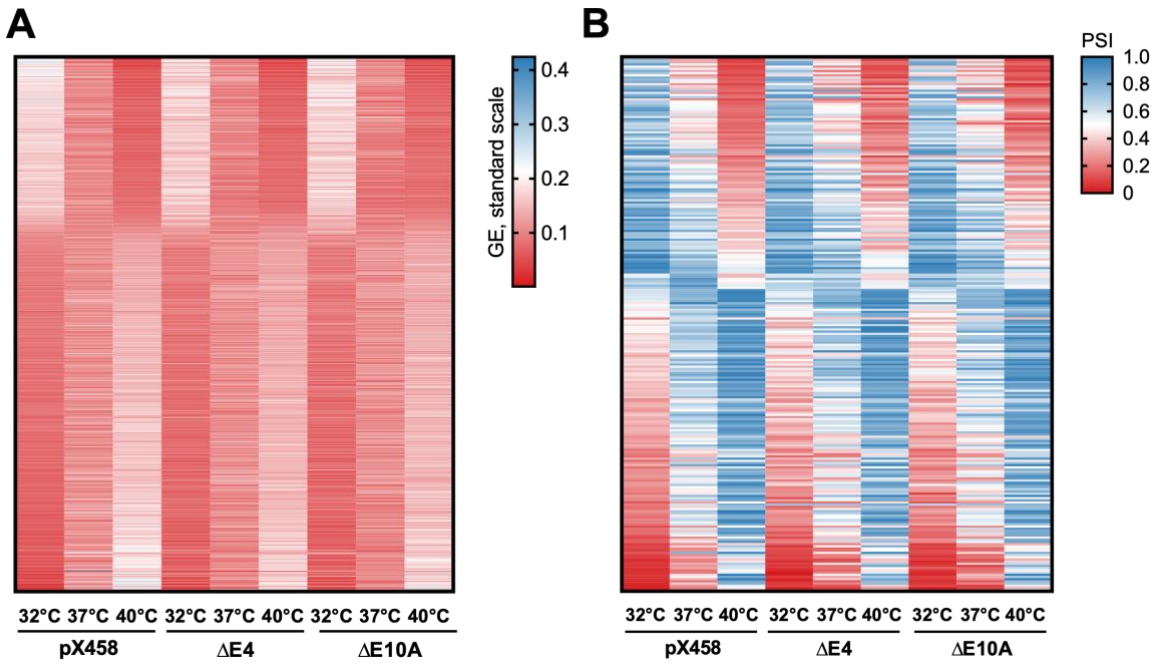

Figure 33. The absence of exon 4 or exon 10A shows similar expression patterns in mRNA and alternative splicing compared to the control in HeLa cells
HeLa CRISPR/Cas9-edited eIF4A2 cells were incubated at 32 °C, 37 °C or 40 °C, total RNA was extracted after 24 hours incubation and analyzed by RNA-seq. The different cell lines show the mean of its two individual clonal cell lines. The first three columns show the control, the following three columns the exon 4 knockout and the last three columns the exon 10A knockout cell lines, each at the indicated temperatures **A** The heatmap shows the normalized mRNA expression values of temperature-responsive genes. Genes were considered significantly changed with a log2 fold change FC > 0.5 (< -0.5) and padj < 0.0001 between 32 °C and 40 °C. The genes are classified based on their FC in temperature between 32 °C and 40 °C in the control cell line. n = 927 **B** The heatmap shows the PSI values of 244 exon skipping events responsive to temperature in the control cell lines. These splicing events were classified based on their FC between 32 °C and 40 °C in the control cell line. AS of exons was considered significant with a temperature-dependent change in PSI > 15 and a p > 0.001.

3.2.9 ACSF2, SPATS2L and GPNMB mRNA expression is similar to that of eIF4A2

Even though we did not observe global eIF4A2-dependent changes in mRNA expression, we still wondered, whether we could identify individual targets regulated by the translation initiation factor. On that account, we compared the control with the exon 4 knockout cell line at 40 °C and found several genes that exhibited similar changes in mRNA expression as eIF4A2 (Figure 34A).

The most prominent gene was eIF4A2 itself, as the absence of exon 4 led to a substantial reduction in mRNA level and the exon 10A knockout resulted in an overexpression. Of the previous identified genes, we selected those which showed similar mRNA expression patterns as eIF4A2 (ACSF2, SPATS2L and GPNMB) and validated these targets in an RT-qPCR (Figure 34B). For ACSF2, SPATS2L and GPNMB we observed a decreased mRNA expression in the exon 4 knockout cell line compared to the control. Interestingly, for ACSF2, the absence of exon 10A led to a constitutively higher mRNA expression at all temperatures and the temperature responsiveness was significantly decreased.

Thus, none of the three targets showed a direct correlation with eIF4A2 protein levels (in the control, exon 4 and exon 10A knockout cell lines), contradicting a direct regulation through eIF4A2.

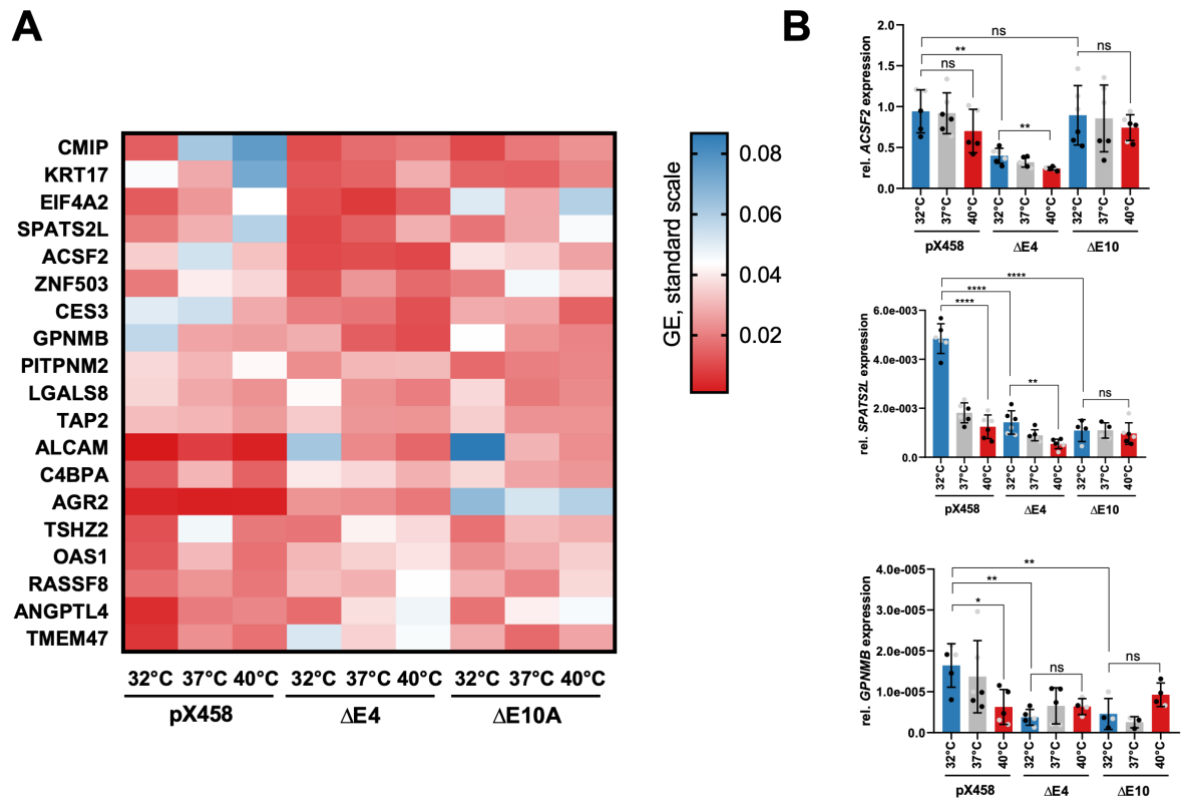

Figure 34. eIF4A2 regulates mRNA expression of ACSF2, SPATS2L and GPNMB
A GE values in response to temperature of eIF4A2 CRISPR/Cas9-edited cell lines are shown in a heatmap. These genes significantly differ between the control and the exon 4 knockout cell line at 40 °C, as well as the control and the exon 10A knockout cell line at 32 °C. RNA was extracted after incubation at 32 °C, 37 °C and 40 °C and analyzed by RNA-seq. Genes were considered significantly changed in an eIF4A2 dependent manner with a log2 FC > 0.5 (< -0.5) and padj < 0.001 between the control cell line and the exon 4 knockout cell line at 40 °C. Genes are classified based on their FC control cell line versus the exon 4 knockout cell line. **B** Genes from (A) with a similar expression pattern as eIF4A2, were validated by RT-qPCR. Clonal HeLa cells were incubated at the indicated temperature and RT-qPCR analysis was performed using gene specific primers. ACSF2 (top), SPATS2L (middle) and GPNMB (bottom) expression levels are shown relative to HPRT levels. (n = 6, mean ± SD, 3 per clone (black/grey)), unpaired t-test and significance is indicated by asterisks: *p < 0.05, **p < 0.01, ***p < 0.001, ****p < 0.0001 all individual data points are shown.

3.2.10 The knockout of eIF4A2 exon 4 leads to an upregulation of a subset of mitochondrial genes that are part of complex I of the respiratory chain

To further investigate the effect of eIF4A2 on the proteome, we first plotted the foldchange in gene expression and the foldchange in peptide abundance between 32 °C and 40 °C in the control cell line. This showed a significant linear correlation between mRNA expression and peptide abundancy in response to changes in temperature, suggesting a regulation of protein levels through RNA levels (Figure 35A). As proof of principle, we highlighted eIF4A2 and two heat shock proteins (HSPA6 and HSPA1B) representing heat-induced proteins and CIRBP and RBM3 as known cold-induced proteins (Danno *et al.*, 1997; Haltenhof *et al.*, 2020; Preußner *et al.*, 2023). We then performed a gene ontology (GO) term enrichment analysis for the factors that were the most significantly upregulated and downregulated at protein level, but were not affected at RNA level, which suggests a regulation through protein synthesis or mRNA decay. We found that the majority of these factors were involved in mitochondrial respiration, as numerous genes expressed proteins of the essential complex I.

Plotting the fold change (FC) in mRNA expression against the FC in peptide abundance between the control cell line and the exon 4 knockout cell line at 32 °C, showed that in the absence of eIF4A2, 132 genes were downregulated and 329 upregulated at protein level, while the mRNA expression remained unaltered (Figure 35B).

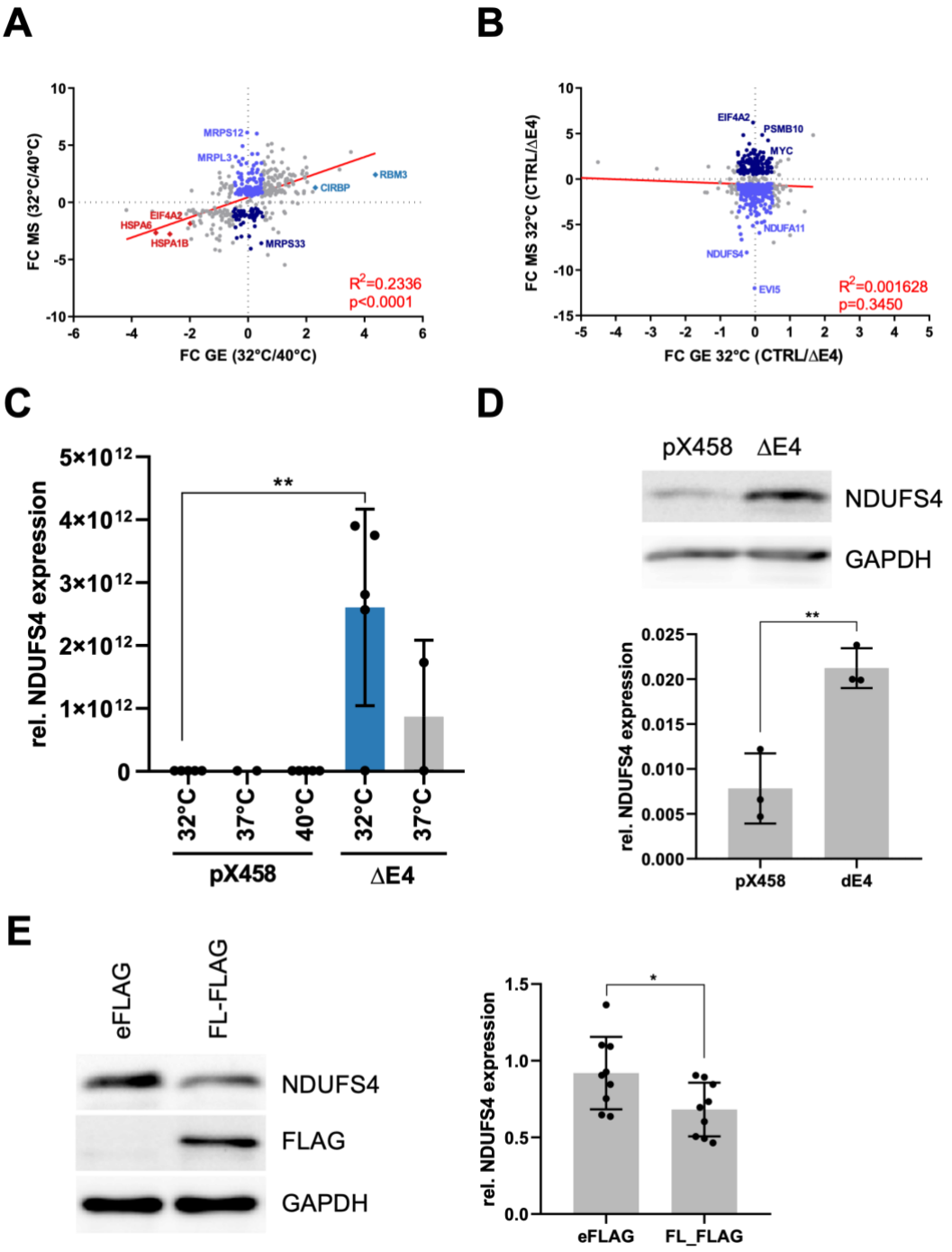

Figure 35. The expression of several mitochondrial proteins is regulated in response to eIF4A2 expression
Analysis and validation of transcriptomics and proteomics data. RNA and proteins were extracted from CRISPR/Cas9-edited eIF4A2 HeLa cells after a 24-hour incubation at 32 °C, 37 °C or 40 °C. RNA was analyzed by RNA-seq and proteins were analyzed by mass spectrometry. Upregulated genes are shown as light purple and downregulated genes as dark purple dots. Heat-induced controls are depicted as red and cold-induced controls as blue diamonds **A** Global correlation in the control cell line of 32 °C versus 40 °C log2 FC gene expression vs log2 FC protein levels. GO term enrichment analysis for "mitochondrial gene expression" and „mitochondrial translation". Proteins were considered significantly changed with a log2 FC > 0.5 (< -0.5) and q-value FDR < 0.05. The red line shows the linear regression, R^2 and p-value are indicated, n = 596. **B** Correlation of control cell line versus exon 4 knockout cell line log2 FC gene expression vs log2 FC protein levels at 32 °C. Genes were considered significantly changed with a log2 FC > 0.5 (< -0.5) and padj < 0.0001 between the control and exon 4 knockout cell lines at 32 °C. Proteins were considered significantly changed with a log2 FC > 0.5 (< -0.5) and q-value FDR < 0.05. Genes associated with the GO terms "mitochondrial respirasome" and „aerobic respiration" are shown. The red line shows the linear regression, R^2 and p-value are indicated, n = 1015 **C** Protein levels of NDUFS4 in control and exon 4 knockout cells were obtained from mass spectrometry (mean ± SD). n = 2 (control)/ n = 4, all individual data points are shown. **D** Validation of NDUFS4 expression predicted by mass spec. Lysates from HeLa control and exon 4 knockout cells were analyzed by immunoblotting for NDUFS4 expression. GAPDH served as a loading control. The quantification is shown on the right, n = 3 (mean ± SD). **E** Rescue of HeLa exon 4 knockout cells via transfection with FLAG-tagged full-length eIF4A2. Subsequently, NDUFS4 expression levels were analyzed by western blot. The quantification is shown on the right n=9 (mean ± SD). In panels D-E, all individual data points are shown. The statistical significance was calculated by unpaired t-test, and indicated by asterisks: *p < 0.05, **p < 0.01.

Results

To further investigate the expression of the identified genes in response to temperature, we performed a GO term analysis, which revealed “mitochondrial gene expression” (GO: 0140053) “and mitochondrial respiratory chain complex I” (GO:0005747) as the most enriched sets of genes. NDUFS4 was one of the proteins whose expression was most highly affected by eIF4A2 levels and was therefore selected for further investigation (Figure 35C). Western blot analysis showed a significant increase in NDUFS4 expression in the absence of eIF4A2, which is consistent with our mass spectrometry data (Figure 35D). To further establish a direct role of exon 4 exclusion in the upregulation of NDUFS4 expression, we performed a rescue experiment by transfecting exon 4 knockout cells with FLAG-tagged full-length eIF4A2 (Figure 35E). Indeed, western blot analysis using both NDUFS4- and FLAG-specific antibodies, showed an increase in NDUFS4 expression upon reintroduction of eIF4A2. This confirms an involvement of the protein in the regulation of NDUFS4 expression.

3.2.11 The impact of eIF4A2 on the respiratory chain is not regulated via the UTRs

To further understand the direct role of the absence of exon 4 in upregulating the expression of mitochondrial genes, we set up a GFP reporter assay where we inserted either the 5’ UTR upstream of the GFP gene or the 3’UTR downstream of the GFP gene (Figure 36A). In this manner, we created reporter constructs for four selected mitochondrial genes, which were co-transfected into HeLa control and exon 4 knockout cells with the red fluorescence tdTomato vector to allow normalization of the GFP expression measured by flow cytometry. We observed a substantial reduction in GFP expression for all reporter constructs regardless of eIF4A2. This reduction was stronger for the 5’UTR than the 3’UTR reporter, especially for NDUFS8 and PSMB10. The absence of eIF4A2 exon 4 did not show a significant effect on GFP expression for any of the selected genes (Figure 36B), suggesting that the eIF4A2-mediated upregulation of mitochondrial proteins is not regulated by the UTRs of these specific proteins.

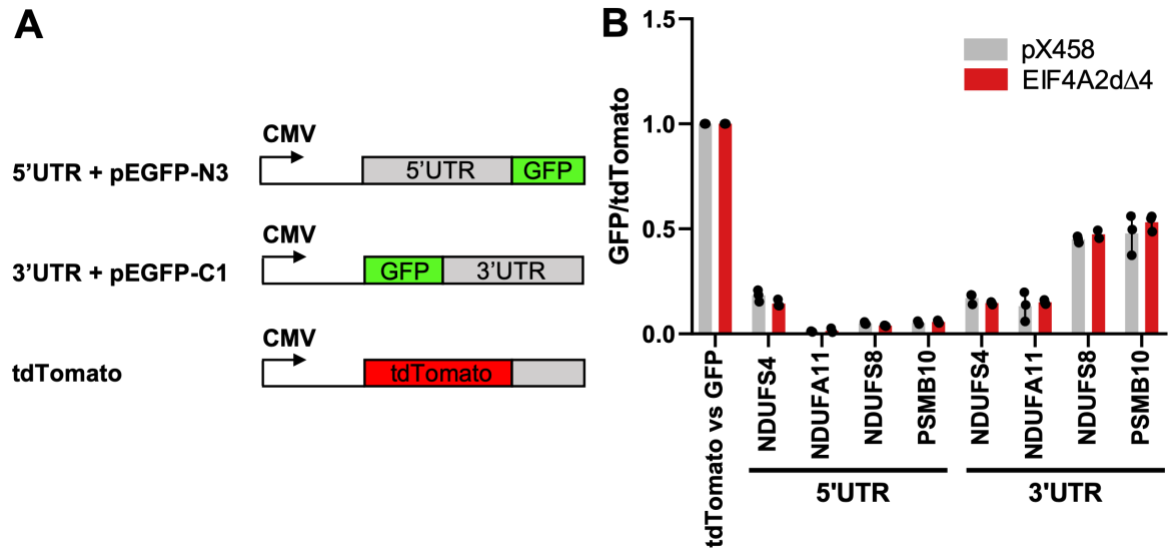

Figure 36. The eIF4A2-mediated regulation of mitochondrial proteins is independent of the UTRs
A The general structure of reporter constructs is shown. **B** The gene expression assay with different GFP reporter constructs measured by flow cytometry is shown. The 3‘ or 5‘ untranslated regions (UTRs) of mitochondrial respiratory chain genes were inserted either upstream or downstream of GFP. The GFP signal was normalized to a co-transfected red fluorescence tdTomato control (mean ± SD). n = 3, all individual data points are shown.

3.3 Temperature-independent alternative splicing of eIF4A2 in response to oxidative stress

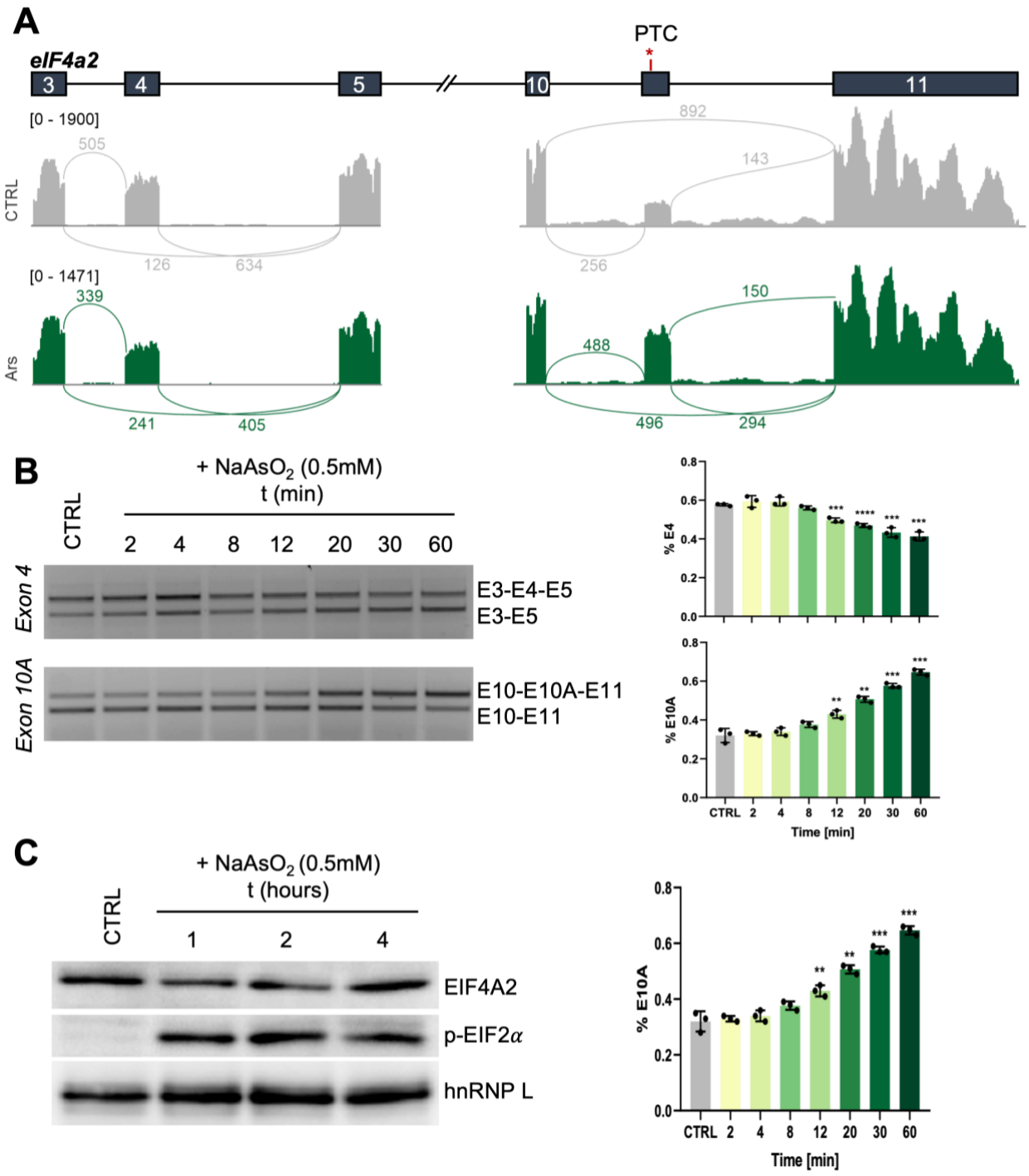

Figure 37. eIF4A2 exon 4 and 10 splicing is regulated in response to oxidative stress
A Top: The exon/intron structure of the eIF4A2 pre-mRNA is shown. Exons are shown as boxes, introns as lines. Bottom: Oxidative stress dependent AS of the eIF4A2 exons 4 and 10A. The sashimi plots show the read distribution for a 1 hour 0.5 mM arsenite treatment (dark green) compared to the control (grey) in HeLa cells (reads per base in brackets). RNA-sequencing reads are indicated by the curved lines, which span the junction of two exons. The RNA-sequencing data were provided by Nabeel-Shah *et al.* (GSE171009 on GEO, Nabeel-Shah *et al.*, 2022). **B** The splice-sensitive RT-PCR, visualized on a 2 % agarose gel, was performed with forward primers annealing to the respective upstream exon and reverse primers annealing to the respective downstream exon of either alternative exon 4 or exon 10A. Cells were treated with 0.5 mM arsenite for 1 hour. The upper panel shows the splicing of exon 4, the lower panel the splicing of exon 10A. The included exons are indicated at the respective band height. The quantification is shown on the right (mean ± SD). **C** Western blot analysis of eIF4A2 levels in arsenite treated cells. HeLa wildtype cells were treated with 0.5 mM arsenite for 1 hour and lysates were investigated for eIF4A2 and p-eIF2α protein expression. hnRNP L served as loading control. The quantification is shown on the right. In panels (B) and (C), (mean ± SD) n = 3, significance of the performed unpaired t-test is indicated by asterisks: *p < 0.05, **p < 0.01, ***p < 0.001, ****p < 0.0001. All individual data points are shown.

Results

eIF4A2 with its two oppositely regulated alternative exons proved to be an excellent model system to investigate the mechanism underlying temperature-dependent alternative splicing. Plotting RNA-sequencing data obtained from arsenite-treated Hek293 cells by Nabeel-Shah *et al.* (2021) against the human reference genome GRCh38/hg38 (Figure 37A) revealed that oxidative stress resulted in exon 4 skipping and exon 10A inclusion, similar to the splicing pattern induced by cold. Thus, we wondered if we could apply the model system, we established to investigate alternative splicing under oxidative stress conditions.

To validate and further investigate these predictions, we performed an RT-PCR of a time course, treating HeLa wildtype cells with 0.5 mM arsenite for the indicated time periods (Figure 37B). We observed that exon 4 and exon 10A showed the first significant stress response in splicing already after twelve minutes. As exon 4 skipping coupled with exon 10A inclusion prevents productive eIF4A2 translation, we wanted to test whether the increase in exon 10A incorporation is also transferred to the protein level in the context of oxidative stress induced by arsenite.

Therefore, we investigated lysates from HeLa cells exposed to 0.5 mM arsenite for one, two or four hours via immunoblotting. As proof of principle, we detected the oxidative stress marker p-eIF2α, to evaluate the effect of $NaAsO_2$ exposure over time. eIF2α phosphorylation increases under $NaAsO_2$-induced stress (Wheeler et al., 2016) and could therefore be used as a control. Indeed, we observed a reduction in eIF4A2 protein levels after one hour of arsenite treatment (Figure 37C). Surprisingly, after two hours, the expression level was still reduced, but slightly increased compared to the one-hour time point. This phenomenon was even more pronounced after four hours of arsenite exposure, as the eIF4A2 protein expression had almost reached the level of the untreated cells. In the course of this, the p-eIF2α level remained equal over time, indicating, that the cell was still under stress conditions.

Taken together, our results show that the expression of eIF4A2 is rapidly modified by arsenite-induced oxidative stress. On RNA level, we observed that alternative splicing already responded already after twelve minutes, and the protein expression followed within an hour. Furthermore, at least at protein level, the cells seemed to be able to adjust to the stress condition with time, as eIF4A2 expression was nearly restored to the initial level after four hours of exposure to arsenite.

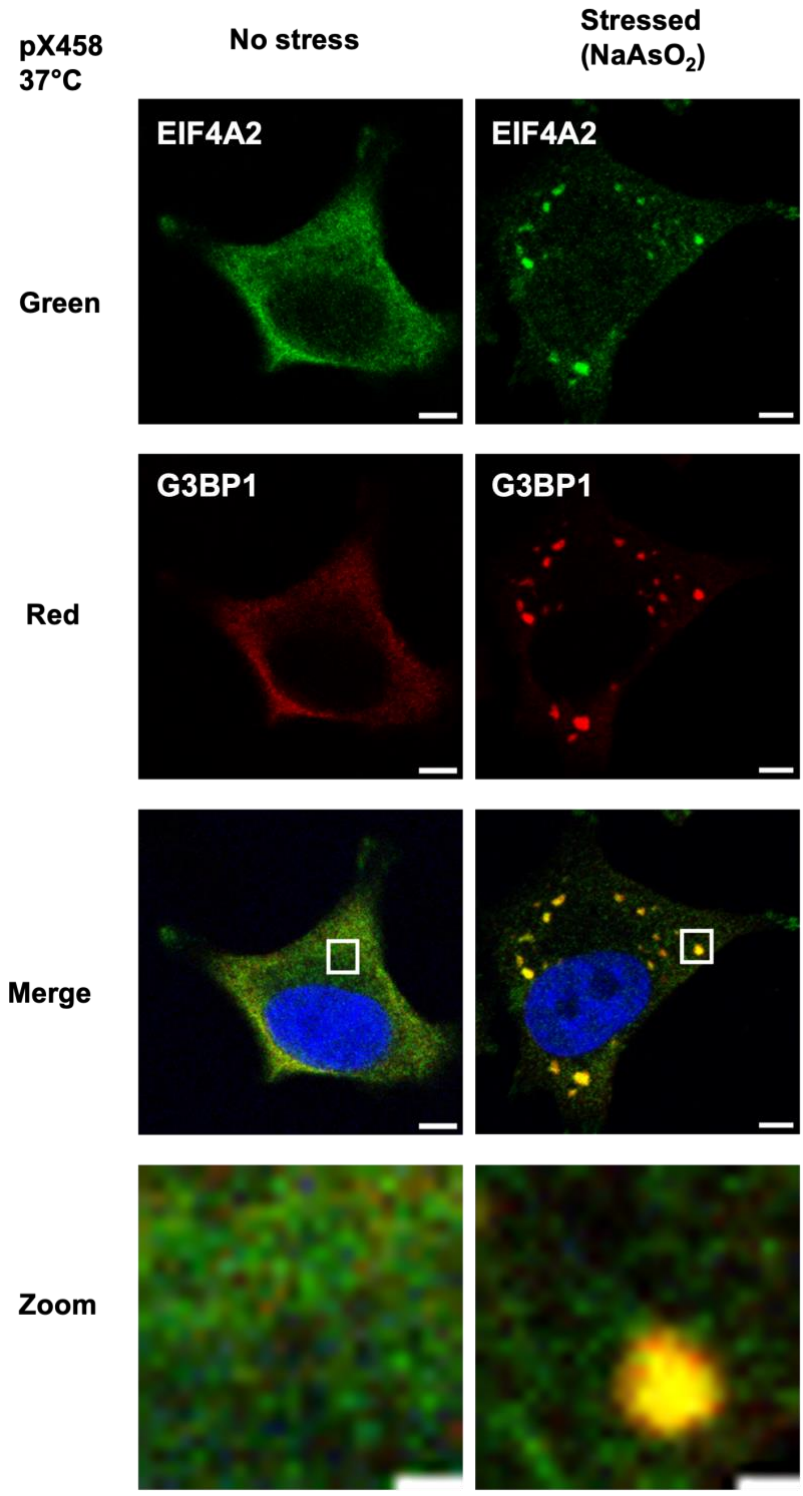

Figure 38. eIF4A2 partitions into stress granules during oxidative stress
Immunofluorescence of eIF4A2 (green) and G3BP1 (red) in SGs. Images display SG formation after 1 h of arsenite treatment (0.5 mM) compared to untreated control cells. Unless otherwise noted all scale bars are 5 µm, zoom: 1 µm.

Different stress stimuli, including oxidative stress, were shown to cause limitation in translation initiation, which in turn results in non-membrane bound RNA-protein (RNP) assemblies, so-called stress granules (Wheeler *et al.*, 2016). Recent findings further demonstrated an important role of eIF4A in SG formation (Tauber *et al.*, 2020). Tauber *et al.* (2020) showed that in U2OS and HeLa cells. Cells, eIF4A1 localizes to SGs after exposure to arsenite, a toxin known to inhibit translation initiation.

Results

As eIF4A2 shares numerous characteristics with eIF4A1 and likewise acts as a translation initiation factor, we wondered how oxidative stress impacts eIF4A2 protein localization within the cells. Since we showed that eIF4A2 responds to arsenite-induced stress on mRNA and protein level, we speculated that eIF4A2 might partition into SGs similar to eIF4A1 (Figure 38). Therefore, we analyzed whether eIF4A2 localizes to SGs in HeLa cells upon 1 h exposure to arsenite, by visualizing eIF4A2 and the canonical SG marker G3BP1 in immunofluorescence microscopy (Tauber *et al.*, 2020). While G3BP1 and eIF4A2 were both localized in the cytoplasm in untreated cells, the eIF4A2 and G3BP1 signals accumulated in SGs upon stress exposure, suggesting that eIF4A2 is indeed recruited into SGs in response to oxidative stress. Surprisingly, while eIF4A1 was reported to localize to the periphery of SGs (Tauber *et al.*, 2020), eIF4A2 seemed to be enriched in the center of the SGs. This would be consistent with the idea that these paralogues exert different functions.

3.4 Global impact of temperature on helicases

Helicases are involved in many cellular processes including DNA replication, RNA transcription and processing, translation, recombination and many more (Patel and Donmez, 2006). We wondered if other important helicases are also expressed in a temperature-dependent manner, like eIF4A2. Therefore, we assessed genes associated with helicases by a GO-term enrichment analysis (GO:0003724, GO:0033678, GO:0033677, GO:0036121, GO0034458, GO0043138, GO0043139, GO0003678, GO0004386) in the human genome. This research revealed around 180 genes encoding for DNA and RNA helicases and chaperones (Figure 39A).

We investigated these 180 genes by merging our RNA sequencing and mass spectrometry datasets. Our analysis indicated a minor global correlation of log 2-fold change in gene expression and log 2-fold change in peptide abundance in response to the temperature shift from 32 °C to 40 °C.

When analyzing all genes associated with RNA helicase activity (GO: 0003724) we found that around 40 % of these genes were temperature responsive on the mRNA but not protein level (Figure 39B). Around 4 % were only regulated on the protein level, while the remaining 4 % were regulated on both mRNA and protein levels. A closer look at the temperature-dependently regulated RNA helicases revealed that of all the helicases downregulated at higher temperatures, only one was affected at both mRNA and protein levels (Figure 39C). We identified this helicase as the DEAD-box protein DDX28. Interestingly, we also found only one helicase to be upregulated at higher temperatures on mRNA and protein levels (Figure 39D). Remarkably, we discovered this helicase to be eIF4A2. This global analysis underlines the importance of eIF4A2 expression in response to temperature.

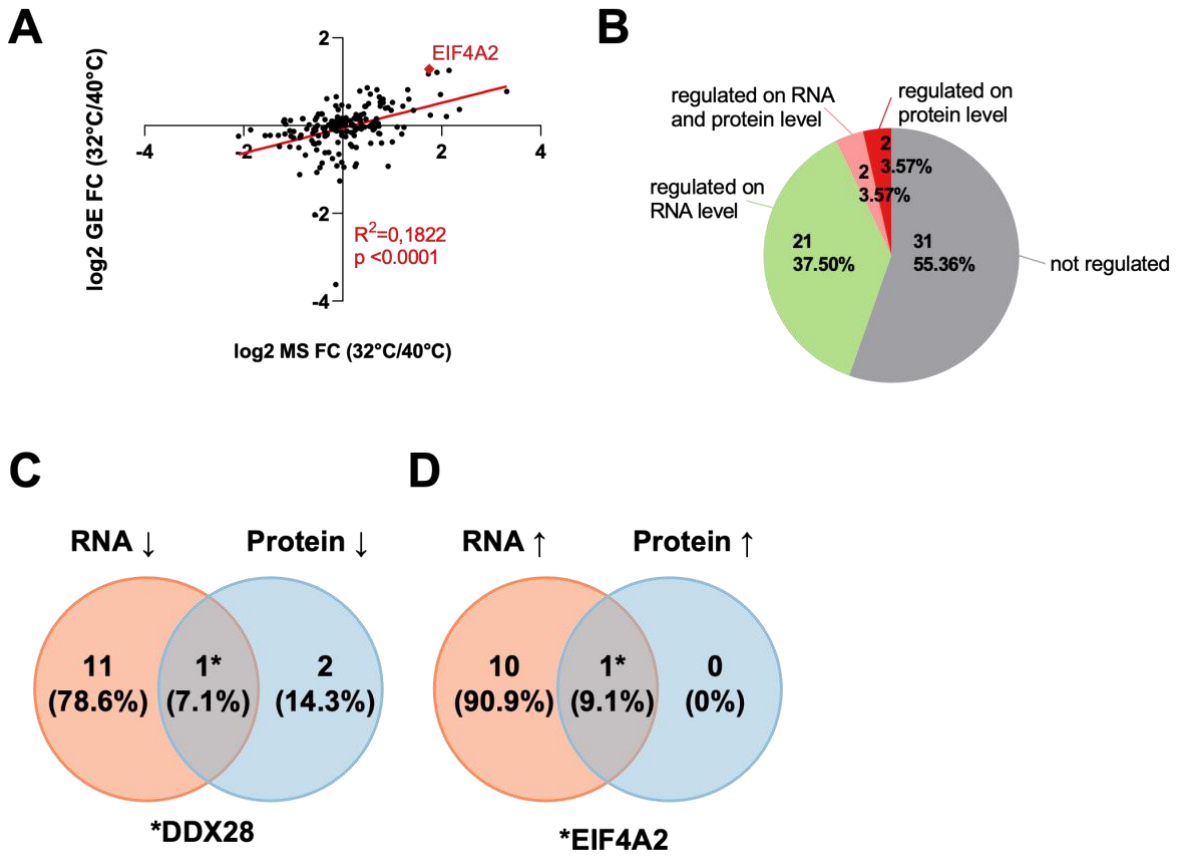

Figure 39. DDX28 and eIF4A2 are the only RNA helicases which are temperature responsive on mRNA and protein levels

RNA-sequencing and mass spectrometry analysis. HeLa cells were incubated for 24 hours at 32 °C, 37 °C or 40 °C. RNA or proteins were extracted and analyzed by RNA-seq or mass spectrometry. Genes were considered significantly changed with a log2 FC > 0.5 (< -0.5) and padj < 0.0001 between 32 °C and 40 °C. Proteins were considered significantly changed with a log2 FC > 0.5 (< -0.5) and q-value FDR < 0.05. **A** Global correlation of gene expression at 32 °C versus 40 °C vs log2 FC protein levels 32 °C versus 40 °C. R^2 and p-value are indicated, n = 180. **B** The pie chart shows the genes associated with the GO term „RNA helicases“. The level on which temperature regulates the helicase expression was investigated, n=56 **C**, **D** Overlap of genes enriched for the GO term „RNA helicases“ that are downregulated (C) on RNA and/or protein level or upregulated (D) on RNA and/or protein level.

4. Discussion

Temperature is an omnipresent factor in the lives of most organisms and is known to have a great influence on many cellular processes, including gene expression (Shiina and Shimizu, 2020). For instance, temperature was shown to affect the speed of RNA polymerase II transcription, which, in turn, is known to affect splicing. In addition, the secondary structure of RNAs is influenced by temperature, which affects the interaction of molecular machines as the spliceosome with the pre-mRNA (Hiller *et al.*, 2007; Capovilla *et al.*, 2015). This way, temperature can impact alternative splice site selection, especially when splicing enhancers and silencers are concerned (Meyer *et al.*, 2011; Somero, 2018). Previous studies mainly focused on alternative splicing in heat-shock proteins (Neves-da-Rocha *et al.*, 2019) or investigated gene expression at colder temperatures. The best-described cold-induced genes to date are the RNA-binding motif protein 3 (RBM3) and the cold-induced binding protein (CIRBP) (Danno *et al.*, 1997; Nishiyama *et al.*, 1997).

Our study is interested in how temperature affects the expression of genes and proteins by analyzing the splicing of alternative exons in response to temperature. We identified the alternative exons in RBM3 and eIF4A2 that are responsible for the temperature-dependent expression of these proteins. In RBM3, we determined exon 3a to be causative for its cold-induced expression. eIF4A2 comprises two alternative exons that respond to temperature changes. We established eIF4A2 exon 4 as one of the most included exons at higher temperatures. Additionally, we identified exon 10A to be strongly cold induced. These two alternative exons make eIF4A2 a perfect model for investigating temperature dependent alternative splicing and its significance for protein expression.

For this purpose, we used a combination of transcriptome- and proteome-wide *in vivo* and *in vitro* approaches. The data obtained in this study revealed that eIF4A2 mRNA and protein expression is regulated by the interplay of the two alternative exons 4 and 10A. The involvement of these two exons in protein expression indicates that alternative splicing functions as a mechanism to regulate protein activity indirectly via influencing protein abundance in the case of eIF4A2.

4.1 Conserved temperature-dependent exons of eIF4A2 do not regulate global mRNA expression

One fundamental question we addressed in this thesis is how temperature changes in the physiological range affect splicing on a global scale. Therefore, we performed an RNA-seq analysis of CRISPR/Cas9-modified eIF4A2 HeLa cells at 32 °C, 37 °C and 40 °C. To rule out any cell-type-specific effects, we compared the data we obtained from HeLa cells with RNA-seq data Haltenhof *et al.* (2020) gathered from Hek293 cells. This comparison showed no global differences. Although the two studies investigate alternative splicing at slightly different temperatures, they demonstrate the conservation of temperature-dependent alternative splicing across the two cell lines. These findings suggest that temperature changes in a physiological range are a robust regulator of alternative splicing in human cells.

We found that most alternative exons in HeLa cells are spliced regardless of temperature. Only, approximately 5 % of all alternative exons responded to temperature within the cut-offs we have specified (Figure 14). Approximately half of the temperature-responsive alternative exons were cold-induced, while the other half was heat-induced. Consistent with previous results (Danno *et al.*, 1997), we identified exon 3a in RBM3 as one of the strongest temperature-dependent exons in heat and essential for temperature-dependent mRNA and protein expression of RBM3 (Preußner *et al.*, 2023). Similar to RBM3 E3a, we identified exon 4 in eIF4A2 as another strongly heat-induced exon. In contrast, we discovered exon 10A to be one of the strongest cold-induced alternative splicing events. Based on our knowledge from RBM3, we predict that eIF4A2 mRNA and protein expression could be regulated by these two strongly temperature-dependent alternative exons.

The precise function of eIF4A2 has been the interest of several studies but has never been fully deciphered. As a DEAD-box RNA helicase, eIF4A2 was shown to have important roles in numerous

cellular processes involving RNA binding and unwinding (Lu *et al.*, 2014; Raza, Waldron and Le Quesne, 2015; Meijer *et al.*, 2019; Liu, Fang and Wu, 2022). The fact that eIF4A2 is a translation initiation factor with a helicase function suggests that it might operate at a genome wide level.

However, investigation of exon 4 (protein loss) and exon 10A (constitutive overexpression) knockout CRISPR/Cas9 genome-edited cell lines in comparison to the control cell line did not reveal significant global differences in mRNA expression and alternative splicing in response to temperature changes.

Previous studies proved the clarification of the eIF4A2 function to be difficult, resulting in many conflicting results. Similar to our exon 10A knockout cell line, most studies investigated eIF4A2 in an oversaturated system (Wilczynska *et al.*, 2019). Unphysiologically high levels of eIF4A2, were shown to cause its association with eIF4G, which under physiological eIF4A2 levels, is more likely bound by eIF4A1 (Mathys *et al.*, 2014; Kuzuoğlu‐Öztürk *et al.*, 2016; Wilczynska *et al.*, 2019). Since the unnaturally high eIF4A2 levels in the exon 10A knockout cell line appear to mimic interactions of its paralogue eIF4A1, it is hard to draw conclusions about the function of eIF4A2 from our exon 10A knockout cell line.

Previous studies disagree on whether eIF4A2 associates with the eIF4F complex, which is involved in translation initiation, or with the CCR4–NOT complex, known for decapping and deadenylation of mRNA to promote its degradation (Wilczynska *et al.*, 2019). Based on an siRNA screen of eIF4F complex components, eIF4A2 was claimed to function in miRNA-mediated translation repression (Meijer *et al.*, 2013), as knockdown resulted in stabilization of their reporter mRNA. However, our RNA-seq analysis revealed that also the knockout of exon 4, which leads to a significant reduction in eIF4A2 levels, had no global effect on mRNA expression in HeLa cells in our experiments. This suggests that, at least on a global level, eIF4A2 does not lead to suppression of mRNA degradation. This is consistent with the findings of Galicia-Vazquez *et al.* (2015), which did not detect any significant consequences of eIF4A2 loss on global protein synthesis or cellular proliferation (Galicia-Vázquez, Chu and Pelletier, 2015).

In summary, our RNA-sequencing data show that eIF4A2 is not a factor that regulates mRNA expression and alternative splicing at a global level.

4.2 The evolutionarily conserved heat-induced poison exon 3a controls temperature-dependent RBM3 expression

Expression of the glycine-rich RNA-binding protein RBM3 was shown to be strongly upregulated at colder temperatures (Danno *et al.*, 1997). The identification of an alternatively spliced poison exon in the RBM3 transcript suggested that this splicing event is coupled to NMD, thus, resulting in a temperature-responsive regulation of RBM3 expression. Our RNA sequencing analyses revealed a dramatic increase in RBM3 mRNA expression at colder temperatures and an oppositely regulated alternative exon 3a that is strongly heat-induced. A more detailed analysis of this alternative exon's sequence revealed the existence seven PTCs, which led to its classification as a poison exon. Inhibition of translation by CHX-exposure stabilized the exon 3a inclusion isoform, clearly demonstrating that this alternative splice event is coupled to NMD (Figure 23). As PTCs lead to degradation of the mRNA via the NMD pathway, they are associated with a decreased mRNA abundance. This coupling mechanism also explains why gene expression is cold-induced while the poison exon is heat-induced: In heat, exon 3a is incorporated into the transcript by alternative splicing, which prevents protein production by induction of NMD. In the cold, the poison exon is skipped and the RBM3 mRNA transcript can be translated into a functional protein by the translational machinery. To unequivocally demonstrate this regulatory mechanism, which is comparable to temperature-dependent expression in CIRPB (Haltenhof *et al.*, 2020), we generated exon 3a knockout cell lines using the CRISPR/Cas9 system. To avoid clonal CRISPR/Cas9 effects or at least reduce their influence on the experimental output, we tested two independent exon 3a knockout cell lines in this study.

Discussion

We, impressively, demonstrated that lacking exon 3a leads not only to the loss of the temperature dependence of RBM3, but also to a constitutive overexpression of the gene (Figure 24). These results incontrovertibly demonstrate that poison exon 3a regulates temperature-dependent RBM3 expression through AS-NMD. To demonstrate this regulatory mechanism in an independent experimental approach, we used a morpholino directed against the 5'SS of exon 3a, resulting in exon exclusion, and investigated the effect on RBM3 mRNA expression via RT-qPCR. Blocking of 5'SS recognition, significantly increased RBM3 transcript levels. This confirmed that targeting splicing of exon 3a can control RBM3 expression in trans (Preußner *et al.*, 2023).

An interesting study by Peretti *et al.* (2015) suggests a function of RBM3 in the reassembly of neuronal synapses. They showed that keeping prion-diseased or Alzheimer-type mice at 16-18 °C for 45 minutes resulted in overexpression of RBM3, which was associated with the prevention of neuronal loss and spongiosis, thus leading to impressive neuroprotection (Peretti *et al.*, 2015). These findings and the results presented in our study are the foundation for the development of an antisense oligo (ASO) that targets exon 3a, which increases RBM3 expression. We are confident that this oligo, which is about to enter pre-clinical studies and toxicity models, could protect against neurodegenerative effects, thus presenting a promising tool in the treatment of neurodegenerative diseases such as Alzheimer's.

4.3 Temperature-dependent alternative exons in the unique heat-induced RNA helicase eIF4A2 regulate gene expression

In our global analysis of the transcriptome at different temperatures, we identified 250 genes that contained two temperature-dependent alternative exons in both HeLa and Hek293 cells (Figure 17). Furthermore, we observed no direct correlation between temperature-dependent splicing of transcripts with two alternative exons and temperature dependence in mRNA expression. Interestingly, the direction in which the exons were regulated and whether they were regulated in the same or opposite directions, did not affect mRNA transcript levels.

Our data, for the first time, reveal exon 4 and exon 10A of eIF4A2 to be spliced in a temperature-dependent manner. Interestingly, while most exons within a transcript are regulated in the same direction, we observed that exon 4 was preferentially included at higher temperatures, while exon 10A was predominantly found at lower temperatures. The existence of two oppositely regulated exons in one transcript is an interesting yet previously uninvestigated phenomenon (Figure 18).

Although we did not determine a global impact of the two temperature-dependent exons on mRNA expression, we observed a clear effect on eIF4A2 transcript levels. Knockout of exon 4 using the CRISPR/Cas9 system resulted in a drastically reduced temperature-sensitivity, as shown by RNA-seq and RT-qPCR. Elimination of exon 10A led to generally increased mRNA levels, which were still somewhat temperature dependent. This demonstrates that the two temperature-responsive exons in eIF4A2 are responsible for the temperature-dependent mRNA expression of eIF4A2.

To support the findings, we obtained from cell lines, we also analyzed temperature-dependent splicing of minigenes comprising exon 4 and/or exon 10A, respectively. Minigenes are not translated and therefore cannot be degraded by the mRNA surveillance pathway. Interestingly, we observed an increase in the exon 4 inclusion/exon 10A exclusion isoform at higher temperatures and an increase in the exon 4 exclusion/exon 10A inclusion isoform at lower temperatures. The splicing pattern of the minigenes is comparable to endogenous eIF4A2 splicing in response to temperature. From this, we can conclude that the two alternative splicing events are regulated by temperature, independently of NMD.

Consistent with our findings on eIF4A2 mRNA level, we also observed a heat-induced eIF4A2 protein expression pattern. Western blot analysis of our CRISPR/Cas9-modified HeLa cells showed that eIF4A2 is significantly less abundant at 32 °C compared to 40 °C. Additionally, the absence of exon 4 led to the loss of protein and the absence of exon 10A to constitutive overexpression of eIF4A2.

Most research on cold-induced proteins focused on RNA binding proteins like CIRBP and RBM3 (Lindquist and Mertens, 2018). However, also numerous RNA helicases are higher expressed at colder temperatures and cold shock-associated (Hunger *et al.*, 2006). Therefore, it is even more remarkable that the RNA helicase eIF4A2 is not only predominantly expressed at higher temperatures but also contains one of the most strongly heat-induced exons in HeLa cells. As many cellular processes are, in one way or another, impacted by changes in temperature, for example, due to the circadian rhythm (Preußner and Heyd, 2016), a temperature-dependent regulation of the expression of helicases seems reasonable. It has been reported that eIF4A2 is involved in, among other things, the immune response, in which rising temperatures are a common feature (Ndzinu *et al.*, 2018).

Impressively, our global analysis of temperature-dependent exons indicated that only 5 % of all exons are regulated in response to temperature. This finding indicates that temperature-dependent AS is not a general or random phenomenon, but a highly specific regulatory mechanism that only affects a small fraction of proteins. The fact that the expression of most RNA helicases is cold-induced while eIF4A2 appears to be the only heat-induced RNA helicase suggests that eIF4A2 fulfils a crucial function in adapting downstream processes in response to subtle temperature changes. Thus, a better understanding of the helicase's operating principles is expedient.

4.4 Exon 10A splicing regulates eIF4A2 protein expression in an all or nothing manner via coupling to NMD

To further explore the extent to which the complete loss of exon 4 affects the production of the eIF4A2 protein, we searched for specific eIF4A2 assignable peptides in the exon 4 knockout cell line. In the sequence of the eIF4A2 mRNA, we identified the start codon at position 37 in exon 1 and a stop codon in exon 11 to mark the boundaries of the predominantly formed full-length isoform (Nielsen and Trachsel, 1988). In addition to the first constitutive start codon, a potential alternative start codon in exon 3 could be found. Furthermore, skipping of exon 4 leads to a frameshift that introduces a stop codon in exon 5 and the inclusion of exon 10A is known to introduce another stop codon to the transcript. As these stop codons result in premature translation termination, they are called premature termination codons (PTCs). Therefore, two potential open reading frames are conceivable for eIF4A2 in exon 4 exclusion conditions. Bicistronic transcripts were shown to lead to the translation of two or more truncated protein fragments, respectively (Königs *et al.*, 2020).

We performed mass spectrometric analysis of our control, exon 4 and exon 10A knockout cell lines at different temperatures and specifically searched for peptides unique for eIF4A2. We found 15 such eIF4A2-specific peptides (Figure 32). However, regardless of the temperature and eIF4A2 levels, we did not find any peptide that begins with the alternative start codon in exon 3 or peptides that end at the alternative stop codons in exon 5 or exon 10A, respectively. It is important to mention, that our experimental set up renders a detection of peptides with a 10A-specific C-terminus impossible, as a lysine is located directly before the PTC. Consequently, the trypsin digest required for a mass spectrometric analysis produces a terminal fragment that only comprises two amino acids, which deceeds the measurable range of the procedure. To compensate for this technical limitation, we compared the ratio of the peptides spanning the exons 5, 6 or 11 with the reference peptide covering the junction between exons 8 and 9. However, we did not observe a higher abundance of peptides spanning the amino acid regions upstream of the PTC (exon 5 or 6) compared to the amino acid regions downstream of the PTC (exon 11). This proves, that were not able to detect the exon 10A inclusion protein isoform in our CRISPR/Cas9-modified cell lines.

In conclusion, our analysis showed impressively and unambiguously that if a protein is synthesized, translation starts in exon 1 and finishes in exon 11 and that skipping of exon 4 leads to the complete loss of the eIF4A2 protein in HeLa cells.

The presence of PTCs in the exon 4 knockout mRNA provides a good explanation why little to no protein could be detected at low temperatures and in the exon 4 knockout cell line. PTCs are known to induce mRNA degradation by the NMD pathway. In contrast to regular stop codons, PTCs are usually

associated with the presence of downstream exon junction complexes and the absence of the poly(A)-binding protein (PABP). As PABP stimulates translation termination, this process is slowed down after PTC-induced ribosome stalling. Furthermore, the EJC delays the termination progression even more to support the dissociation of the ribosome along with the recruitment of NMD factors, which then scan the mRNA and promote its degradation by the NMD machinery (Powers, Szeto and Schaffitzel, 2020).

Previous studies described a link between AS and NMD to be responsible for temperature-dependent gene regulation (McGlincy and Smith, 2008; da Costa, Menezes and Romão, 2017; Neumann *et al.*, 2020), suggesting that the temperature-sensitive splicing of exon 4 and exon 10A serves as a mechanism to regulate eIF4A2 protein expression.

Roughly 35 % of all alternative isoforms in humans are predicted to be NMD targets. Interestingly, SR proteins and hnRNPs are commonly regulated by AS-NMD. This coupling is causative for an autoregulatory feedback loop allowing a self-limiting range of protein expression. Consequently, this process enables the regulation of unproductive splicing and translation (RUST). The fact that fundamental factors such as SR proteins and hnRNPs are regulated via AS-NMD emphasizes the importance of this process (da Costa, Menezes and Romão, 2017).

Inhibition of translation in HeLa and Hek293 cells via CHX treatment led to a substantial stabilization of the PTC containing exon 10A inclusion isoform (Figure 28). Since CHX targets the ribosome, not the NMD machinery, our study only provides indirect evidence that the exon 10A inclusion isoform is a direct target for NMD. However, the knockdown of the RNA helicase UPF1, which is a known inducer of NMD, was shown to stabilize the exon 10A inclusion mRNA isoform (Huth *et al.*, 2022), supporting our suggestion that exon 10A causes the degradation of the eIF4A2 mRNA via the NMD pathway.

The contribution of the PTC in exon 5, introduced by exon 4 exclusion, is not clear at the moment. Splicing-sensitive PCR did not show an increase in the exon 4 inclusion variant upon CHX treatment, which indicates that at least in our experimental setup the induced PTC in exon 5 does not promote NMD. To determine which PTC (or both) is responsible for activating the NMD machinery, individually mutating the PTCs and investigating eIF4A2 pre-mRNA splicing after CHX exposure could provide further information.

Interestingly, Huth *et al.* (2022) investigated WT and NMD-deficient embryonic stem cells (ESCs) by western blot analysis and described the appearance of a truncated eIF4A2 protein ($eIF4A2^{PTC}$) upon NMD inhibition. Considering the fact that exon 10A comprises a PTC, they suggest that this protein isoform corresponds to a variant ending in exon 10A. It is not clear whether this isoform comprises exon 4 or not. Huth *et al.* (2022) assume that all previous exons are included but did not further investigate or mention the alternative splicing in this region. Based on our findings we would anticipate that the inclusion of exon 10A is accompanied by the absence of exon 4, however, the fact that we were not able to detect any other variant apart of the full-length protein, indicates significant differences between our cellular and/or technical systems. It is possible that the formation of a truncated eIF4A2 variant is a cell type-specific effect.

To examine if it is possible at all to express this truncated isoform, we further designed a GFP overexpression construct. Immunoblotting confirmed the presence of this protein isoform, which, however, was highly unstable and poorly expressed (data not shown). Together with our mass spectrometry data, these results suggest that the $eIF4A2^{PTC}$ protein detected by Huth *et al.* (2022) does not exist in HeLa cells. This supports our speculation that $EIF4A2^{PTC}$ might be cell type-specific or that this isoform can only be detected under specific conditions such as NMD effector protein knockout in ESCs or overexpression in HeLa cells.

4.5 Temperature-dependent exon 4 splicing determines alternative splicing of exon 10A in eIF4A2

Our investigations revealed that the absence of exon 4 results in the loss of the eIF4A2 protein. To investigate whether this phenomenon is based on the co-regulation of exon 4 and exon 10A, we performed a splicing analysis using eIF4A2 minigenes (Figure 27).

These minigenes comprised either the region around exon 4 or exon 10A, respectively and were transfected into HeLa or Hek293 cells individually or concomitantly. Splicing-sensitive PCR showed that the addition of exon 10A did not affect the inclusion of exon 4, while the presence of exon 4 favored the exclusion of exon 10A. This is consistent with the RNA-seq analysis of our exon 4 and exon 10A knockout CRISPR/Cas9 cell lines.

Since this effect can be observed in our minigene system, we conclude that elements located close to the alternative exon 4 are involved in the regulation of both exons. A linear regression of exon 4 and exon 10A incorporation in human and mice tissues also revealed a correlation between their inclusion, which supports the notion of the two exons being co-regulated. However, as exon 10A has no influence on the splicing of exon 4, we suggest a unidirectional regulation rather than a bidirectional coupling. Additionally, the analysis of the intron removal of eIF4A2 indicated that splice site selection of exon 4 takes place before the definition of exon 10A (Bergeron *et al.*, in revision). This observation is consistent with the results we obtained in the RNA-sequencing and splicing analysis of our CRISPR/Cas9-edited eIF4A2 cell lines as well as our minigene assay, which all cohesively showed that exon 4 splicing has a stronger impact on the splicing of exon 10A than the other way around (Figure 26 and Figure 27).

4.6 eIF4A2 is predominantly localized in the cytoplasm of HeLa cells

To examine whether the changes in eIF4A2 protein expression impact the localization of the protein within the cell, we performed immunofluorescence staining of our eIF4A2 CRISPR/Cas9-modified HeLa cell lines. We observed moderate levels of endogenous eIF4A2 in the control and high eIF4A2 levels in the cytoplasm of the exon 10A knockout cell line. Surprisingly, we could detect little to no endogenous eIF4A2-specific signal in exon 4 knockout cells. Based on the facts that our antibody specifically detects eIF4A2 and that our proteome analysis excluded the expression of any eIF4A2-specific peptide in the exon 4 knockout cell line, we can rule out that this signal refers to eIF4A1. This suggests that the immunofluorescence signal corresponds to unspecific staining or an autofluorescence signal.

Consequently, we can exclude that the endogenous levels of eIF4A2 affect its protein localization within the cell. As temperature also plays a crucial role in the subcellular localization of proteins (Martinez *et al.*, 1991; Upadhyay, Bhadauriya and Ganesh, 2016), we performed immunofluorescence staining of eIF4A2 at different temperatures. In the range of 10 °C to 42 °C (data shown only for 32 °C and 40 °C) eIF4A2 was located exclusively in the cytoplasm of HeLa cells, independent of the temperature. Consistent with the fact that eIF4A2, being a translation factor, is associated with ribosomes, we find eIF4A2 exclusively in the cytoplasm. Furthermore, we did not observe any changes in the eIF4A2 localization with its increasing protein abundance in response to temperature. These results indicate that temperature changes do not cause the recruitment of eIF4A2 to the nucleus or any other change of subcellular localization. Therefore, we suggest that eIF4A2 is not involved in cellular processes that take place in the nucleus.

4.7 Model for how temperature regulates mRNA and protein expression of eIF4A2

Combining the information obtained from the transcriptome and proteome analyses of HeLa cells, we generated a model for how temperature might lead to the different mRNA isoforms of eIF4A2 causing different outcomes on the protein level (Figure 40). We propose that higher temperatures lead to the inclusion of exon 4 and the exclusion of exon 10A, resulting in a high abundance of eIF4A2 mRNA. This

transcript gets translated into an annotated protein starting in exon 1 and terminating in exon 11. At colder temperatures, exon 4 is preferentially excluded, while exon 10A is incorporated. The inclusion of exon 10A causes the introduction of a PTC that renders this isoform an NMD target and results in the degradation of the mRNA. Consequently, the mRNA levels are drastically reduced, which leads to the loss of protein formation. Taken together, we conclude that temperature-dependent alternative splicing functions as a switch in the regulation of eIF4A2 abundance. Higher temperatures causing the absence of exon 10A lead to a constitutive overexpression of eIF4A2. Instead, lower temperatures cause the absence of exon 4, resulting in a complete loss of protein.

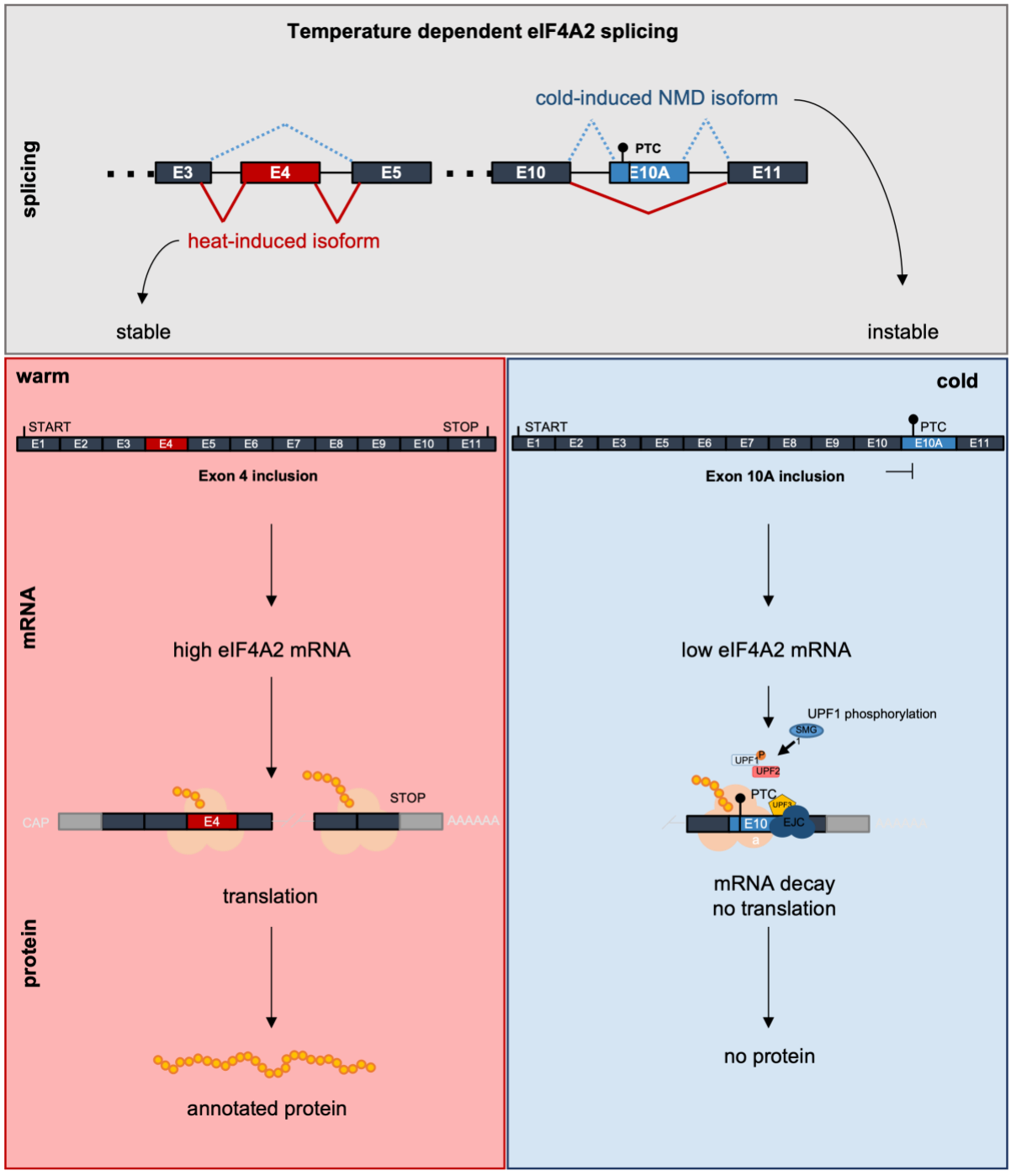

Figure 40. Model for how temperature regulates the eIF4A2 expression on the transcriptomic and proteomic level
eIF4A2 alternative splicing is regulated by temperature, which causes a heat-induced exon 4 and a cold-induced exon 10A inclusion isoform. At higher temperatures, the inclusion of exon 4 promotes the exclusion of exon 10A and leads to higher eIF4A2 mRNA levels. This results in the translation of an annotated protein. At lower temperatures, the inclusion of the poison exon 10A is coupled to the exclusion of exon 4. This poison exon induces mRNA degradation by NMD and no protein formation.

4.8 Tissue-specific eIF4A expression proposes unique functions for eIF4A2 during neuronal development

The eIF4A protein family consists of three proteins: eIF4A1, eIF4A2 and eIF4A3. The highly similar isoforms eIF4A1 and eIF4A2 share an amino acid sequence identity of almost 90 %. The third member, eIF4A3, shares approximately 60 % homology with eIF4A1 and eIF4A2 (Lu *et al.*, 2014). Neither eIF4A1 nor eIF4A3 are predicted to have any alternative exons. We could confirm this prediction by our RNA-sequencing analysis, irrespective of the temperature.

Initial research on eIF4A1 and eIF4A2 proposed a functional redundancy of the two paralogues, based on their high sequence homology (Nielsen and Trachsel, 1988). However, recent studies, investigating the expression of these two paralogues in different tissues, propose that the mRNA of eIF4A1 is preferentially synthesized and translated in dividing cells, whereas the mRNA of eIF4A2 is more likely to be expressed in growth-starved cell types. For instance, the eIF4A2 mRNA is 20-30 times higher expressed in mouse brain tissues compared to the lower expression levels in the liver, while moderate eIF4A2 levels were observed in the lung (Nielsen and Trachsel, 1988). We observed similar expression distributions in our RNA-seq analysis of publicly available datasets from mouse and human tissues (Fagerberg *et al.*, 2014; Tanikawa *et al.*, 2017), which we could verify via splicing-sensitive PCR and RT-qPCR in mouse samples. These data showed higher eIF4A2 transcript and protein levels in the brain compared to liver and spleen. In contrast, the eIF4A1 mRNA is generally higher expressed in most tissues, except for the brain (Galicia-Vázquez *et al.*, 2012).

The different expression distributions of the eIF4A1 and eIF4A2 mRNAs led to the conclusion that the two paralogues have different functions (Rogers, Komar and Merrick, 2002). This is consistent with the finding, that although eIF4A2 was shown to interact with eIF4A1-specific binding partners when it is oversaturated (Wilczynska *et al.*, 2019), its upregulation could not rescue the translational and cell proliferation suppression caused by the loss of eIF4A1 function (Raza, Waldron and Le Quesne, 2015). Interestingly, it has been reported that inhibition of eIF4A1 results in enhanced eIF4A2 transcription (Xue *et al.*, 2021). Furthermore, our RNA-seq analysis of eIF4A2 CRISPR/Cas9-edited HeLa cells showed that eIF4A1 transcript levels are independent of eIF4A2. This suggests that eIF4A1 mRNA levels unidirectionally regulate the abundance of the eIF4A2 mRNA oppositely to its own levels. Interestingly, in some mouse and human cancer types, high eIF4A1 (and low eIF4A2) levels are associated with a high probability of death, while high eIF4A2 (and low eIF4A1) levels in other cancer types are often associated with a better prognosis, suggesting different roles in proliferation (Raza, Waldron and Le Quesne, 2015) and as a result different survivability of the organism. These findings strongly suggest that eIF4A1 and eIF4A2 implement distinct, if not opposite functions in cancer cells and different tissues/organs.

As eIF4A2 is most highly expressed in the brain, a function in brain development is conceivable. This is in line with a recent publication of Paul *et al.*, which showed that deletion or missense mutation of a single amino acid results in severe neurodevelopmental diseases such as intellectual disability, hypotonia and epilepsy (Paul *et al.*, 2023). These findings underline the importance of the alternative splicing mechanism in eIF4A2, as incorrect splicing can result in a defective protein, which, as described, causes severe neuronal damage during development.

Consistent with the observation that eIF4A2 possesses an essential function during brain formation, analysis of data generated by Harnett *et al.* (2022) showed that the eIF4A2 mRNA is more abundant during neuronal development in the cortex of mice (Harnett *et al.*, 2022) and eIF4A2 expression increases during neuronal development in the embryogenesis (neurulation) in *Xenopus*. Furthermore, overexpression of eIF4A2 mRNA in *Xenopus* was shown to induce the expression of neural fold genes as well as the upregulation of genes which are expressed early in the neural plate border. (Morgan and Sargent, 1997). Large-scale studies in human tissues further demonstrated major changes in the eIF4A2 mRNA expression levels between fetal and adult tissues, with eIF4A2 expression in the adult brain being reduced by a factor of eight compared to the fetal brain (Galicia-Vázquez *et al.*, 2012). This

expression pattern is consistent with the fact that the body temperature of an adult organism is lower than in a fetus (Keil, Cummings and de Magalhães, 2015).

Using the freely available web resource "cortexomics", we showed that eIF4A2 expression at RNA and protein levels increased two-fold from stage E14 to E15.5 in mice (Figure 41). We could validate the increase in protein expression via immunoblotting (experiments in neuronal samples were performed in the lab of Matthew Kraushar; data not shown). The translation efficiency predicted by the “cortexomics” tool did not differ during embryonic development. The dependence of neuronal development on the formation of functional eIF4A2 in human, mouse, *Xenopus* and *Drosophila* indicates that eIF4A2 expression in the brain is highly conserved across many species and highlights the importance of the protein for proper brain formation (Morgan and Sargent, 1997; Galicia-Vázquez *et al.*, 2012; Raza, Waldron and Le Quesne, 2015; Paul *et al.*, 2023). Thus, eIF4A2 appears to have an individual and important role, especially in the brain and during its development.

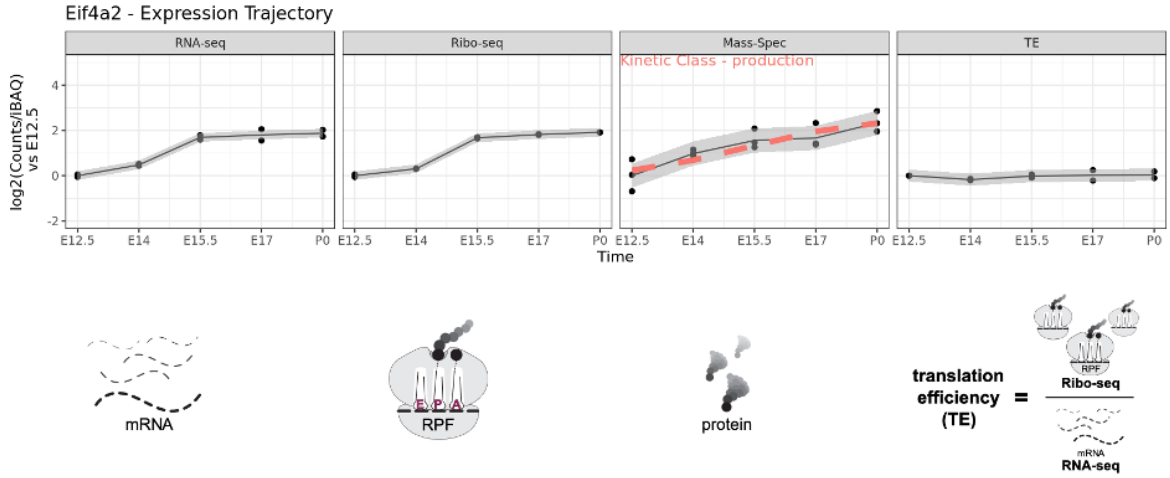

Figure 41. Expression trajectory of eIF4A2 in mouse neocortex developmental translatome
Modeling of eIF4A2 in the developmental neocortex translatome generated with the open-source resource “cortexomics” (Harnett *et al.*, 2022). Depicted are the embryonic days from 12.5 (E12.5) to 18 (E18) and the postnatal day 0 (P0).

4.9 eIF4A2 regulates protein expression of a subset of mitochondrial genes involved in the respiratory chain

Mitochondria are crucial organelles that produce most of a cell’s energy in the form of ATP through a proton gradient in the respiratory chain. Therefore, mitochondria are referred to as the powerhouse of the cell. Especially complex I plays an important role in the respiratory chain (Hirst, 2013). Gene ontology (GO) analysis was performed on the RNA sequencing and mass spectrometry datasets obtained from HeLa control cells at 32 °C compared to 40 °C. This analysis revealed a subset of temperature-dependent genes that are regulated at protein level but not mRNA levels. Interestingly, these temperature-regulated genes belong to a set of mitochondrial ribosomal proteins, suggesting that temperature may regulate processes in the human mitochondrion.

Additionally, the absence of eIF4A2 (exon 4 knockout) is causative for the upregulation of a subset of mitochondrial genes. The GO analysis identified the majority of proteins that constitute the NADH:ubiquinone oxidoreductase supernumerary subunits (NDUF) gene family, which are predominantly part of the respiratory chain complex I.

As these genes were predominantly regulated at the protein, but not the mRNA level, eIF4A2 appears to control their expression directly at the protein level, either by managing protein synthesis or degradation. It is likely that eIF4A2 either activates translation by binding to the 5’UTR or represses translation either through miRNAs or by replacing eIF4A1, which might be more active, at the 5’UTR (Galicia-Vázquez, Chu and Pelletier, 2015; Wilczynska and Bushell, 2015; Wilczynska *et al.*, 2019).

eIF4A2 is known to be involved in reducing translation initiation. However, the underlying mechanism is only poorly understood. eIF4A2 binds preferentially to mRNAs that contain purine rich motifs in the 5'UTR (Wilczynska *et al.*, 2019) and decreases their translation. To investigate whether the binding of eIF4A2 to one of the UTRs is responsible for regulating their expression, we designed GFP reporter constructs containing the 5' or 3' UTRs of four different eIF4A2-dependent mitochondrial genes. Of these genes three were upregulated (NDUFS4, NDUFA11, NDUFS8) and one was downregulated (PSMB10) in the absence of eIF4A2. The GFP reporter constructs were co-transfected with the red fluorescence construct tdTomato into HeLa cells (control cell line and exon 4 knockout cell line) and subsequently the fluorescence signal was measured by flow cytometry.
Surprisingly, none of the GFP reporters with the distinct UTRs showed a noteworthy change in expression between the control and the exon 4 knockout cell line. This suggests that neither the 5'UTR nor the 3'UTR is preferentially bound by eIF4A2.

We further investigated NDUFS4 as a representative of the NDUF family. The mass spectrometry data suggested a higher NDUFS4 abundance in the absence of eIF4A2, which was validated by western blot analysis. In a rescue experiment, we overexpressed full-length eIF4A2 in the exon 4 knockout cell line and determined NDUFS4 protein expression via western blot. This showed a reduction in NDUFS4 level upon eIF4A2 overexpression, suggesting NDUFS4 expression (and maybe of other NDUF proteins) is regulated by eIF4A2.

It is possible that eIF4A2 functions as a thermosensor in a regulatory pathway, which adapts the ATP levels in response to heat-stress. Mass spectrometric analysis of our exon 4 knockout cell line showed that in the absence of eIF4A2 the majority of NDUF genes are upregulated. Similarly, overexpressing eIF4A2 using FLAG-tagged full-length constructs, resulted in the downregulation of a representative member of the NDUF protein family. As NDUFs are fundamental components of the essential complex I in the respiratory chain, their upregulation likely leads to a higher electron transfer rate and as a result, an increased ATP synthesis (Annesley and Fisher, 2019). Consequently, a downregulation of NDUFs at higher temperatures would be associated with a reduced generation of ATP. Interestingly, a temperature increase of 2.4 °C in the mitochondria of HeLa cells was reported to decrease the ATP level by 75 % during oxidative phosphorylation (Qiao *et al.*, 2018). Even though the regulation of the NDUF proteins by eIF4A2 is temperature independent, the protein abundance of eIF4A2 is regulated in response to temperature, suggesting that eIF4A2 acts as a link between temperature changes and NDUF protein expression regulation. This notion is coherent with the fact that under heat stress conditions the demand for ATP is diminished, as helicase expression is downregulated, and translation is globally reduced (Bresson *et al.*, 2020).

Taken together, eIF4A2, the only known RNA helicase upregulated at higher temperatures, might act as a temperature detector that triggers a regulatory pathway to adjust ATP production via the NDUF protein family.

Connections between helicases and energy production have already been described previously. In endothelial cells of mice, silencing of the ATP-dependent RNA DEAH-box helicase 15 (DHX15) was shown to affect the expression of numerous proteins involved in ATP biosynthesis. This included NDUFS1, whose downregulation was associated with an impaired mitochondrial respiratory chain activity (Ribera *et al.*, 2021).

Interestingly, the cyano bacterial RNA helicase crhR was shown to be regulated through the electron transport chain. Thereby, the helicase's expression is increased at conditions that promote the reduction of the chain, such as low temperature or salt stress as well as dark-light transition (Kujat and Owttrim, 2000). The observation that RNA helicase activity not only affects the functionality of the chain but also the inverted effect does exist, indicates a strong connection between helicases and the ETC.

Discussion

4.10 Oxidative stress induced by arsenite regulates alternative splicing of eIF4A2 which is recruited into stress granules

Stress can have severe consequences for the cell depending on its intensity and duration. In stress situations, the cell needs to adapt its metabolism to survive under these harmful conditions. A mechanism to respond rapidly to stress on a genome-wide scale is alternative splicing. In addition, gene silencing by miRNAs plays an important role in gene regulation under stress conditions. Especially during transient stress, post-transcriptional mechanisms help to rapidly regulate the synthesis, stability, and localization of different mRNA isoforms. In the course of our study, we looked at eIF4A2 splicing in publicly available RNA-sequencing data. Consistent with the RNA-seq predictions, we showed that acute physiological stress preferentially stimulates the generation of the alternatively spliced eIF4A2 exon 10A inclusion isoform. Taken together, our findings suggest that in HeLa and Hek293 cells oxidative stress favors the inclusion of exon 10A over exon 4 in response to arsenite (Figure 37).

It would be interesting to demonstrate whether oxidative stress leads to increased formation of the exon 10A isoform, which is a known NMD target. Investigation of the involvement of NMD in the degradation of the stress-induced exon 10A isoform, would require the inhibition of NMD factors (UPF1, for example), followed by examination of exon 10A inclusion isoform levels. If stress results in an increased expression despite UPF1 inhibition, this result would provide evidence that NMD is not involved in the stress-induced splicing of the eIF4A2 mRNA.

In addition to the effects observed at the RNA level, we were also able to detect an impact of oxidative stress on eIF4A2 protein formation. Already after one and two hours of exposure to arsenite, we discovered that the amount of eIF4A2 protein was decreased significantly. This can be explained by the higher inclusion of the PTC in exon 10A, which we detected in a splicing-sensitive PCR. Surprisingly, the protein level increased again after four hours of arsenite treatment, almost reaching control levels. Nevertheless, western blot analysis of the arsenite-treated cells demonstrated the presence of phosphorylated eIF2a, which is an established indicator for arsenite stress conditions. It is possible that the cell is able to develop some kind of adaptation mechanism to stress over time. However, the underlying mechanism remains unclear.

It is known that the exposure to stress induces the formation of stress granules. These have an important task in protecting the cell from damage and enabling a fast resumption of translation. It has been demonstrated that stress granule formation plays a repressive role in translation, as many translational repressors partition in stress granules. As a consequence, it was shown that stress granule formation correlates with reduced global translation (Anderson and Kedersha, 2009). However, SG formation is not a prerequisite for global translational repression (Buchan and Parker, 2009).

Previous studies indicated that many eukaryotic initiation factors like eIF4E, eIF4G, eIF4A or eIF4B are recruited into stress granules (Buchan and Parker, 2009). For example, arsenite induces the partition of eIF4A1 in the periphery of SGs (Tauber *et al.*, 2020). To assess the localization of eIF4A2 within the cell during stress conditions, we induced oxidative stress by arsenite treatment for one hour. Based on immunofluorescence staining, eIF4A2 partitions in stress granules in the cytoplasm of HeLa cells (Figure 38). Interestingly, our fluorescence staining created the impression that eIF4A2 is enriched in the center of SGs. Stress granule disassembly is important for rapid resumption of translation and therefore correlates with the recovery of protein synthesis. However, complete SG resolution is not a prerequisite for translation resumption (Buchan and Parker, 2009). Taken together, these observations allude to the idea that eIF4A2 is involved in mRNA repression during stress response but is not essential for the fast revival of translation. To obtain a clearer picture of the role of eIF4A2, further experiments would be required. For instance, high-resolution fluorescence microscopy could present a more precise picture of the localization of eIF4A2 in the context of SGs, while ribosome profiling would provide a quantitative determination of the translation efficiency.

4.11 DNA and RNA helicase levels determine the efficiency of many cellular processes

Proteins with helicase activity were originally described in *Escherichia coli* in the 1970s. Since then, the existence of DNA and RNA helicases has been established in many organisms. Additionally, mutations in helicases were shown to be associated with various diseases. Especially in virus replication, helicases play an important role (Patel and Donmez, 2006). The class of DEAD-box helicases use ATP to unwind RNA secondary structures, whereby the stability of the secondary structure limits the unwinding efficiency (Linder and Jankowsky, 2011). The RNA secondary structures within mRNAs increase in complexity at colder temperatures and impede the translation elongation, RNA turnover and the binding of microRNAs. Thus, it is plausible that the expression of temperature-sensitive RNA helicases is associated with colder temperatures in prokaryotes and higher eukaryotes (Rosana, Chamot and Owttrim, 2012).

To further investigate the temperature dependency of RNA helicases we took a closer look at their gene and protein expression in our bioinformatic datasets, in which we could detect around 80-90 % of all annotated human RNA helicases. Approximately half of the RNA helicases we found were not temperature controlled (Figure 39). The majority of the temperature-controlled RNA helicases were temperature dependent only on the RNA level. Interestingly, only two RNA helicases were regulated on RNA and protein levels. At lower temperatures, we identified the mitochondrial DEAD-box protein 28 (DDX28) as the only RNA helicase that was upregulated on both RNA and protein levels. DDX28 is localized in mitochondria and partially in the nucleus (Valgardsdottir, Ottersen and Prydz, 2004). Although not much is known about the function of DDX28, it seems to be involved in the biogenesis of mitochondrial ribosomes (Antonicka and Shoubridge, 2015).

Additionally, we found only one RNA helicase to be upregulated at higher temperatures, both on RNA and protein levels. This RNA helicase was eIF4A2. Interestingly, both RNA helicases that could be identified as temperature controlled on RNA and protein levels, are both DEAD-box helicases that interact with the ribosome. While DDX28 has a function in mitoribosome biogenesis (Tu and Antoni, 2016), eIF4A2 interacts with the cellular ribosome.

Our data classify eIF4A2 as the strongest temperature-dependent RNA helicase in HeLa cells. The role of the eIF4A homologs in translation initiation is to unwind RNA secondary structures, thereby creating single-stranded RNAs that enable binding of the ribosome (Sen *et al.*, 2015). Investigation of translation revealed a reduction in the translation rate at colder temperatures in *E. coli* (Friedman, H., Lu, P. & Rich, 1969; Broeze, Solomon and Pope, 1978). Between 25 °C and 37 °C, an increase in temperature causes a raise in translation rate (Farewell and Neidhardt, 1998). This is consistent with the previous suggestion that eIF4A2 mimics the function of eIF4A1 in promoting translation initiation when higher temperatures result in overexpression-like levels of eIF4A2 (Wilczynska *et al.*, 2019). To expand our current knowledge on the specific functions of eIF4A2 during translation, a quantitative measurement of the translation efficiency at different eIF4A2 levels by ribosome profiling could be performed.

While many RNA helicases are predominantly expressed at colder temperatures (Rossana et al), we found eIF4A2 to be the only RNA helicase that was strongly heat-induced, suggesting an extraordinary role of eIF4A2. Temperatures above 39 °C are challenging to human cells, consequently an organism depends on mechanisms to protect itself against heat stress. This is achieved by repressing translation and recruiting most components belonging to the 48S-preinitiation complex into SGs. Under these conditions, the cell relies on translating only mRNAs necessary for stress defense.

eIF4A2 predominantly binds to the N-terminus of mRNAs and unwinds secondary structures in the 5' UTRs. At higher temperatures, the secondary structures of the mRNA are less stable, consequently reducing the requirement for helical activity. Previous studies have shown that eIF4A2-bound mRNAs are repressed in translation initiation (Wilczynska *et al.*, 2019). It is possible that, at least under heat stress, the function of eIF4A2 is independent from its helicase activity. Under these conditions, a higher expression could contribute to the regulation of translational repression through binding to non-stress

related mRNAs. Some of these transcripts might be stored in SGs, until resumption of normal gene expression, as we discussed earlier.

Cautiously speaking, temperature-dependent helicases seem to play a crucial role in protein synthesis, but the evidence gathered up to this point does not allow drawing solid conclusions. Further experiments of temperature-dependent protein synthesis in the cell and mitochondria, are required to gain more insights into the mechanism of temperature-controlled RNA helicases in (mito)ribosomal assembly.

4.12 eIF4A2 and DDX28 are host factors in the replication of HIV-1

A common feature of eIF4A2 and DDX28 is their involvement in the human immunodeficiency virus 1 (HIV-1) replication (Williams *et al.*, 2015; Ndzinu *et al.*, 2018). eIF4A2 was identified as a host factor required for HIV-1 replication by unwinding the viral RNA and regulating viral cDNA synthesis (Ndzinu *et al.*, 2018). The replication of HIV-1 is dramatically increased at a febrile temperature (39.5 °C) (Roesch *et al.*, 2012). This is consistent with our findings which show that eIF4A2 expression is elevated at higher temperatures, suggesting that the increase in temperature due to viral inflammation raises the eIF4A2 level, which then induces HIV-1 replication. While eIF4A2 is necessary for unwinding viral RNA, DDX28 expression was shown to be required for infectious particle production, and lower DDX28 levels were shown to cause a reduction in the infectivity of HIV-1 (Williams *et al.*, 2015). Interestingly, our data reveal that DDX28 is downregulated at higher temperatures. This raises the possibility of a temperature-dependent interplay between DDX28 and eIF4A2 expression in the response to HIV-1 infection. Additional studies are required to clarify the role of DDX28 in HIV-1 replication and a potential interaction between these two helicases to allow a more profound interpretation of these effects.

4.13 Perspectives

This thesis aimed to clarify the role of temperature-sensitive alternative exons in mRNA and protein expression of eIF4A2. The establishment of CRISPR/Cas9 genome-edited cell lines resulted in an excellent tool to study the effects of temperature on alternative splicing in general and the expression of eIF4A2 in particular. However, using CRISPR/Cas9-edited cell lines is always associated with the possibility of clonal effects. Thus, it would be important for future investigations to confirm existing results in other systems. For example, an siRNA-mediated eIF4A2 knockdown would be suitable to confirm the effects of the exon 4 knockout cell line. This would complement our overexpression system, which verified the accuracy of our exon 10A knockout cell line. The combination of a reliable knockout and overexpression cell culture system provides a valuable foundation for an even more thorough investigation of the role of eIF4A2 in different processes such as translation initiation, viral and oxidative stress response, brain development and function or electron transfer in the respiratory chain.

In this study, we could show that eIF4A2 gene expression is controlled by its two temperature-dependent exons 4 and 10A. At this point, it is not entirely clear how the interaction between the two exons is mediated during alternative splicing, especially as splice site selection of exon 4 takes place before the definition of exon 10A. One possibility is that he presence of exon 4 promotes the skipping of exon 10A and that this inhibitory effect is disrupted when exon 4 is excluded. Alternatively, if exon 4 alternative splicing does not actively impact the splicing of exon 10A, exon 10A might be spliced in a temperature- or tissue-specific manner, regardless of exon 4. A genome-edited cell line where exon 4 is permanently included would be a suitable system to investigate this phenomenon as it allows a mechanistic investigation independent of other factors such as temperature or oxidative stress, which are known to determine eIF4A2 mRNA splicing.

Unfortunately, the specific study of the eIF4A2 function within the cell proved difficult, as eIF4A1 and eIF4A2 are highly homologous and unphysiologically high eIF4A2 levels are anticipated to imitate eIF4A1-specific enzymatic functions.

At this point, it is not entirely clear how eIF4A2 regulates the translation initiation and impacts the aerobic respiration. A good way to investigate the role of eIF4A2 in translation initiation would be to measure

gene expression in our knockout cell lines at the translational level via ribosome footprinting (Ribo-Seq). To study the interaction between mRNA and ribosomes in response to temperature or eIF4A2 levels polysome profiling could be performed. Together, the above-mentioned experiments would enable an in-depth investigation of the translatome under the impact of different eIF4A2 abundancies and temperatures changes.

To investigate the impact of eIF4A2 on the respiratory chain, a seahorse assay measuring the oxygen consumption rate (OCR) and extracellular acidification rate (ECAR) of living cells could be performed in the different CRISPR/Cas9 cell lines. This procedure assesses and quantifies the rate at which ATP is simultaneously produced from the glycolytic and mitochondrial systems in living cells and would, thus, provide a profound understanding of the role of eIF4A2 in mitochondria.

This study impressively showed how versatile the regulation of eIF4A2 is. As an RNA helicase, eIF4A2 is involved in many cellular processes that depend on RNA unwinding. The unique temperature dependence of this helicase opens many possibilities to study cellular processes in response to temperature.

5. References

Andersen, C.B.F. *et al.* (2006) 'Structure of the exon junction core complex with a trapped DEAD-Box ATPase bound to RNA', *Science*, 313(5795), pp. 1968–1972. Available at: https://doi.org/10.1126/science.1131981.

Anderson, P. and Kedersha, N. (2009) 'RNA granules: Post-transcriptional and epigenetic modulators of gene expression', *Nature Reviews Molecular Cell Biology*, 10(6), pp. 430–436. Available at: https://doi.org/10.1038/nrm2694.

Annesley, S.J. and Fisher, P.R. (2019) 'Mitochondria in Health and Disease', *Cells*, 8(7), p. 680. Available at: https://doi.org/10.3390/cells8070680.

Antonicka, H. and Shoubridge, E.A. (2015) 'Mitochondrial RNA Granules Are Centers for Posttranscriptional RNA Processing and Ribosome Biogenesis', *Cell Reports*, 10(6), pp. 920–932. Available at: https://doi.org/10.1016/j.celrep.2015.01.030.

Asangani, I.A. *et al.* (2008) 'MicroRNA-21 (miR-21) post-transcriptionally downregulates tumor suppressor Pdcd4 and stimulates invasion, intravasation and metastasis in colorectal cancer', *Oncogene*, 27(15), pp. 2128–2136. Available at: https://doi.org/10.1038/sj.onc.1210856.

Ballut, L. *et al.* (2005) 'The exon junction core complex is locked onto RNA by inhibition of eIF4AIII ATPase activity', *Nature Structural and Molecular Biology*, 12(10), pp. 861–869. Available at: https://doi.org/10.1038/nsmb990.

Baralle, F.E. and Giudice, J. (2017) 'Alternative splicing as a regulator of development and tissue identity', *Nature Reviews Molecular Cell Biology*, 18(7), pp. 437–451. Available at: https://doi.org/10.1038/nrm.2017.27.

Bergfort, A. *et al.* (2022) 'A multi-factor trafficking site on the spliceosome remodeling enzyme BRR2 recruits C9ORF78 to regulate alternative splicing', *Nature Communications*, 13(1), pp. 1–16. Available at: https://doi.org/10.1038/s41467-022-28754-2.

Black, D.L. (2003) 'Mechanisms of alternative pre-messenger RNA splicing', *Annual Review of Biochemistry*, 72, pp. 291–336. Available at: https://doi.org/10.1146/annurev.biochem.72.121801.161720.

Blencowe, B.J. (2006) 'Alternative Splicing: New Insights from Global Analyses', *Cell*, 126(1), pp. 37–47. Available at: https://doi.org/10.1016/j.cell.2006.06.023.

Bresson, S. *et al.* (2020) 'Stress-Induced Translation Inhibition through Rapid Displacement of Scanning Initiation Factors', *Molecular Cell*, 80(3), pp. 470-484.e8. Available at: https://doi.org/10.1016/j.molcel.2020.09.021.

Broeze, R.J., Solomon, C.J. and Pope, D.H. (1978) 'Effects of low temperature on in vivo and in vitro protein synthesis in Escherichia coli and Pseudomonas fluorescens', *Journal of Bacteriology*, 134(3), pp. 861–874. Available at: https://doi.org/10.1128/jb.134.3.861-874.1978.

Buchan, J.R. and Parker, R. (2009) 'Eukaryotic Stress Granules : The Ins and Out of Translation What are Stress Granules ?', *Molecular cell*, 36(6), p. 932.

Capovilla, G. *et al.* (2015) 'Role of alternative pre-mRNA splicing in temperature signaling', *Current Opinion in Plant Biology*, 27, pp. 97–103. Available at: https://doi.org/10.1016/j.pbi.2015.06.016.

Chalabi Hagkarim, N. and Grand, R.J. (2020) *The Regulatory Properties of the Ccr4-Not Complex*, *Cells*. Available at: https://doi.org/10.3390/cells9112379.

Chomyn, A. *et al.* (1986) 'URF6, last unidentified reading frame of human mtDNA, codes for an NADH dehydrogenase subunit', *Science*, 234(4776), pp. 614–618. Available at: https://doi.org/10.1126/science.3764430.

Clawson, G.A., Feldherr, C.M. and Smuckler, E.A. (1985) 'Nucleocytoplasmic RNA transport', *Molecular and Cellular Biochemistry*, 67(2), pp. 87–99. Available at: https://doi.org/10.1007/BF02370167.

Cooper, T.A. (2005) 'Use of minigene systems to dissect alternative splicing elements', *Methods*, 37(4),

pp. 331–340. Available at: https://doi.org/10.1016/j.ymeth.2005.07.015.

da Costa, P.J., Menezes, J. and Romão, L. (2017) 'The role of alternative splicing coupled to nonsense-mediated mRNA decay in human disease', *International Journal of Biochemistry and Cell Biology*, 91, pp. 168–175. Available at: https://doi.org/10.1016/j.biocel.2017.07.013.

Crick, F. (1970) 'Central Dogma of Molecular Biology', *Nature*, 227(5258), pp. 561–563. Available at: https://doi.org/10.1038/227561a0.

Danno, S. *et al.* (1997) 'Increased transcript level of RBM3, a member of the glycine-rich RNA-binding protein family, in human cells in response to cold stress', *Biochemical and Biophysical Research Communications*, 236(3), pp. 804–807. Available at: https://doi.org/10.1006/bbrc.1997.7059.

Dobin, A. *et al.* (2013) 'STAR: Ultrafast universal RNA-seq aligner', *Bioinformatics*, 29(1), pp. 15–21. Available at: https://doi.org/10.1093/bioinformatics/bts635.

Dresios, J. *et al.* (2005) 'Cold stress-induced protein Rbm3 binds 60S ribosomal subunits, alter microRNA levels, and enhances global protein synthesis', *Proceedings of the National Academy of Sciences of the United States of America*, 102(6), pp. 1865–1870. Available at: https://doi.org/10.1073/pnas.0409764102.

Evans, S.S., Repasky, E.A. and Fisher, D.T. (2015) 'Fever and the thermal regulation of immunity: the immune system feels the heat', *Nature Reviews Immunology*, 15(6), pp. 335–349. Available at: https://doi.org/10.1038/nri3843.

Fagerberg, L. *et al.* (2014) 'Analysis of the human tissue-specific expression by genome-wide integration of transcriptomics and antibody-based proteomics', *Molecular and Cellular Proteomics*, 13(2), pp. 397–406. Available at: https://doi.org/10.1074/mcp.M113.035600.

Fairman-Williams, M.E., Guenther, U.-P. and Jankowsky, E. (2010) 'SF1 and SF2 helicases: family matters', *Current Opinion in Structural Biology*, 20(3), pp. 313–324. Available at: https://doi.org/10.1016/j.sbi.2010.03.011.

Farewell, A. and Neidhardt, F.C. (1998) 'Effect of temperature on in vivo protein synthetic capacity in Escherichia coli', *Journal of Bacteriology*, 180(17), pp. 4704–4710. Available at: https://doi.org/10.1128/jb.180.17.4704-4710.1998.

Fatscher, T., Boehm, V. and Gehring, N.H. (2015) 'Mechanism, factors, and physiological role of nonsense-mediated mRNA decay', *Cellular and Molecular Life Sciences*, 72(23), pp. 4523–4544. Available at: https://doi.org/10.1007/s00018-015-2017-9.

Fica, S.M. *et al.* (2017) 'Structure of a spliceosome remodelled for exon ligation', *Nature*, 542(7641), pp. 377–380. Available at: https://doi.org/10.1038/nature21078.

Friedman, H., Lu, P. & Rich, A. (1969) 'Ribosomal Subunits produced by Cold Sensitive Initiation of Protein Synthesis', 223, pp. 909–913. Available at: https://doi.org/10.1038/223909a0.

Fu, X.-D. and Ares, M. (2014) 'Context-dependent control of alternative splicing by RNA-binding proteins', *Nature Reviews Genetics*, 15(10), pp. 689–701. Available at: https://doi.org/10.1038/nrg3778.

Galicia-Vázquez, G. *et al.* (2012) 'A cellular response linking eIF4AI activity to eIF4AII transcription', *Rna*, 18(7), pp. 1373–1384. Available at: https://doi.org/10.1261/rna.033209.112.

Galicia-Vázquez, G., Chu, J. and Pelletier, J. (2015) 'EIF4AII is dispensable for miRNA-mediated gene silencing', *Rna*, 21(10), pp. 1826–1833. Available at: https://doi.org/10.1261/rna.052225.115.

Garneau, N.L., Wilusz, J. and Wilusz, C.J. (2007) 'The highways and byways of mRNA decay', *Nature Reviews Molecular Cell Biology*, 8(2), pp. 113–126. Available at: https://doi.org/10.1038/nrm2104.

Gehring, N.H. and Roignant, J.Y. (2021) 'Anything but Ordinary – Emerging Splicing Mechanisms in Eukaryotic Gene Regulation', *Trends in Genetics*, 37(4), pp. 355–372. Available at: https://doi.org/10.1016/j.tig.2020.10.008.

Geuens, T., Bouhy, D. and Timmerman, V. (2016) 'The hnRNP family: insights into their role in health and disease', *Human Genetics*, 135(8), pp. 851–867. Available at: https://doi.org/10.1007/s00439-016-1683-5.

References

Green, M.R. (1986) 'PRE-mRNA SPLICING', *Annual Review of Genetics*, 20(1), pp. 671–708. Available at: https://doi.org/10.1146/annurev.ge.20.120186.003323.

Haltenhof, T. *et al.* (2020) 'A Conserved Kinase-Based Body-Temperature Sensor Globally Controls Alternative Splicing and Gene Expression', *Molecular Cell*, 78(1), pp. 57-69.e4. Available at: https://doi.org/10.1016/j.molcel.2020.01.028.

Harnett, D. *et al.* (2022) 'A critical period of translational control during brain development at codon resolution', *Nature Structural and Molecular Biology*, 29(12), pp. 1277–1290. Available at: https://doi.org/10.1038/s41594-022-00882-9.

Heinrichs, V. *et al.* (1990) 'U1-specific protein C needed for efficient complex formation of U1 snRNP with a 5′ splice site', *Science*, 247(4938), pp. 69–72. Available at: https://doi.org/10.1126/science.2136774.

Heyd, F. and Lynch, K.W. (2011) 'DEGRADE, MOVE, REGROUP: signaling control of splicing proteins', *Trends in Biochemical Sciences*, 36(8), pp. 397–404. Available at: https://doi.org/10.1016/j.tibs.2011.04.003.

Hiller, M. *et al.* (2007) 'Pre-mRNA secondary structures influence exon recognition', *PLoS Genetics*, 3(11), pp. 2147–2155. Available at: https://doi.org/10.1371/journal.pgen.0030204.

Le Hir, H. *et al.* (2000) 'The spliceosome deposits multiple proteins 20-24 nucleotides upstream of mRNA exon-exon junctions', *EMBO Journal*, 19(24), pp. 6860–6869. Available at: https://doi.org/10.1093/emboj/19.24.6860.

Hirst, J. (2013) 'Mitochondrial Complex I', *Annual Review of Biochemistry*, 82(1), pp. 551–575. Available at: https://doi.org/10.1146/annurev-biochem-070511-103700.

Holbrook, J.A. *et al.* (2004) 'Nonsense-mediated decay approaches the clinic', *Nature Genetics*, 36(8), pp. 801–808. Available at: https://doi.org/10.1038/ng1403.

Houseley, J. and Tollervey, D. (2009) 'The Many Pathways of RNA Degradation', *Cell*, 136(4), pp. 763–776. Available at: https://doi.org/10.1016/j.cell.2009.01.019.

Hu, Y. *et al.* (2022) 'RBM3 is an outstanding cold shock protein with multiple physiological functions beyond hypothermia', *Journal of Cellular Physiology*, 237(10), pp. 3788–3802. Available at: https://doi.org/10.1002/jcp.30852.

Hunger, K. *et al.* (2006) 'Cold-induced putative DEAD box RNA helicases CshA and CshB are essential for cold adaptation and interact with cold shock protein B in Bacillus subtilis', *Journal of Bacteriology*, 188(1), pp. 240–248. Available at: https://doi.org/10.1128/JB.188.1.240-248.2006.

Huth, M. *et al.* (2022) 'NMD is required for timely cell fate transitions by fine-tuning gene expression and regulating translation', *Genes and Development*, 34(5), pp. 348–367. Available at: https://doi.org/10.1101/gad.347690.120.

Jackson, R.J., Hellen, C.U.T. and Pestova, T. V. (2010) 'The mechanism of eukaryotic translation initiation and principles of its regulation', *Nature Reviews Molecular Cell Biology*, 11(2), pp. 113–127. Available at: https://doi.org/10.1038/nrm2838.

Jacob, F. and Monod, J. (1961) 'Genetic regulatory mechanisms in the synthesis of proteins', *Journal of Molecular Biology*, 3(3), pp. 318–356. Available at: https://doi.org/10.1016/S0022-2836(61)80072-7.

Jewer, M., Findlay, S.D. and Postovit, L.M. (2012) 'Post-transcriptional regulation in cancer progression Microenvironmental control of alternative splicing and translation', *Journal of Cell Communication and Signaling*, 6(4), pp. 233–248. Available at: https://doi.org/10.1007/s12079-012-0179-x.

Ji, H. *et al.* (2020) 'Identification, functional prediction, and key lncRNA verification of cold stress-related lncRNAs in rats liver', *Scientific Reports*, 10(1), pp. 1–14. Available at: https://doi.org/10.1038/s41598-020-57451-7.

Ji, P. *et al.* (2003) 'MALAT-1, a novel noncoding RNA, and thymosin β4 predict metastasis and survival in early-stage non-small cell lung cancer', *Oncogene*, 22(39), pp. 8031–8041. Available at: https://doi.org/10.1038/sj.onc.1206928.

References

Kedersha, N. *et al.* (2005) ‘Stress granules and processing bodies are dynamically linked sites of mRNP remodeling’, *Journal of Cell Biology*, 169(6), pp. 871–884. Available at: https://doi.org/10.1083/jcb.200502088.

Keil, G., Cummings, E. and de Magalhães, J.P. (2015) ‘Being cool: how body temperature influences ageing and longevity’, *Biogerontology*, 16(4), pp. 383–397. Available at: https://doi.org/10.1007/s10522-015-9571-2.

Königs, V. *et al.* (2020) ‘SRSF7 maintains its homeostasis through the expression of Split-ORFs and nuclear body assembly’, *Nature Structural and Molecular Biology*, 27(3), pp. 260–273. Available at: https://doi.org/10.1038/s41594-020-0385-9.

Krämer, A. (1996) ‘THE STRUCTURE AND FUNCTION OF PROTEINS INVOLVED IN MAMMALIAN PRE-mRNA SPLICING’, *Annual Review of Biochemistry*, 65(1), pp. 367–409. Available at: https://doi.org/10.1146/annurev.bi.65.070196.002055.

Kujat, S.L. and Owttrim, G.W. (2000) ‘Redox-regulated RNA helicase expression’, *Plant Physiology*, 124(2), pp. 703–713. Available at: https://doi.org/10.1104/pp.124.2.703.

Kuzuoğlu-Öztürk, D. *et al.* (2016) ‘ mi RISC and the CCR 4– NOT complex silence mRNA targets independently of 43S ribosomal scanning ’, *The EMBO Journal*, 35(11), pp. 1186–1203. Available at: https://doi.org/10.15252/embj.201592901.

Kyono, K., Miyashiro, M. and Taguchi, I. (2002) ‘Human eukaryotic initiation factor 4AII associates with hepatitis C virus NS5B protein in vitro’, *Biochemical and Biophysical Research Communications*, 292(3), pp. 659–666. Available at: https://doi.org/10.1006/bbrc.2002.6702.

Laggerbauer, B., Achsel, T. and Lührmann, R. (1998) ‘The human U5-200kD DEXH-box protein unwinds U4/U6 RNA duplices in vitro’, *Proceedings of the National Academy of Sciences of the United States of America*, 95(8), pp. 4188–4192. Available at: https://doi.org/10.1073/pnas.95.8.4188.

Lambowitz, A.M. and Zimmerly, S. (2011) ‘Group II Introns: Mobile Ribozymes that Invade DNA’, *Cold Spring Harbor Perspectives in Biology*, 3(8), pp. a003616–a003616. Available at: https://doi.org/10.1101/cshperspect.a003616.

Laube, E. *et al.* (2022) ‘Conformational changes in mitochondrial complex I of the thermophilic eukaryote Chaetomium thermophilum’, *Science Advances*, 8(47), pp. 1–15. Available at: https://doi.org/10.1126/sciadv.adc9952.

Lewis, B.P., Green, R.E. and Brenner, S.E. (2003) ‘Evidence for the widespread coupling of alternative splicing and nonsense-mediated mRNA decay in humans’, *Proceedings of the National Academy of Sciences of the United States of America*, 100(1), pp. 189–192. Available at: https://doi.org/10.1073/pnas.0136770100.

Li, Q. *et al.* (1999) ‘Eukaryotic Translation Initiation Factor 4AIII (eIF4AIII) Is Functionally Distinct from eIF4AI and eIF4AII’, *Molecular and Cellular Biology*, 19(11), pp. 7336–7346. Available at: https://doi.org/10.1128/mcb.19.11.7336.

Lin, C.J. *et al.* (2008) ‘c-Myc and eIF4F are components of a feedforward loop that links transcription and translation’, *Cancer Research*, 68(13), pp. 5326–5334. Available at: https://doi.org/10.1158/0008-5472.CAN-07-5876.

Linder, P. and Jankowsky, E. (2011) ‘From unwinding to clamping ĝ€" the DEAD box RNA helicase family’, *Nature Reviews Molecular Cell Biology*, 12(8), pp. 505–516. Available at: https://doi.org/10.1038/nrm3154.

Linder, P. and Slonimski, P.P. (1988) ‘Sequence of the genes TIF1 and TIF2 from Saccharomyces cerevisiae coding for a translation initiation factor’, *Nucleic Acids Research*, 16(21), p. 10359. Available at: https://doi.org/10.1093/nar/16.21.10359.

Lindquist, J.A. and Mertens, P.R. (2018) ‘Cold shock proteins: From cellular mechanisms to pathophysiology and disease’, *Cell Communication and Signaling*, 16(1), pp. 1–14. Available at: https://doi.org/10.1186/s12964-018-0274-6.

Liu, L. *et al.* (2022) ‘The splicing factor RBM17 drives leukemic stem cell maintenance by evading

References

nonsense-mediated decay of pro-leukemic factors', *Nature Communications*, 13(1). Available at: https://doi.org/10.1038/s41467-022-31155-0.

Liu, Q., Fang, L. and Wu, C. (2022) 'Alternative Splicing and Isoforms: From Mechanisms to Diseases', *Genes*, 13(3). Available at: https://doi.org/10.3390/genes13030401.

Liu, Y. *et al.* (2017) 'Impact of Alternative Splicing on the Human Proteome', *Cell Reports*, 20(5), pp. 1229–1241. Available at: https://doi.org/10.1016/j.celrep.2017.07.025.

Los, B. *et al.* (2022) 'Body temperature variation controls pre-mRNA processing and transcription of antiviral genes and SARS-CoV-2 replication', *Nucleic Acids Research*, 50(12), pp. 6769–6785. Available at: https://doi.org/10.1093/nar/gkac513.

Love, M.I., Huber, W. and Anders, S. (2014) 'Moderated estimation of fold change and dispersion for RNA-seq data with DESeq2', *Genome Biology*, 15(12), pp. 1–21. Available at: https://doi.org/10.1186/s13059-014-0550-8.

Lu, W.T. *et al.* (2014) 'The diverse roles of the eIF4A family: You are the company you keep', *Biochemical Society Transactions*, 42(1), pp. 166–172. Available at: https://doi.org/10.1042/BST20130161.

Madhani, H.D. and Guthrie, C. (1992) 'A novel base-pairing interaction between U2 and U6 snRNAs suggests a mechanism for the catalytic activation of the spliceosome', *Cell*, 71(5), pp. 803–817. Available at: https://doi.org/10.1016/0092-8674(92)90556-R.

Maier, T., Güell, M. and Serrano, L. (2009) 'Correlation of mRNA and protein in complex biological samples', *FEBS Letters*, 583(24), pp. 3966–3973. Available at: https://doi.org/10.1016/j.febslet.2009.10.036.

Martinez, J. *et al.* (1991) 'Cellular localization and cell cycle regulation by a temperature-sensitive p53 protein', *Genes and Development*, 5(2), pp. 151–159. Available at: https://doi.org/10.1101/gad.5.2.151.

Mateju, D. *et al.* (2020) 'Single-Molecule Imaging Reveals Translation of mRNAs Localized to Stress Granules', *Cell*, 183(7), pp. 1801-1812.e13. Available at: https://doi.org/10.1016/j.cell.2020.11.010.

Mathys, H. *et al.* (2014) 'Structural and Biochemical Insights to the Role of the CCR4-NOT Complex and DDX6 ATPase in MicroRNA Repression', *Molecular Cell*, 54(5), pp. 751–765. Available at: https://doi.org/10.1016/j.molcel.2014.03.036.

McGlincy, N.J. and Smith, C.W.J. (2008) 'Alternative splicing resulting in nonsense-mediated mRNA decay: what is the meaning of nonsense?', *Trends in Biochemical Sciences*, 33(8), pp. 385–393. Available at: https://doi.org/10.1016/j.tibs.2008.06.001.

Meijer, H. a *et al.* (2013) 'Translational Repression and eIF4A2 Activity Are Critical for MicroRNA-Mediated Gene Regulation', *Science*, 340(6128), pp. 82–85. Available at: https://doi.org/10.1126/science.1231197.

Meijer, H.A. *et al.* (2019) 'DEAD-box helicase eIF4A2 inhibits CNOT7 deadenylation activity', *Nucleic Acids Research*, 47(15), pp. 8224–8238. Available at: https://doi.org/10.1093/nar/gkz509.

Merendino, L. *et al.* (1999) 'Inhibition of msl-2 splicing by Sex- lethal reveals interaction between', *Nature*, 402(December), pp. 1–4.

Merrick, W.C. and Pavitt, G.D. (2018) 'Protein synthesis initiation in eukaryotic cells', *Cold Spring Harbor Perspectives in Biology*, 10(12), pp. 1–22. Available at: https://doi.org/10.1101/cshperspect.a033092.

Meyer, M. *et al.* (2011) 'Deciphering 3'ss Selection in the Yeast Genome Reveals an RNA Thermosensor that Mediates Alternative Splicing', *Molecular Cell*, 43(6), pp. 1033–1039. Available at: https://doi.org/10.1016/j.molcel.2011.07.030.

Mockenhaupt, S. and Makeyev, E. V. (2015) 'Non-coding functions of alternative pre-mRNA splicing in development', *Seminars in Cell and Developmental Biology*, 47–48, pp. 32–39. Available at: https://doi.org/10.1016/j.semcdb.2015.10.018.

Moldave, K. (1985) 'EUKARYOTIC PROTEIN SYNTHESIS', *Annual Review of Biochemistry*, 54(1), pp. 1109–1149. Available at: https://doi.org/10.1146/annurev.bi.54.070185.005333.

References

Moore, M.J. and Sharp, P.A. (1993) 'Evidence for two active sites in the spliceosome provided by stereochemistry of pre-mRNA splicing', *Nature*, 365(6444), pp. 364–368. Available at: https://doi.org/10.1038/365364a0.

Morgan, R. and Sargent, M.G. (1997) 'The role in neural patterning of translation initiation factor eIF4AII; induction of neural fold genes', *Development*, 124(14), pp. 2751–2760. Available at: https://doi.org/10.1242/dev.124.14.2751.

Nair, L., Chung, H. and Basu, U. (2020) 'Regulation of long non-coding RNAs and genome dynamics by the RNA surveillance machinery', *Nature Reviews Molecular Cell Biology*, 21(3), pp. 123–136. Available at: https://doi.org/10.1038/s41580-019-0209-0.

Ndzinu, J.K. *et al.* (2018) 'eIF4A2 is a host factor required for efficient HIV-1 replication', *Microbes and Infection*, 20(6), pp. 346–352. Available at: https://doi.org/10.1016/j.micinf.2018.05.001.

Neumann, A. *et al.* (2020) 'Alternative splicing coupled mRNA decay shapes the temperature-dependent transcriptome', *EMBO reports*, 21(12), pp. 1–17. Available at: https://doi.org/10.15252/embr.202051369.

Neves-da-Rocha, J. *et al.* (2019) 'Alternative splicing in heat shock protein transcripts as a mechanism of cell adaptation in Trichophyton rubrum', *Cells*, 8(10). Available at: https://doi.org/10.3390/cells8101206.

Nielsen, P.J. and Trachsel, H. (1988) 'The mouse protein synthesis initiation factor 4A gene family includes two related functional genes which are differentially expressed.', *The EMBO journal*, 7(7), pp. 2097–2105. Available at: https://doi.org/10.1002/j.1460-2075.1988.tb03049.x.

Nishiyama, H. *et al.* (1997) 'A glycine-rich RNA-binding protein mediating cold-inducible suppression of mammalian cell growth', *Journal of Cell Biology*, 137(4), pp. 899–908. Available at: https://doi.org/10.1083/jcb.137.4.899.

Othumpangat, S., Kashon, M. and Joseph, P. (2005) 'Sodium arsenite-induced inhibition of eukaryotic translation initiation factor 4E (eIF4E) results in cytotoxicity and cell death', *Molecular and Cellular Biochemistry*, 279(1–2), pp. 123–131. Available at: https://doi.org/10.1007/s11010-005-8284-2.

Palacios, I.M. *et al.* (2004) 'An eIF4AIII-containing complex required for mRNA localization and nonsense-mediated mRNA decay', *Nature*, 427(6976), pp. 753–757. Available at: https://doi.org/10.1038/nature02351.

Pan, Q. *et al.* (2008) 'Deep surveying of alternative splicing complexity in the human transcriptome by high-throughput sequencing', *Nature Genetics*, 40(12), pp. 1413–1415. Available at: https://doi.org/10.1038/ng.259.

Patel, S.S. and Donmez, I. (2006) 'Mechanisms of helicases', *Journal of Biological Chemistry*, 281(27), pp. 18265–18268. Available at: https://doi.org/10.1074/jbc.R600008200.

Patro, R. *et al.* (2017) 'Salmon provides fast and bias-aware quantification of transcript expression', *Nature Methods*, 14(4), pp. 417–419. Available at: https://doi.org/10.1038/nmeth.4197.

Paul, M.S. *et al.* (2023) 'Rare EIF4A2 variants are associated with a neurodevelopmental disorder characterized by intellectual disability, hypotonia, and epilepsy', *American Journal of Human Genetics*, 110(1), pp. 120–145. Available at: https://doi.org/10.1016/j.ajhg.2022.11.011.

Peretti, D. *et al.* (2015) 'RBM3 mediates structural plasticity and protective effects of cooling in neurodegeneration', *Nature*, 518(7538), pp. 236–239. Available at: https://doi.org/10.1038/nature14142.

Powers, K.T., Szeto, J.Y.A. and Schaffitzel, C. (2020) 'New insights into no-go, non-stop and nonsense-mediated mRNA decay complexes', *Current Opinion in Structural Biology*, 65, pp. 110–118. Available at: https://doi.org/10.1016/j.sbi.2020.06.011.

Preußner, M. *et al.* (2017) 'Body Temperature Cycles Control Rhythmic Alternative Splicing in Mammals', *Molecular Cell*, 67(3), pp. 433-446.e4. Available at: https://doi.org/10.1016/j.molcel.2017.06.006.

Preußner, M. *et al.* (2023) '<scp>ASO</scp> targeting <scp>RBM3</scp> temperature-controlled

References

poison exon splicing prevents neurodegeneration *in vivo*', *EMBO Molecular Medicine* [Preprint]. Available at: https://doi.org/10.15252/emmm.202217157.

Preußner, M. and Heyd, F. (2016) 'Post-transcriptional control of the mammalian circadian clock: implications for health and disease', *Pflugers Archiv European Journal of Physiology*, 468(6), pp. 983–991. Available at: https://doi.org/10.1007/s00424-016-1820-y.

Protter, D.S.W. and Parker, R. (2016) 'Principles and Properties of Stress Granules', *Trends in Cell Biology*, 26(9), pp. 668–679. Available at: https://doi.org/10.1016/j.tcb.2016.05.004.

Qiao, J. *et al.* (2018) 'Simultaneous Monitoring of Mitochondrial Temperature and ATP Fluctuation Using Fluorescent Probes in Living Cells', *Analytical Chemistry*, 90(21), pp. 12553–12558. Available at: https://doi.org/10.1021/acs.analchem.8b02496.

Ran, F.A. *et al.* (2013) 'Genome engineering using the CRISPR-Cas9 system', *Nature Protocols*, 8(11), pp. 2281–2308. Available at: https://doi.org/10.1038/nprot.2013.143.

Ray, B.K. *et al.* (1985) 'ATP-dependent unwinding of messenger RNA structure by eukaryotic initiation factors', *Journal of Biological Chemistry*, 260(12), pp. 7651–7658. Available at: https://doi.org/10.1016/s0021-9258(17)39658-8.

Raza, F., Waldron, J.A. and Le Quesne, J. (2015) 'Translational dysregulation in cancer: EIF4A isoforms and sequence determinants of eIF4A dependence', *Biochemical Society Transactions*, 43, pp. 1227–1233. Available at: https://doi.org/10.1042/BST20150163.

Refinetti, R. (2010) 'The circadian rhythm of body temperature', *Frontiers in Bioscience*, 15(2), pp. 564–594. Available at: https://doi.org/10.2741/3634.

Ribera, J. *et al.* (2021) 'The loss of DHX15 impairs endothelial energy metabolism, lymphatic drainage and tumor metastasis in mice', *Communications Biology*, 4(1), pp. 1–15. Available at: https://doi.org/10.1038/s42003-021-02722-w.

Robinson, J.T. *et al.* (2011) 'Integrative Genome Viewer', *Nature Biotechnology*, 29(1), pp. 24–6. Available at: https://doi.org/10.1038/nbt.1754.Integrative.

Roesch, F. *et al.* (2012) 'Hyperthermia stimulates HIV-1 replication', *PLoS Pathogens*, 8(7), p. 35. Available at: https://doi.org/10.1371/journal.ppat.1002792.

Rogers, G.W., Komar, A.A. and Merrick, W.C. (2002) 'eIF4A: The godfather of the DEAD box helicases', *Progress in Nucleic Acid Research and Molecular Biology*, 72, pp. 307–331. Available at: https://doi.org/10.1016/s0079-6603(02)72073-4.

Rosana, A.R.R., Chamot, D. and Owttrim, G.W. (2012) 'Autoregulation of RNA Helicase Expression in Response to Temperature Stress in Synechocystis sp. PCC 6803', *PLoS ONE*, 7(10). Available at: https://doi.org/10.1371/journal.pone.0048683.

Schwanhäusser, B. *et al.* (2011) 'Global quantification of mammalian gene expression control', *Nature*, 473(7347), pp. 337–342. Available at: https://doi.org/10.1038/nature10098.

Schwer, B. and Guthrie, C. (1991) 'PRP16 is an RNA-dependent ATPase that interacts transiently with the spliceosome', *Nature*, 349(6309), pp. 494–499. Available at: https://doi.org/10.1038/349494a0.

Seetharaman, M. *et al.* (2006) 'Structure of a self-splicing group II intron catalytic effector domain 5: Parallels with spliceosomal U6 RNA', *Rna*, 12(2), pp. 235–247. Available at: https://doi.org/10.1261/rna.2237806.

Shaoyan, X. *et al.* (2013) 'Downregulation of EIF4A2 in non-small-cell lung cancer associates with poor prognosis', *Clinical Lung Cancer*, 14(6), pp. 658–665. Available at: https://doi.org/10.1016/j.cllc.2013.04.011.

Shatkin, A.J. and Manley, J.L. (2000) 'The ends of the affair: Capping and polyadenylation', *Nature Structural Biology*, 7(10), pp. 838–842. Available at: https://doi.org/10.1038/79583.

Shi, H. *et al.* (2019) 'Regulating glycolysis, the TLR4 signal pathway and expression of RBM3 in mouse liver in response to acute cold exposure', *Stress*, 22(3), pp. 366–376. Available at: https://doi.org/10.1080/10253890.2019.1568987.

References

Shiina, T. and Shimizu, Y. (2020) 'Temperature-dependent alternative splicing of precursor mRNAs and its biological significance: A review focused on post-transcriptional regulation of a cold shock protein gene in hibernating mammals', *International Journal of Molecular Sciences*, 21(20), pp. 1–19. Available at: https://doi.org/10.3390/ijms21207599.

Shirai, Y.T. *et al.* (2014) 'Multifunctional roles of the mammalian CCR4-NOT complex in physiological phenomena', *Frontiers in Genetics*, 5(AUG), pp. 1–11. Available at: https://doi.org/10.3389/fgene.2014.00286.

Sinitcyn, P. *et al.* (2023) 'Global detection of human variants and isoforms by deep proteome sequencing.', *Nature biotechnology* [Preprint]. Available at: https://doi.org/10.1038/s41587-023-01714-x.

Somero, G.N. (2018) 'RNA thermosensors: How might animals exploit their regulatory potential?', *Journal of Experimental Biology*, 221(4). Available at: https://doi.org/10.1242/jeb.162842.

Staley, J.P. and Guthrie, C. (1999) 'An RNA switch at the 5' splice site requires ATP and the DEAD box protein Prp28p', *Molecular Cell*, 3(1), pp. 55–64. Available at: https://doi.org/10.1016/S1097-2765(00)80174-4.

Sterne-Weiler, T. *et al.* (2018) 'Efficient and Accurate Quantitative Profiling of Alternative Splicing Patterns of Any Complexity on a Laptop', *Molecular Cell*, 72(1), pp. 187-200.e6. Available at: https://doi.org/10.1016/j.molcel.2018.08.018.

Sudo K., Yakahashi E., and N.Y. (1995) 'Isolation and mapping of the human EIF4A2 gene hommologous to the murine protein synthesis initiation factor 4A-II gene Eif4a2', *Nucl. Phys.*, 13(1), pp. 104–116.

Tanikawa, C. *et al.* (2017) 'The Transcriptional Landscape of p53 Signalling Pathway', *EBioMedicine*, 20, pp. 109–119. Available at: https://doi.org/10.1016/j.ebiom.2017.05.017.

Tauber, D. *et al.* (2020) 'Modulation of RNA Condensation by the DEAD-Box Protein eIF4A', *Cell*, 180(3), pp. 411-426.e16. Available at: https://doi.org/10.1016/j.cell.2019.12.031.

Temin, H.M. and Mizutani, S. (1970) 'Viral RNA-dependent DNA Polymerase: RNA-dependent DNA Polymerase in Virions of Rous Sarcoma Virus', *Nature*, 226(5252), pp. 1211–1213. Available at: https://doi.org/10.1038/2261211a0.

Tu, Y.-T. and Antoni, B. (2016) 'The Human Mitochondrial DEAD-Box Protein DDX28 Resides in RNA Granules and Functions in Mitoribosome Assembly', *Cell Rep.*, 176(3), pp. 854–864.

Turunen, J.J. *et al.* (2013) 'The significant other: Splicing by the minor spliceosome', *Wiley Interdisciplinary Reviews: RNA*, 4(1), pp. 61–76. Available at: https://doi.org/10.1002/wrna.1141.

Upadhyay, M., Bhadauriya, P. and Ganesh, S. (2016) 'Heat shock modulates the subcellular localization, stability, and activity of HIPK2', *Biochemical and Biophysical Research Communications*, 472(4), pp. 580–584. Available at: https://doi.org/10.1016/j.bbrc.2016.03.035.

Valgardsdottir, R., Ottersen, O.P. and Prydz, H. (2004) 'Regulated compartmentalization of the putative DEAD-box helicase MDDX28 within the mitochondria in COS-1 cells', *Experimental Cell Research*, 299(2), pp. 294–302. Available at: https://doi.org/10.1016/j.yexcr.2004.05.019.

Vercellino, I. and Sazanov, L.A. (2022) 'The assembly, regulation and function of the mitochondrial respiratory chain', *Nature Reviews Molecular Cell Biology*, 23(2), pp. 141–161. Available at: https://doi.org/10.1038/s41580-021-00415-0.

Virgili, G. *et al.* (2013) 'Structural Analysis of the DAP5 MIF4G Domain and Its Interaction with eIF4A', *Structure*, 21(4), pp. 517–527. Available at: https://doi.org/10.1016/j.str.2013.01.015.

Wang, E.T. *et al.* (2008) 'Alternative isoform regulation in human tissue transcriptomes', *Nature*, 456(7221), pp. 470–476. Available at: https://doi.org/10.1038/nature07509.

Wang, S.H. *et al.* (2021) 'LncRNA H19 governs mitophagy and restores mitochondrial respiration in the heart through Pink1/Parkin signaling during obesity', *Cell Death and Disease*, 12(6). Available at: https://doi.org/10.1038/s41419-021-03821-6.

References

Weatheritt, R.J., Sterne-Weiler, T. and Blencowe, B.J. (2016) 'The ribosome-engaged landscape of alternative splicing', *Nature Structural & Molecular Biology*, 23(12), pp. 1117–1123. Available at: https://doi.org/10.1038/nsmb.3317.

Wetsel, W.C. (2011) 'Sensing hot and cold with TRP channels', *International Journal of Hyperthermia*, 27(4), pp. 388–398. Available at: https://doi.org/10.3109/02656736.2011.554337.

Wheeler, J.R. *et al.* (2016) 'Distinct stages in stress granule assembly and disassembly', *eLife*, 5(Se), pp. 1–25. Available at: https://doi.org/10.7554/eLife.18413.

Wilczynska, A. *et al.* (2019) 'EIF4A2 drives repression of translation at initiation by Ccr4-Not through purine-rich motifs in the 5′UTR', *Genome Biology*, 20(1), pp. 1–21. Available at: https://doi.org/10.1186/s13059-019-1857-2.

Wilczynska, A. and Bushell, M. (2015) 'The complexity of miRNA-mediated repression', *Cell Death and Differentiation*, 22(1), pp. 22–33. Available at: https://doi.org/10.1038/cdd.2014.112.

Will, C.L. *et al.* (2002) 'Characterization of novel SF3b and 17S U2 snRNP proteins, including a human Prp5p homologue and an SF3b DEAD-box protein', *EMBO Journal*, 21(18), pp. 4978–4988. Available at: https://doi.org/10.1093/emboj/cdf480.

Will, C.L. and Luhrmann, R. (2011) 'Spliceosome Structure and Function', *Cold Spring Harbor Perspectives in Biology*, 3(7), pp. a003707–a003707. Available at: https://doi.org/10.1101/cshperspect.a003707.

Williams, C.A. *et al.* (2015) 'Identification of RNA helicases in human immunodeficiency virus 1 (HIV-1) replication – A targeted small interfering RNA library screen using pseudotyped and WT HIV-1', *Journal of General Virology*, 96, pp. 1484–1489. Available at: https://doi.org/10.1099/vir.0.000092.

Xue, C. *et al.* (2021) 'Expression and Functional Roles of Eukaryotic Initiation Factor 4A Family Proteins in Human Cancers', *Frontiers in Cell and Developmental Biology*, 9(November), pp. 1–12. Available at: https://doi.org/10.3389/fcell.2021.711965.

Yamamoto, H. *et al.* (2014) 'Structure of the mammalian 80S initiation complex with initiation factor 5B on HCV-IRES RNA', *Nature Structural and Molecular Biology*, 21(8), pp. 721–727. Available at: https://doi.org/10.1038/nsmb.2859.

Yang, H.J. *et al.* (2018) 'Cold shock induced protein RBM3 but not mild hypothermia protects human SH-SY5Y neuroblastoma cells from MPP+-induced neurotoxicity', *Frontiers in Neuroscience*, 12(MAY), pp. 1–8. Available at: https://doi.org/10.3389/fnins.2018.00298.

Zhang, D. and Rosbash, M. (1999) 'Identification of eight proteins that cross-link to pre-mRNA in the yeast commitment complex', *Genes and Development*, 13(5), pp. 581–592. Available at: https://doi.org/10.1101/gad.13.5.581.

Zhang, M. and Green, M.R. (2001) 'Identification and characterization of yUAP/Sub2p, a yeast homolog of the essential human pre-mRNA splicing factor hUAP56', *Genes and Development*, 15(1), pp. 30–35. Available at: https://doi.org/10.1101/gad.851701.

Zhang, M.Q. (1998) 'Statistical features of human exons and their flanking regions', *Human Molecular Genetics*, 7(5), pp. 919–932. Available at: https://doi.org/10.1093/hmg/7.5.919.

6. Appendix

6.1 Abbreviations

3’SS	3‘ splice site
5’SS	5‘ splice site
Δ	Depletion/mutant
A	Adenosine/ampere
aa	Amino acid
Alt3’SS	Alternative 3’SS
Alt5’SS	Alternative 5’SS
Amp	Ampicillin
APS	Ammonium peroxodisulfate
ATP	Adenosine triphosphate
BCA	Bicinchoninic acid
bp	Base pair
BP	Branch point
BPS	Branch point sequence
BS	Branch site
BSA	Bovine serum albumin
°C	Degree celsius
C	Cytosine / Carboxy
Cex	Cassette exon
Ci	Curie
cm	Centimetre
cpm	Counts per minute
CTD	C-terminal domain
CTRL	Control
d	desoxy
dd	Double distilled/ didesoxy
Da	Dalton

Appendix

DExD/H	Consensus sequence of helicases
DMSO	Dimethyl sulfoxide
DNA	Desoxyribonucleic acid
DTT	Dithiothreitol
ECL	Enhanced chemiluminescence
EDTA	Ethylendiamintetraacetate
EJC	Exon junction complex
EM	Electron microscopy
et al.	*Et alii*
FBS	Fetal bovine serum
FL	Full length
Fwd	forward
G	Guanosine
g	Gram / centrifugal force
GTP	Guanosine triphosphate
h	Hour
h. sapiens	*Homo sapiens*
H_2O	Water
HeLa	Henrietta Lacks
k	Kilo
kb	Kilo bases
kDa	Kilodalton
L	Liter
LB	Luria Bertani
M	Molar
m	Milli / meter
µ	Micro
min	Minutes
$MgCl_2$	Magnesium chloride
mM	Millimolar
mRNA	Messenger RNA

MS	Mass spectrometry
MW	Molecular weight
N	Amino
n	Nano
NTD	N-terminal domain
NTP	Nucleoside triphosphate
nt	Nucleotides
OD	Optical density
PAGE	Polyacrylamide gel-electrophoresis
PCI	Phenol-chloroform-isoamyl alcohol
PCR	Polymerase chain reaction
pH	Preponderance of hydrogen ions
PMSF	Phenylmethylsulfonylfluoride
PY	Polypyrimidine
Pre-mRNA	Precursor-mRNA
%	Percent
R	Purine base
Rev	reverse
RNA	Ribonucleic acid
RNAi	RNA interference
RNase	Ribonuclease
RNP	Ribonucleoprotein
rpm	Revolutions per minute
RRM	RNA recognition motif
RT	Room temperature/ Reverse transcription
s	Second
SDS	Sodium dodecylsulfate
siRNA	Small interfering RNA
sn	Small nuclear
snRNP	Small nuclear ribonucleoparticles
T	Thymin

Appendix

TEMED	N, N, N’, N’-Tetramethylethylendiamine
Tris	Tris-(hydroxymethyl)-aminomethane
tRNA	Transfer RNA
U	Uridine/unit
UV	Ultraviolet
V	Volt
Vol	Volume
W	Watts
Y	Pyrimidine base

6.2 List of figures

Appendix

6.3 List of tables

Appendix

6.4 Acknowledgements

Firstly, I want to express my sincere gratitude to Prof. Dr. Florian Heyd for the opportunity to work in his lab and for introducing me to the fascinating field of mRNA splicing. Thank you for your continuous support and motivation during the entire time.

A very special thank you to Dr. Marco Preußner. Thank you for your helpful and endless supervision and for working side-by-side in the lab. I highly appreciate that you shared your challenging project with me, all the things I have learned from you and that you've never lost your patience.

Furthermore, I would like to thank Prof. Sutapa Chakrabarti, who immediately expressed her willingness to review my thesis and be part of my Thesis Committee. You and your lab have always been very kind and helpful in any regard.

I also want to thank Antje Grünwald, Bobby Draegert and Karin Hesse for making life in and around the lab much easier. It's nice having people around the lab that care about everything.

Further, I want to acknowledge my dearest lab companions who joined me on my way to submitting this thesis. I've never experienced such a strong community and a working atmosphere where people care about each other. I'm going to miss seeing and talking to you guys every day. Especially Felix, Bruna, Mateusz, and Silvia. Joining the big office brought us so much closer together. I enjoyed working with you, having you as my work family and more than that, calling you friends. Even in tough times, I always appreciated your sense of humor, kindness, and caring nature.

A big thank you also to Ioana for the many hours together at the microscope and your valuable tips while writing this thesis. Without your patience and support, I would never have been able to take immunofluorescence images on my own!

My dearest Bruna, we have been together on this journey from the beginning to the end. You were always there for me and cheered me up when I needed it. I am grateful to have made this long and sometimes difficult journey with you. I will deeply miss your dark sense of humor. I hope that no matter where life takes us, we will stay in touch. Because what is life without two grown-ups sending cute animal videos to each other?!

One of the best things that happened to me in my time here is to find true friendship in you, Sandra, and Miri. I hope life will never separate us over time, and we are staying as close as we became over the last four years. I especially want to thank Sandra for all the tips and proofreading of this thesis! You made writing less stressful, always cheered me up and motivated me. I don't know how I would have survived this time without your boundless help and your two cute dogs Oskar and Gustaf.

With all my heart, I want to thank all my friends who make life worth living. Thanks for the unforgettable moments and the privilege of having true friends like you!

You are the most important person in my life, dear Rebecca. I am infinitely happy and grateful to have the most wonderful big sister in the world. Thank you for always believing in me and always supporting me with your love and care over the past 28 years. I wouldn't be where I am today if we didn't have each other. I think I can speak for everyone in the world when I say that the greatest gift is to share your whole life with someone as warm-hearted as you.

Finally, I would like to thank Marius. Thank you for never leaving my side during all this time. You have given me so many opportunities for personal growth. Even though times have not always been easy, you have never stopped believing in me and providing me with love, affection and most important: food! With you, I could always be me. Thanks for listening to my million monologues about everything and nothing and pretending to be listening. Thank you for dragging me through the final phase of this thesis and covering my back wherever you could. Thank you for all the incredible journeys and personal growth over the last five years.